Mechanical behavior of

unsaturated compacted Iowa loess

by

Sonal Singhal

A thesis submitted to the graduate faculty

in partial fulfillment of the requirements for the degree of

MASTER OF SCIENCE

Major: Civil Engineering (Geotechnical Engineering)

Program of Study Committee:
Radhey S. Sharma (Major Professor)
Vernon R. Schaefer
Matthew J. Helmers

Iowa State University
Ames, Iowa
2005

Graduate College

Iowa State University

This is to certify that the master's thesis of

Sonal Singhal

has met the thesis requirements of Iowa State University

TABLE OF CONTENTS

LIST OF FIGURES

LIST OF TABLES

ACKNOWLEDGEMENTS

I am grateful to my supervisor Dr. Radhey S. Sharma. Without his guidance, expertise and suggestions the completion of this project was not possible. I am also thankful to my committee members Dr. Vernon R. Schaefer and Dr. Matthew J. Helmers for their time and suggestions to improve my thesis.

I am also indebted to Dr. Kumar for his help and encouragement through out the project. Furthermore, I am thankful to Don Davidson, Laboratory Assistant for his continuous support in learning the utilization of various available laboratory facilities. I am also thankful to Dr. Warren E. Straszeim in the MARL lab for carrying out SEM tests and explaining them to me.

Additionally, I am grateful to all my friends from Institute of Technology, Banaras Hindu University and Iowa State University for their continued moral support.

Finally, I am forever indebted to my mother for her understanding, endless patience and encouragement when it was most required. I am also grateful to my sister Sheetal and brother Pranav for their love, care and support.

ABSTRACT

The collapsible soils possess a high apparent strength at their low natural moisture content but undergo large reduction in volume upon wetting. The volume change and shear strength behavior of a laboratory compacted loess soil was studied and presented. Collapse tests and partial collapse tests were conducted using conventional oedometer. Undrained shear strength was measured from Torvane shear tester. Penetration tests were also performed on collapsible soil specimens. Undrained cohesion, c_u, was obtained from the measured values of penetration resistance using Sanglerat's equation. Correlations were proposed to relate collapse potential with the penetration resistance. Tests were conducted to determine the variation of water content with suction for loess. The unsaturated soil behavior was investigated for nine conditions produced by varying initial water contents and compactive efforts. The initial water content was replaced with suction and the effect of initial suction on the collapse potential was studied.

The collapse potential of loess was found to be dependent on the initial water content, initial dry unit weight and flooding stress (vertical stress at inundation). The amount of partial collapse increased with increase in degree of saturation. The effect of variation in initial water content was more significant as compared to the effect of compactive effort on soil water characteristic curves. Undrained cohesion obtained from Torvane shear tests and penetration tests were found to tally and to give a good correlation. The collapse potential increased with increase in initial suction. However, the percentage increase in collapse on increasing suction reduced as the compactive effort increased.

CHAPTER 1

INTRODUCTION

AN OVERVIEW OF PROBLEMATIC SOILS

Design and construction of foundations in problematic soils such as expansive soils and collapsible soils, is common in the practice of geotechnical engineering. These problematic soils expand, collapse, disperse, undergo excessive settlement, have a distinct lack of strength or are corrosive. Such detrimental characteristics of soil may be understood by their composition, the nature of their pore fluids, their mineralogy or their fabric (Bell and Culshaw, 2001). With the exception of peat, the formation of soil takes place due to breakdown of rock masses, either by weathering or by erosion. The engineering behavior of soils depends on the type of weathering process. Hence, residual soils and transported soils show different engineering behavior. Climatic conditions such as precipitation and evapotranspiration play an important role in governing the engineering behavior of soils.

Most soils are sensitive to seasonal changes in moisture regime. The soils which respond quickly to changes in moisture regime may lead to deleterious consequences (Chen, 1988) such as swell, collapse, or loss of strength upon wetting. The problem of wetting may arise from a variety of sources, such as changes in surface and ground water regimes. Wetting of soils well above their natural moisture contents leads to problematic subsoil conditions. If the material is highly plastic, initially dry, and lightly confined then it swells

on wetting, or if the material is non-plastic or slightly plastic, initially dry, and heavily confined then the result is collapse on wetting (Houston *et al.* 2001).

The most noteworthy among the problematic soils are swelling/shrinking clays, collapsible soils, quick sands, frozen soils and peat. The presence of minerals such as montmorillonite in clays is the main cause of expansiveness (Grim, 1962). The volume change potential or swell potential is controlled by the initial moisture content, initial dry density, the initial microstructure and the initial vertical stress, as well as the type of clay minerals and their quantity present (e.g., Mitchell, 1976; Chen, 1988; Rao *et al.* 1991). Soft clays existing at high natural water content and loose sands having a low relative density undergo excessive settlements, exhibit low shear strength and create difficult subsoil conditions.

Partially decomposed and disintegrated plant remains preserved under incomplete aeration and high water conditions give birth to peat. It usually has an organic content well in excess of 50%, void ratios between 9 and 35 and water contents over 500 % (Bell and Culshaw, 2001). The engineering problems posed by peat are differential and excessive settlement. Saturated sands and silts acquire 'quick' condition when the weight of submerged soil is balanced by an equal and opposite acting seepage force reducing effective pressure to zero. Loosely packed finer sands and coarser silts are more susceptible to quick condition as compared to coarser sands due to their relatively low permeabilities which do not allow easy dissipation of pore water pressure. Sudden shocks caused by heavy machinery such as pile driving, activities such as blasting and earthquakes can also cause liquefaction (Bell and Culshaw, 2001; Seed and Idriss, 1971).

Collapsible soils, which consist mainly of wind-blown silt, are susceptible to large reductions in volume upon wetting either under overburden pressure, or under additional imposed load (Tadepalli *et al.* 1992). Sometimes, the soil collapses due to the application of imposed load under natural moisture conditions also by virtue of being in a loose state. Such soils have porous structure, high void ratios and relatively low densities in dry conditions (Lutenegger and Saber, 1988; Lawton *et al.* 1989).

The cost of repair to damage done to civil engineering structures by these problematic soils is very heavy in various countries such as £3 billion in Britain and $2.3 billion in USA (Jones and Holtz, 1973; Bell and Culshaw, 2001).

AIM OF THE RESEARCH PROJECT

This thesis deals with a study on collapsible soil, loess obtained from Turin, Western Iowa. The main objectives of this study are as follows:

- To summarize and synthesize the previous research on collapsible soils thereby developing an understanding of the collapse mechanism of loess.
- To evaluate the various available experimental techniques on collapsible soils.
- To investigate the influence of initial placement conditions and flooding stress (vertical stress at inundation) on the collapse potential of loess.
- To study the volume change behavior of loess under controlled and uncontrolled flooding conditions.
- To interpret the behavior of soil water characteristic curves developed at different initial placement conditions.

- To develop correlations between suction and volume change behavior of collapsible soils.
- To develop initial correlations to predict field collapse from laboratory test results.

OUTLINE OF THESIS

Chapter 1 gives an introduction to various problematic soils and presents the objectives of this research. Chapter 2 deals with a detailed review of literature on collapsible soils.

Basic characteristics of the collapsible soil used for testing, experimental investigation carried out, preparation of the soil specimens, the tests performed and the procedures thereof have been explained in Chapter 3.

Chapter 4 presents a detailed discussion and an analysis of test results from collapse tests. Soil suction study and various correlations drawn from the test program have been presented in Chapter 5.

Conclusions drawn from this experimental study and recommendations for future work are presented in Chapter 6.

CHAPTER 2

REVIEW OF LITERATURE

COLLAPSIBLE SOILS

Of the various problems posed by different problematic soils (e.g. swelling/shrinkage, collapse and dispersion), those triggered by collapsible soils can also be very disconcerting. For example, the cost of repair to damage from collapse of loess deposits in Bulgaria during 1956 to 1986 was estimated to be about $150 million (Evstatiev, 1995). The cost of remedial measures required to repair structures at a cement plant in Central Utah located on collapsible soils was more than $20 million (Hepworth and Langfelder, 1988). A conservative estimate of cost of repair to damage from collapsible soils in US annually is more than $100 million dollars. Collapsible soils are those soils which exhibit a sudden detrimental reduction in volume on inundation or increase of water content at a constant total stress (Lutenegger and Saber, 1988; Lawton *et al.* 1989; Tadepalli *et al.* 1992). They are characterized by a sudden decrease in bearing capacity following collapse or subsidence (Reznik, 1992).

Formation and existence of collapsible soils

The formation of collapsible soils is favored by arid environments, where evaporation exceeds rain fall (Houston *et al.* 2001). The primary depositional processes (aeolian deposition, alluvial and flood depositions and sediment deposition in shallow or deep sea and lake) are generally common to various types of collapsible soils such as debris flow deposits,

alluvial deposit and wind-blown deposits (Houston *et al.* 1995a). However, collapsible soils are not confined only to arid regions, as they occur in most parts of the world. Almost all naturally occurring collapsible soil deposits (Houston *et al.* 2001) are either debris flow deposits or loess deposits (wind-blown silts). Loess consists chiefly of silt sized particles (typically 20-30 μm), which are transported by great rivers (e.g. Hwang He, the Danube and the Rhine) from the source such as tectonically active mountains like the Himalayan and the Alpine mountains. On subsequent flooding of the rivers the silt particles are deposited on the flood plain. Upon drying, however, the particles are detached and transported by winds (Jefferson *et al.* 2001).

Loess deposits are abundant in the mid-continent areas in North America, Europe and Asia. In United States, the damages due to collapse problems have been reported in 17 states. Figure 1 shows the major loess deposits in the US along with other sites of reported collapsible soils. They exist in the US from Indiana to Nebraska, and from Illinois to Tennessee and Mississippi. They exist in China also (Handy, 1995). In North China loess covers an area of over 640,000 km^2 of which collapsible behavior has been observed over an area of 380,000 km^2. In some of the places in North China the thickness of loess has been found to be more than 300 m (Derbyshire *et al.* 1995; Miao *et al.* 2002).

Loesses are widespread the world over. The main loess covered areas in the world are shown in Figure 2. It is reported that loess deposits of thickness of approximately 20-30 m occupy vast territories in Russia with a total area of 3,500,000 km^2. The collapsibility of the soil and the overburden has been reported to vary from 5 to over 50-100 cm (Osipov and Sokolov, 1995). More than 60% of the land area in Mediterranean Europe consists of loess deposits (Poesen and Wesemael, 1995). It has been recorded that 13% of the territory of

Bulgaria consists of loess deposits, covering an area of about 14,000 km^2. The thickness of loess deposits has been found to be of the order of 40-50 m (Evstatiev, 1995). The following table (Table 1) shows a detailed distribution of various collapsible soils all over the world.

Table 1 - Distribution of collapsible soils the world over (after Rogers, 1995).

Name of the collapsible soil	Name of the country/place
Granitic sands	South Africa
Collapsible aeolian sands	Saharan fringes
Kalahari sands	South Africa
Volcanic dust	South America, Japan, New Zealand
Loess	China, East Europe, Central Asia, North America, South America
Quick clays	Scandinavia, Canada
Parna (a cemented sandy clay, which collapses on leaching)	Australia
Cemented soils	Northern Nigeria
Saline soils	China

Types of collapsible soils

Loess, brickearth and wind-blown silts have the potential for collapse and therefore, may be classed as collapsible soils. These soils generally consist of 50 to 90% silt particles. However, some soils have been found to consist of sandy and clayey particles also (Clevenger, 1958). Brickearth means the earth used for manufacturing bricks. Brickearth is composed largely of silt-sized particles. The brickearth deposits are yellowish brown in color and slightly plastic in nature (Jefferson *et al.* 2001; Bell and Culshaw, 2001). Some alluvial soils deposited from water in dry places are also collapsible. The most abundant collapsible soil is *loess*, which is wind deposited silt. Loess derives its name from a German word

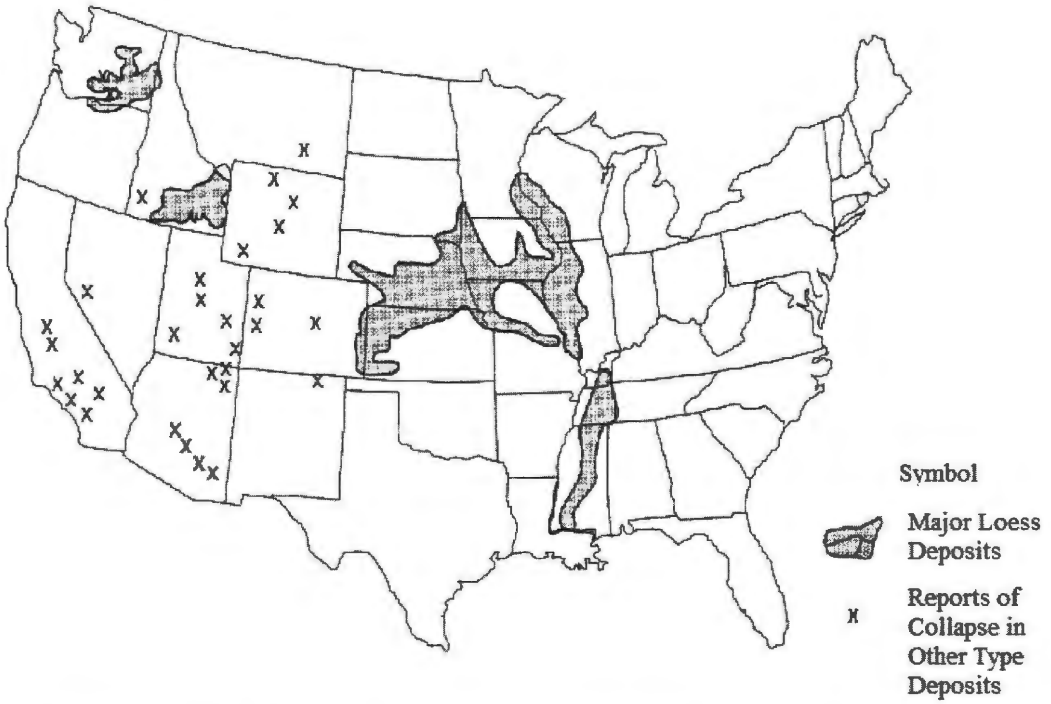

Figure 1 - Major loess deposits in the US along with other sites of reported collapsible soils (Coduto, 2002).

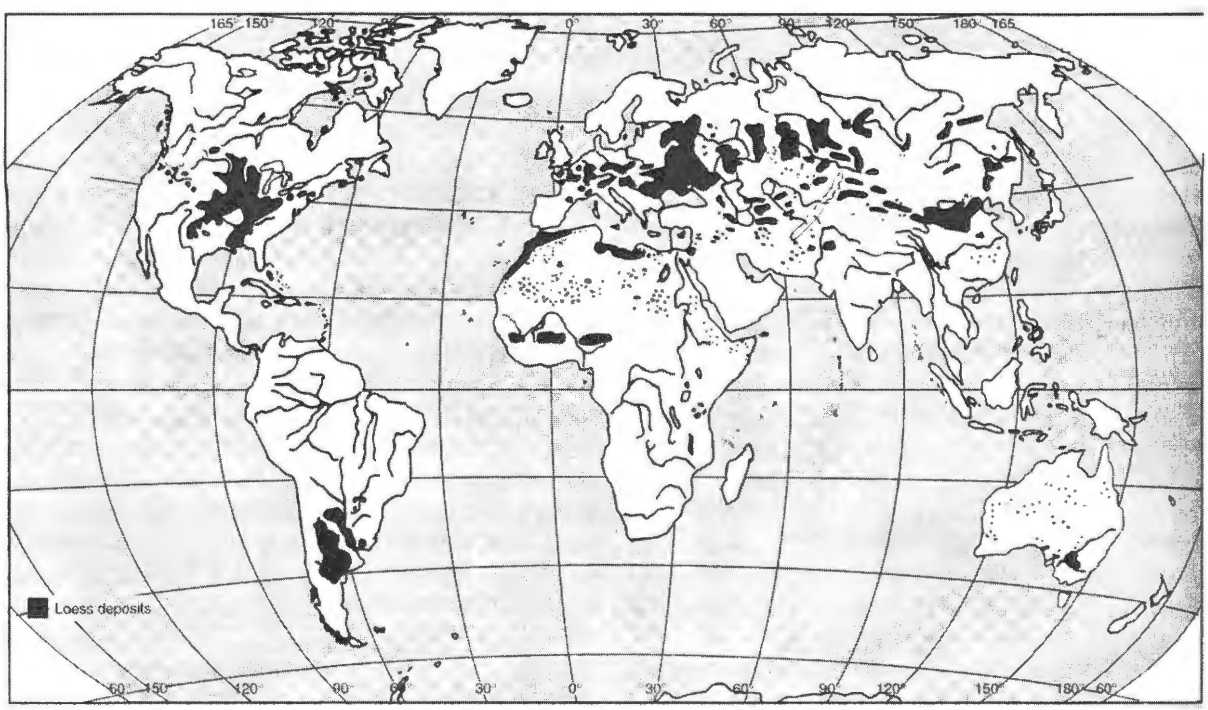

Figure 2 - Main loess covered areas in the world (after Livingstone and Warren, 1996).

"*loëss*" which means loose (Handy, 1995). Loess is generally characterized by its high content of dusty particles (as a rule, not less than 50%) (Osipov and Sokolov, 1995).

Material characteristics of loess

(i) Particle size

Loess deposits are comprised predominantly of particles with size ranging from silt to fine sands (Haq and Kibria, 1994; Houston *et al.* 2001; Bell and Culshaw, 2001; Jefferson *et al.* 2001) though varying clay contents have been found all over the world. The typical index properties of some collapsible soils are shown in Table 2.

Table 2 - Index properties of some collapsible soils (after Tadepalli *et al.* 1992; Pereira, 1996; Pereira and Fredlund, 2000).

Index Property	Indian Head Silty Sand	Mississippi Delta Silt (Vicksburg)	Residual Silty Sand (Ceara, Brazil)
Grain-size distribution	Sand sizes = 62%	Sand sizes = 5.9%	Sand sizes = 52%
	Silt sizes = 32%	Silt sizes = 84.3%	Silt sizes = 35%
	Clay sizes = 6%	Clay sizes = 9.8%	Clay sizes = 13%
	D_{10} = 0.0034 mm	D_{10} = 0.002 mm	D_{10} = 0.0006 mm
	D_{30} = 0.025 mm	D_{30} = 0.043 mm	D_{30} = 0.016 mm
	D_{60} = 0.090 mm	D_{60} = 0.017 mm	D_{60} = 0.022 mm
Coefficient of uniformity, C_u	$C_u = D_{60}/D_{10}$ = 26.4	$C_u = D_{60}/D_{10}$ = 8.5	$C_u = D_{60}/D_{10}$ = 36.6
Atterberg limits	Liquid limit, w_L = 22.2%	Liquid limit, w_L = 35.5%	Liquid limit, w_L = 29%
	Plastic limit, w_P = 16.6%	Plastic limit, w_P = 21.55%	Plastic limit, w_P = 17%
	Plastic index, *PI*= 5.6%	Plastic index, *PI* = 14.0%	Plastic index, *PI* = 12.0%
Specific gravity, G_s	2.68	2.68	2.64

(ii) Mineral composition

Loesses are polymineral materials, composed of over 50 various minerals. The silty and sandy fractions mostly consist of quartz, feldspar, carbonates, micas, gypsum and other minerals. While, clay fractions are dominated by hydromica, montmorrilonite, mixed-layered, Kaolinite, fine-dispersed quartz and calcite (Osipov and Sokolov, 1995). Most loesses are characterized by:

Carbonate content – 1% to 15-25%

Gypsum content (medium soluble mineral) – 4% to 10%

Chlorides content (readily soluble salt) – under 2%

Oxides and hydroxides (half soluble) – under 2.4%

Humus (in humus interstrata and loess subsoils) - less than 1-2% humus (Ananyev, 1964; Sargeev *et al.* 1986; Osipov and Sokolov, 1995).

It has been believed by a majority of researchers investigating loessial soils that the collapsibility of loess decrease with an increase in content of low soluble salts and clay minerals, particularly of smectite and mixed – layered groups. However, no direct correlation between these factors and collapse potential was established (Osipov and Sokolov, 1995).

(iii) Moisture content and index properties

The amount of water present in collapsible soils which depends on natural humidity has a very significant role to play in the phenomenon of collapse. The general index of initial water content for collapse of loess is defined as the minimum natural humidity to initiate collapse. Previous research shows that the initial degree of saturation for most collapses of loess varies from 15 to 19% (Osipov and Sokolov, 1995). The natural water content of most

loess soils has been found to vary from 4 to 23% (Qian *et al.* 1985; Derbyshire *et al.* 1995). Though most of the collapsible soils are of low plasticity, their plasticity index varies. A general range of plasticity index for collapsible soils based on previous research can be considered as 5 to 32. The range of dry densities over which most collapsible soil deposits exist has been found to be 12.50 -17.50 kN/m^3 (Qian *et al.* 1985; Derbyshire *et al.* 1995; Bell and Culshaw, 2001).

The high void ratios of the collapsible soil deposits range from 0.55 to 0.82. Collapsible loess soils are characterized by a high porosity, which has been found to vary between 35 and 45% (Derbyshire and Mellors, 1988; Osipov and Sokolov, 1995; Bell and Culshaw, 2001). Loesses with aggregative structures are known to be the most porous. The porosity formed by the largest and medium size inter-grain and inter-aggregate pores called as "active" porosity, which plays an important role in loess collapsibility (Osipov and Sokolov, 1995). It may be mentioned here that, in spite of a lot of research on the importance of porosity in loess collapsibility, there are no precise quantitative relationships between porosity characteristics and loess collapsibility. Table 3 shows some of the significant index properties of different collapsible soils.

(iv) Structure and texture

Collapsible soil deposits possess porous textures and high void ratios and, therefore, exist at relatively low densities in dry conditions (Bell and Culshaw, 2001). After collapse, however, the soil particles rearrange themselves into a denser state of packing. These soils possess a high apparent strength at their low natural moisture content but undergo large

Table 3 - Representative values of index properties of collapsible soils (after Derbyshire and Mellors, 1988).

Location	G_s	ρ_d (kN/m^3)	e	n (%)	LL (%)	PL (%)	PI (%)
Pine Farm Quarry	2.70	14.8	0.82	45	32	22	10
Ford	2.70	14.9	0.81	45	34	19	15
Pegwell Bay	2.69	16.4	0.64	39	29	18	11
Pegwell Bay buried channel	2.69	17.4	0.55	36	33	20	13
Reculver	2.68	16.2	0.65	39	33	20	13
Sturry	2.69	16.9	0.59	37	44	22	22
Northgleet	2.70	16.0	0.68	41	32	19	13
Average	2.69	16.2	0.68	40	34	20	14

reduction in volume upon wetting. This means that the metastable structure collapses on wetting. Figures 3(a) and 3(b) show the structure of loess before collapse and after collapse respectively. The fabric of collapsible soils takes the form of a loose skeleton of grains (generally quartz) and micro-aggregates (groups of clay or clay and silty clay particles). Surface coatings of clay minerals may also be present on coarser grains (Bell and Culshaw, 2001). The sand and silt sized particles are sub-angular to sub-rounded, and may be in grain to grain contact or separate from each other as shown in Figure 4 (Jefferson *et al.* 2001). Investigations have shown that the inner part or the nucleus of the grains, which is formed by a primary mineral (usually, quartz or feldspar), is divided into separate blocks of size 0.1 mm (Osipov and Sokolov, 1995). Different morphological types of loess structure have been identified, namely, grainy, aggregative-grainy, grainy-aggregative and aggregative structures which are shown in Figures 5(a) to 5(d).

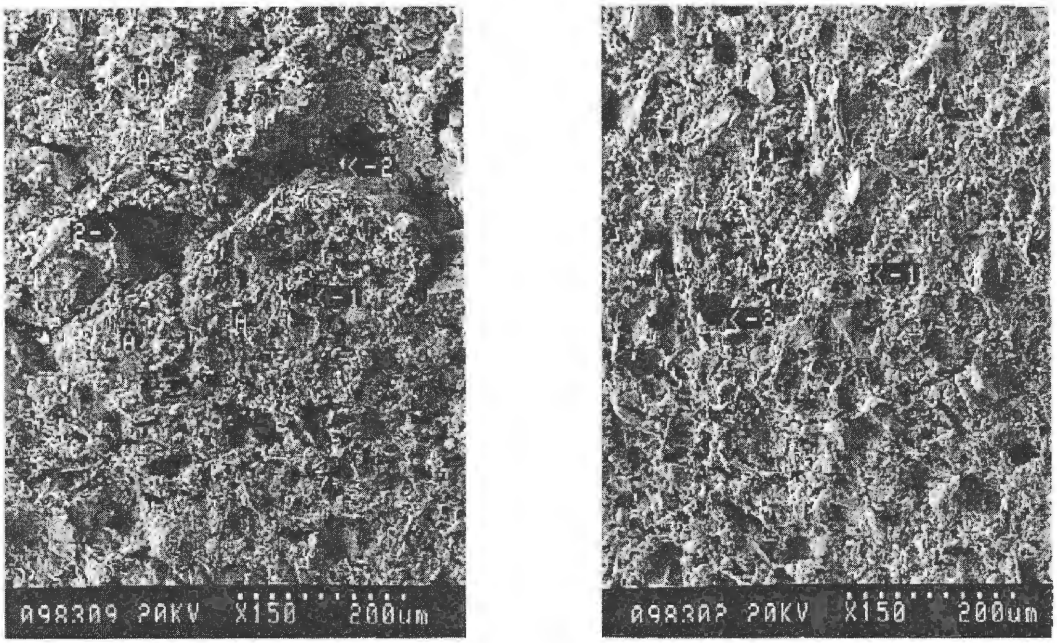

(a) (b)

Figure 3 - Loess structure before and after collapse: (1) Intra-aggregate pores; (2) Interaggregate pores; A-aggregates (after Osipov and Sokolov, 1995).

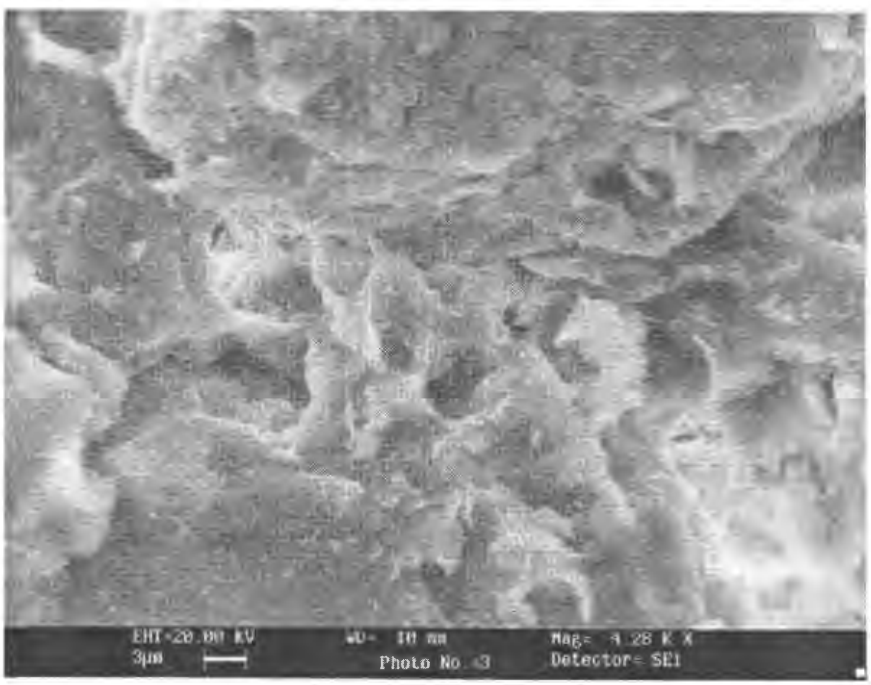

Figure 4 - Bonded quartz particles in brickearth (loess) (after Jefferson *et al.* 2001).

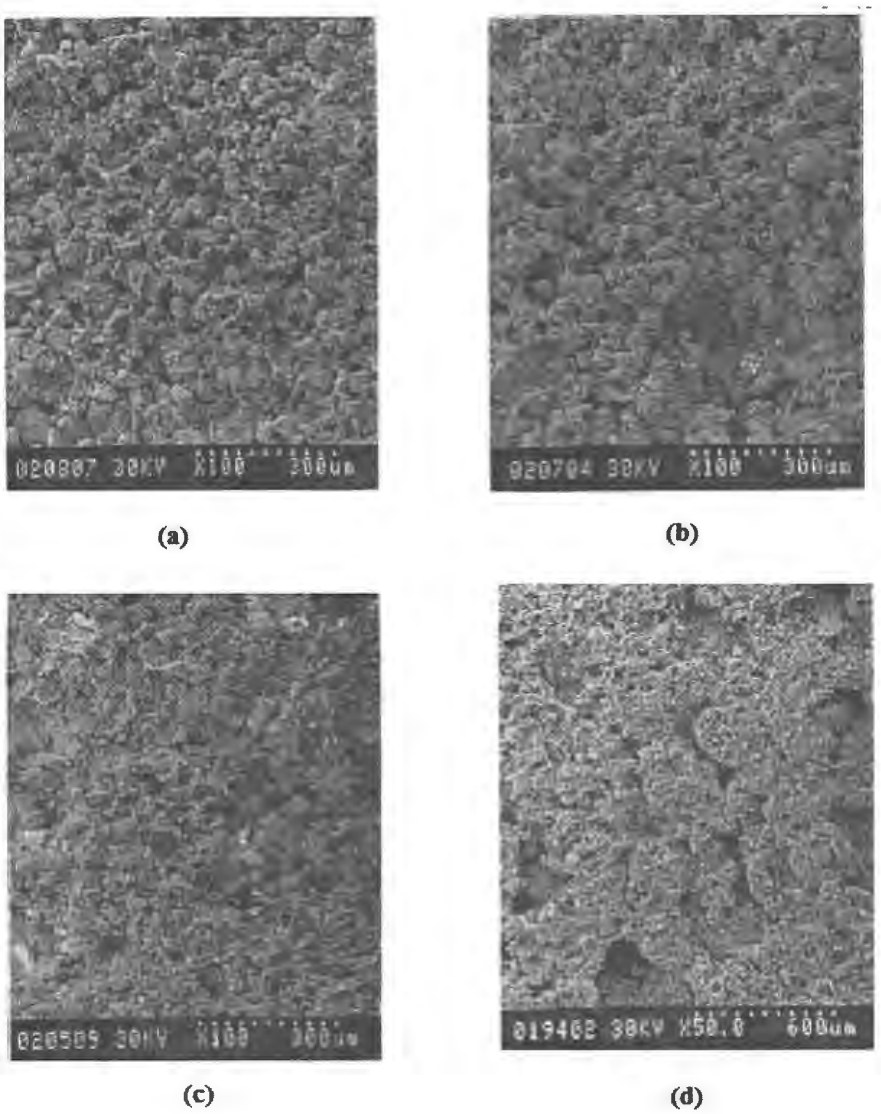

Figure 5 - Different morphological types of loess structure: (a) grainy; (b) aggregative-grainy; (c) grainy-aggregative; (d) aggregative (after Osipov and Sokolov, 1995; Sergeev *et al.* 1986; Larionov, 1971).

(v) Essential factors for collapse

The following pre-requisite conditions have been identified for collapse to occur in a soil (Barden *et al.* 1973; Mitchell, 1976; Rogers, 1995; Al-Amoudi and Abduljauwad, 1994; Lawton *et al.* 1989). They are:

a) An open, partially unstable and unsaturated fabric,

b) A high void ratio,

c) A low dry density,

d) A high porosity,

e) Increase in water content of the soil reducing soil suction and destroying bonding agents, and

f) A relatively high level of total stress acting on the soil.

The first four features are interconnected and facilitate volume reduction and the consequential particle rearrangement. In fact, all the first four factors are *prima facie* indicators to a potential of the soil for collapse. Higher amount of soil suction present in the soil in its unsaturated condition causes bonding or cementing and thus stabilizes the soil (Sharma, 1998; Gallipoli *et al.* 2003; Wheeler *et al.* 2003). However, with the increase in water content, degree of saturation increases and suction decreases. Hence, the soil loses bonding between particles, thus becoming unstable (Rogers, 1995; Houston *et al.* 2001). Volume reduction of soil takes place when the vertical compressive stress is increased. For collapse to occur in loess, a limiting value of vertical compressive stress was identified, defined as the *collapse pressure* (Popescu, 1986). It was observed that volume reduction of soil increased appreciably beyond collapse pressure. The soils in which collapse occurs at a collapse pressure less than the vertical overburden pressure can cause detrimental subsidence.

This means that these soils cannot support even the weight of the overburden when saturated. This kind of collapse may be called water-induced collapse, which is more dramatic than stress-induced collapse, which takes place on increase of stress (Rogers, 1995). The soils in which collapse occurs at a collapse pressure higher than the vertical overburden pressure may be termed as conditionally collapsible soils, because these soils are capable of supporting a certain level of stress even on saturation. Therefore, they are pseudo-stable (Popescu, 1986). Soils having lower moisture contents were observed to collapse at a critical pressure greater than that for soils with higher moisture contents (Phien-wej *et al.* 1992). Previous research also recorded that collapse occurred essentially at constant total stress, suggesting a collapse potential of the soil at the flooding stress level (Lawton *et al.* 1989). A stress pulse from an earthquake, which increases the stress significantly above the static value, can cause a more dramatic collapse (Rogers, 1995).

MECHANISMS OF COLLAPSE

Classification of collapse

Collapse is broadly classified as (i) local collapse and (ii) total collapse. Soil attains a metastable condition on change of initial placement conditions (increase of water content). During metastable state, collapse takes place and the soil regains a stable state. If the collapse is of a smaller extent, being confined mainly to the weaker regions resulting in the homogenization of soil, then the collapse is called local collapse. In this state the soil has further capacity to reach the state of full equilibrium (Feda, 1995). Total collapse, however, is the result of complete equilibrium acquired by the soil on complete failure of the system followed by the reconstruction of the soil structure.

Micromechanics of collapse

Micromechanics of collapse deals with the study of the role of various structural components of collapsible soils such as structural units (consists of grains, particles and their aggregates and clusters), fabric, bonding and internal stress (Feda, 1995). Four collapse mechanisms have been identified from the micromechanical point of view as shown in Figure 6. They are (1) debonding, (2) grain-breakage, (3) fabric transition, and (4) softening and hardening. Collapse by debonding is the most frequent example and the soils showing such a collapse are commonly termed as collapsible soils. Collapse usually occurs by water inundation which destroys the bonds between particles and causes demolition of capillary forces. On flooding with water, adsorption of water molecules takes place on the newly formed surfaces of soil particles, which decreases the surface energy and hence, the strength of the parent material. Adsorption of water molecules to the planes of discontinuities not only reduces the strength but also encapsulates the pore air, thereby breaking the soil structure (cementation bonds). The second type of micromechanism of collapse is collapse due to grain-breakage or grain-crushing (see Figure 6). This occurs because of isotropic compression at high compressive stresses. Coarser grains of equal diameters are broken more easily than a mixture of grain sizes, because well-graded materials resist crushing better than poorly-graded materials (Feda, 1995).

The third type of micromechanically classified collapse is fabric transition which is a consequence of shearing rather than a factor governing the collapse. This type of mechanism can be seen in triaxial K_0-measurements in which specimens are unloaded axially so that their overconsolidation ratio (OCR) increased, where, K_0 is the coefficient of earth pressure at rest. The increase in K_0 stops at some critical value of overconsolidation ratio followed by

reduction in K_0 values thereafter. This phenomenon is attributed to the fabric-induced structural changes. During the consolidation stage, contact planes of individual grains tend to orient themselves in a direction perpendicular to the applied load, forming a kind of compression fabric. Unloading beyond OCR > 1, the directional load is radial which develops an inconsistent situation gradually between the direction of newly developed directional load and the old fabric with the tendency of the fabric being to reorient according to the former one. This change in fabric, leading to collapse, must be preceded by some debonding (Feda, 1995). The last type of micromechanism of collapse occurs because of a periodical softening-hardening occurrence. This has been found to occur especially in fissured clays, which have strength anisotropy, wherein the pattern of fissures is incompatible with the triaxial failure mode. The interference of laboratory boundary conditions with the soil weakness planes' kinematics leads to this type of collapse more than any of the aforementioned collapses. Though the different micromechanics of collapse, as mentioned above, have been identified, it is possible that a mixed collapse might occur combining some or all of these different mechanisms of collapse (Smith *et al.* 1994).

Macromechanics of collapse

Macromechanics of collapse concerns with the relationships of macromechanical or measured quantities such as stress or strain. Figure 6 shows the causes of collapse from macromechanical point of view. Collapse induced by critical stress, which may depend on the stress path is the most common of all collapses. Collapse triggered by wetting is governed by water content or suction. The hardening-softening process seems to occur due to perturbations which result from the breakage of clusters of particles. Two types of creep have

been identified, namely, distortional creep and volumetric creep. Collapse due to increase in pore water pressure has also been recognized. The two possibilities of collapse under pore water pressure increase are

(i) Pore water pressure increase being independent of soil deformation (external source), and

(ii) The breakdown of soil skeleton inducing an increase in pore water pressure (internal source).

Collapse has been identified as a state of instability of soil triggered by internally caused pore water pressure increase (Feda, 1995).

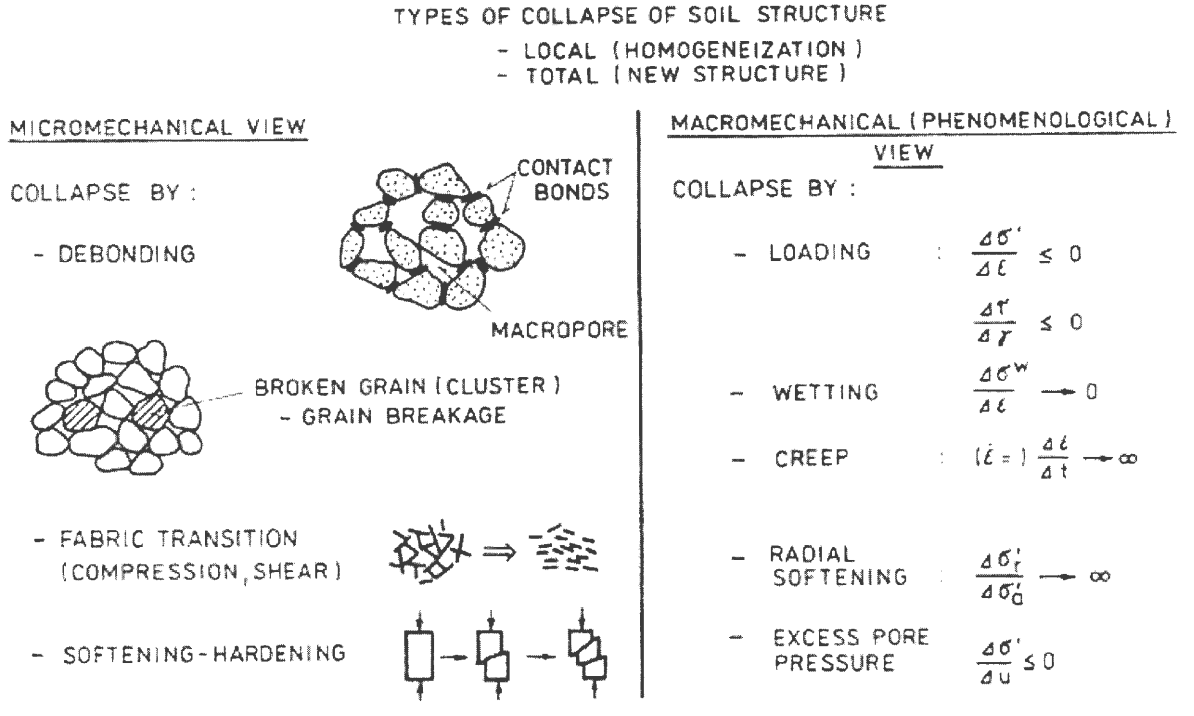

Figure 6 - Classification of collapse mechanisms (after Feda, 1995).

DEFINITIONS OF COLLAPSE AND COLLAPSE POTENTIAL

The term collapse is applied to unsaturated soils which show drastic rearrangement of particles leading to loss of volume on inundation with or without increase in loading (Jennings and Knight, 1957; Jennings and Burland, 1962). Collapse can be directly measured in the laboratory by conducting one-dimensional consolidation tests on undisturbed samples. In general, there are two types of test procedures that can be employed for the laboratory determination of collapse potential. The definition of collapse potential varies depending on the test procedure used.

Single oedometer collapse test

The definition of collapse potential, i_e as first suggested by Abelev (1948) for an undisturbed soil specimen at natural moisture content loaded to a stress of 300 kPa in an oedometer and then inundated, is as follows:

$$i_e = \frac{\Delta e_c}{1 + e_1} \tag{1}$$

where, Δe_c = Change in void ratio upon wetting under flooding stress (300 kPa) i.e., e_1 - e_f,

e_1 = Void ratio at the point of flooding

e_f = Final equilibrium void ratio under flooding stress (vertical stress at inundation).

Knight (1963) used 200 kPa as flooding stress and defined collapse potential as the ratio of the change in void ratio on inundation at the flooding stress to specific volume. It is expressed as,

$$i_e = \frac{\Delta e}{1 + e_o} \tag{2}$$

where, Δe = Change in void ratio of the specimen on flooding i.e., e_o - e_f, and

e_o = Equilibrium void ratio after the placement of first vertical stress in oedometer test.

e_f = Final equilibrium void ratio under flooding stress.

This definition of collapse potential referred to by Equation (2) was later modified (Jennings and Knight, 1975) by replacing Δe with Δe_c, which signifies the change in void ratio upon flooding with respect to the initial void ratio at the flooding stress, as follows:

$$i_e = \frac{\Delta e_c}{1 + e_o} \tag{3}$$

The difference in Equation (1) and Equation (3) apart from difference in stress level is in the choice of initial void ratio taken for obtaining the volumetric strain. The two definitions give almost the same results if only a little compression of specimen occurs up to the flooding stress level. Also, Equation (1) considers the amount of compression that occurs only as a result of collapse and does not include compression which occurs because of the loading applied prior to the flooding stress (Lutenegger and Saber, 1988).

Figure 7 shows the typical e-log σ_v curve showing the collapse at a given flooding stress. The two stages of the sample at natural water content and the inundated water content are shown.

Double oedometer collapse test

Jennings and Knight (1957) proposed an alternative method to predict collapse potential by using results of the "double oedometer" test. The method consists of two oedometer tests on samples having the same initial placement conditions. One of the samples is loaded at the initial placement conditions, while the other is saturated even before loading.

The difference between the e-log σ_v curves obtained from the two oedometer tests at any stress level quantifies the amount of deformation that would occur if the sample is saturated at that particular stress level during its loading history. Figure 8 gives a schematic representation of results from a double oedometer test.

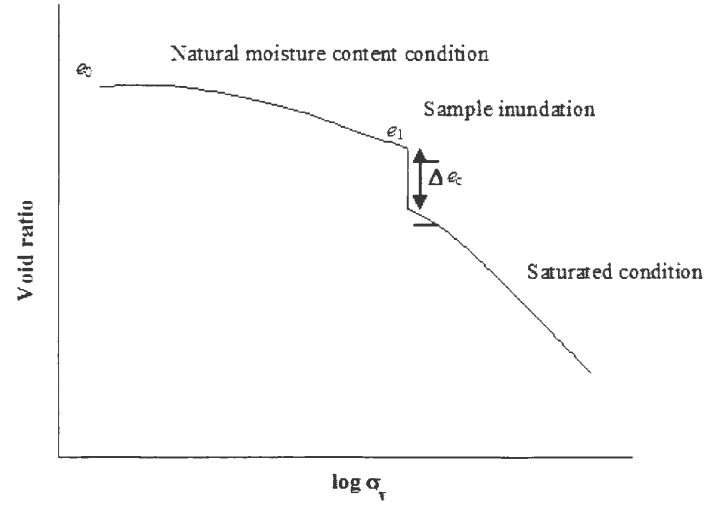

Figure 7 - Single oedometer collapse test (after Abelev, 1948; Jennings and Knight, 1975; Jennings and Burland, 1962).

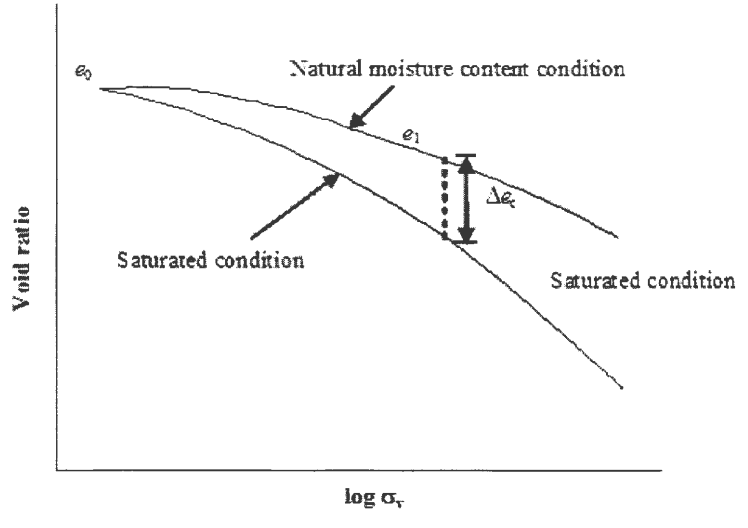

Figure 8 - Double oedometer collapse test (after Jennings and Knight, 1957).

There may be significant differences in the values of collapse potential obtained from the single and the double oedometer tests depending on the texture and other properties (such as intrinsic inhomogeneities when trimming small specimens and sample size) of the soils being tested. A double oedometer test which measures the difference in compression between unsaturated and fully saturated soil samples, assumes that the mechanism producing collapse also produces this difference in deformation behavior. However, this assumption may not be true. Due to this reason and due to the difficulty in preparing specimens having similar initial placement conditions, it is always preferred to use single oedometer collapse test (Lutenegger and Saber, 1988).

MEASUREMENT OF COLLAPSE POTENTIAL

Precise measurement of the amount of collapse is extremely important in the identification of a collapsible soil so that a suitable foundation may be designed and post-construction collapse may be avoided. Identification of collapsible soils can be done through (*a*) indirect correlations between collapse potential and index properties, (*b*) direct measurement of collapse potential in the laboratory, and (*c*) field measurement of collapse potential.

Indirect correlations

Qualitative and semi-qualitative correlations between collapse potential and various index properties have been developed. Mostly the criteria used in these correlations are dry unit weight or consistency limits, or combinations thereof. Table 4 summarizes the criteria that can be used for the identification of collapsible soils (Saber, 1987). One of the

commonly used correlations to distinguish collapsible soils from non-collapsible soils based on dry unit weight and liquid limit is shown in Figure 9.

Table 4 - Summary of criteria reported by different authors for the identification of collapsible soils (after Lutenegger and Saber, 1988; Das, 1995).

Criteria used for characterization of collapsible soils	Reference
Coefficient of subsidence, $K = e_L/e_0$	Denisov (1951)
K = 0.5 – 0.75: highly collapsing soils	
K = 1.0: non-collapsible loams	
K = 1.5 – 2.0: non-collapsible soils	
$K_D = (w_0 - w_P)/I_P$	Priklonski (1952)
K_D < 0: highly collapsible soils	
K_D > 0.5: non collapsible soils	
K_D > 1.0: swelling soils	
If dry density less than 1.26 g/cm^3, settlement will be large;	Clevenger (1958)
Dry density greater than 1.44 g/cm^3, settlement will be small	
Collapse ratio, $R = w_S/w_L$	Gibbs (1961)
This was also shown graphically	
$L = (e_0 - e_L)/(1+e_0)$ for S_0 < 60%, if L > -0.1, it is a collapsing soil	Soviet Building Code (1962)
$K_L = (w_0/S_0) - (w_P/I_P)$ for S_0 < 100%, if K_L > 0.85, it is a subsident soil	Feda (1964)
If initial porosity, n_0 > 40%, the soil is susceptible to collapse	Feda (1966)
A dispersion test where 2 g of soil sample is poured into 12 ml of distilled water and the time taken by the soil for dispersion is noted; dispersion times of 20-30 s were obtained for collapsing Arizona soils	Benites (1968)
Collapse ratio R where	Anderson (1968)
$R = 5.5 - 3.82 \log (w_L/w_P) - 1.63 \log w_P - 1.24 \log C_u - 0.918 \log P_{10} - 0.303 P_{200} + 0.465 \log (D_{60}/D_{40}) - 0.45 \log(D_{99}/D_{50})$	
Iowa loess with clay (< 0.002 mm) contents	Handy (1973)
< 16% : high probability of collapse	
16 to 24% : probably collapsible	
24 to 32% : less than 50% probability	
> 32% :usually safe form collapse	

Definitions of symbols used in Table 4:

e_L = void ratio at liquid limit.

e_0 = natural void ratio.

w_0 = natural water content.

w_S= saturation water content.

w_L = liquid limit.

w_P = plastic limit.

I_P = plasticity index.

S_0 = natural degree of saturation.

P_{200} = fraction passing No. 200 (75-μm) sieve.

P_{10} = fraction passing No. 10 (2.00-mm) sieve.

C_u = uniformity coefficient.

D_P = diameter of grain corresponding to percentage P on the grain size curve.

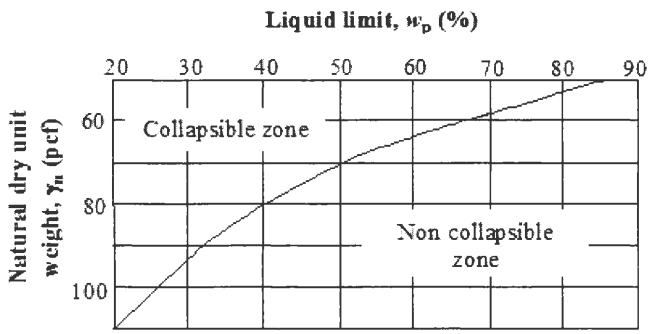

Figure 9 - Commonly used criterion for determination of collapsibility (after Lutenegger and Saber, 1988).

These correlations are certainly helpful in identifying collapsible soils. But, the disadvantage with these correlations with index properties is that there is a considerable

scatter, and the quality of collapse potential prediction is not good enough to be used for subsequent settlement analysis (Houston *et al.* 2001). Hence, the most effective way of identifying collapsible soils is to perform actual collapse tests either in laboratory or *in situ* for the direct measurement of collapse potential.

Direct measurement of collapse potential

Different testing techniques have been devised for the measurement of amount of collapse. Among these techniques there are both laboratory experimental techniques and *in situ* testing techniques. Results from laboratory and *in situ* tests can be used for the direct measurement of collapse potential.

Laboratory experimental techniques

The most commonly performed laboratory test for the measurement of collapse potential is the conventional one-dimensional oedometer test. In a one-dimensional single oedometer collapse measurement test, the specimen is placed in the oedometer ring at the *in situ* moisture content and subjected to compression under different applied stresses, and the respective compression of the specimen is noted. The specimen is inundated under the anticipated *in situ* stress and the collapse settlement observed. The amount of collapse potential given by Equation (1) is obtained from e-log σ_v curve of the test specimen. Unloading of the specimen is done to study the rebound and swelling index.

Table 5 shows the characterization of collapse potential indicating the degree of severity of collapse based on the amount of collapse potential (%) determined at a flooding stress of 200 kPa as given by Jennings and Knight (1975).

Table 5 - Degree of severity of collapse at a flooding stress of 200 kPa (after Jennings and Knight, 1975).

Collapse potential (%)	Degree of severity
0-1	No problem
1-5	Moderate trouble
5-10	Trouble
10-20	Severe trouble
Above 20	Very severe trouble

The effect of specimen size on collapse potential values was studied by Lutenegger and Saber (1988). Air-dried specimens of 50.8, 63.5, 76.2 and 101.6 mm diameter were used and tested at a stress of 300 kPa. A constant height to diameter ratio of 0.25 was used. A poor agreement between the collapse potential values measured from different sizes of specimen was found. This type of behavior of specimens could be partially attributed to the random nature of soil fabric. It was reported that the larger the samples of soil, the more representative will the soil structure be as compared to smaller size samples. Therefore, smaller size samples may give more random results.

Kezdi (1974) demonstrated the influence of stress level on collapse potential by reporting that the collapse potential of loess in the Danube Valley of Hungary increased linearly on increasing stresses up to a stress level of about 400 kPa and thereafter remained constant. A similar observation was made by Lutenegger and Saber (1988) on performing single and double oedometer tests on three different air-dried soils at stress levels ranging from 100 to 600 kPa in increments of 100 kPa. This suggests that in such cases collapse potential can be expressed in terms of percent deformation per unit stress up to a limiting value of stress after which collapse potential remains almost constant. The value of limiting stress for any collapsible soil is related to maximum packing arrangement of soil particles. It

is not necessary that this behavior to be observed in all collapsing soils and it may be possible that in some soils the value of collapse potential at high stresses is quite low. This happens particularly if the yielding of soil or crushing of particles has already occurred during loading of specimen in an oedometer ring (Feda, 1966).

It was found that compacted soils are susceptible to compression upon wetting (Houston *et al.* 2001). The response of compacted soils to inundation depends on the type of the soil, compactive effort, compaction water content and stress level at the time of inundation (Houston and Houston, 1997). Identification of collapsible soils is achieved by testing soil specimens compacted at different water contents and dry densities over a range of stress levels anticipated *in situ*. Appropriate compaction specifications and construction controls leading to minimization of collapse can be achieved by identifying the conditions leading to collapse of a soil in the laboratory (Houston *et al.* 2001).

The laboratory test data on collapse of soil on inundation, which corresponds to complete saturation, can be used in estimating the *in situ* collapse settlement of a soil deposit expected on full wetting corresponding to a high degree of saturation. Figure 10 shows a wetted stress-strain curve of a collapsible soil. Curve AB represents the dry compression curve. Curves AC, AD and AE depict higher amounts of collapse. Curve H'FG represents the wetted curve falling within the band representing a large amount of values of collapse compression on complete wetting. The total collapse settlement is computed by integrating the strain profile over the extent of the zone of wetting. The path D'H' in the figure represents the wetting at a lower stress for a laboratory test specimen.

The compression curve for medium to large scale footings on dry collapsible soils is flat and similar to the curve AB. The curve AD represents collapse due to sample

disturbance, which would have occurred due to wetting. Hence, irrespective of whether the sample is disturbed or not, it falls within the shaded band. Therefore, the collapse strain on flooding of a sample at a particular stress is the full strain from the origin to the wetted curve.

The collapse settlements predicted from the collapse potential obtained in the laboratory of a specimen completely inundated may not be realized in the field. The reason for this is that complete saturation of the entire soil layer *in situ* is not possible. The variation of collapse potential with the amount of initial suction or initial degree of saturation can be obtained in the laboratory by conducting the one-dimensional consolidation collapse test over a range of degrees of saturation. These results are mainly useful for forensic studies and for the assessment of mitigation alternatives such as prewetting prior to construction and controlled wetting after construction in case of differential settlement of foundations (Houston *et al.* 2001).

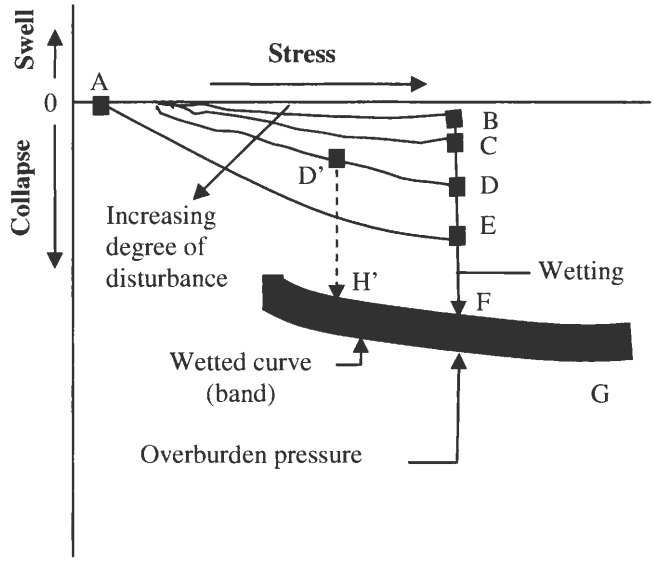

Figure 10 - Wetted stress-strain curve for a collapsible soil (after Houston *et al.* 2001).

1. Suction monitored oedometer collapse test:

Tadepalli *et al.* (1992) suggested a simple experimental procedure for the measurement of changes in matric suction and soil volume during inundation of collapsible soils. The experimental measurements provide data which can be used for verifying the applicability of unsaturated soil mechanics to the behavior of collapsible soils. This is done by relating changes in the stress-state variable to total volume change during inundation. It was found that the matric suction was the only stress-state variable which changed during inundation (Tadepalli and Fredlund, 1991). Matric suction was measured with the help of tensiometer prior to and during inundation. The ceramic cup of the tensiometer is inserted into the soil specimen. Equilibrium with suction pressures is established as water in the tensiometer tube flows in or out through the ceramic cup. The flow of water stops when equilibrium is reached. Hence, water in the tensiometer tube will be under tension which is recorded by a vacuum gauge. The vacuum gauge reading at equilibrium is equivalent to the soil matric suction.

2. Computer-controlled isotropic compression test:

Isotropic compression of collapsible soil in computer-controlled modified triaxial cell is one of the laboratory techniques adopted for measuring different salient quantities such as volume change, degree of saturation and suction (Habibagahi and Mokhberi, 1998). The standard triaxial cell needed to be modified in order to deal with volume change behavior of unsaturated soil specimens. Figure 11 shows the modified triaxial cell used by Habibagahi and Mokhberi (1998). The special pedestal shown in the figure had a high air entry ceramic disk sealed in it with the help of which suction was measured during the test. An annular high

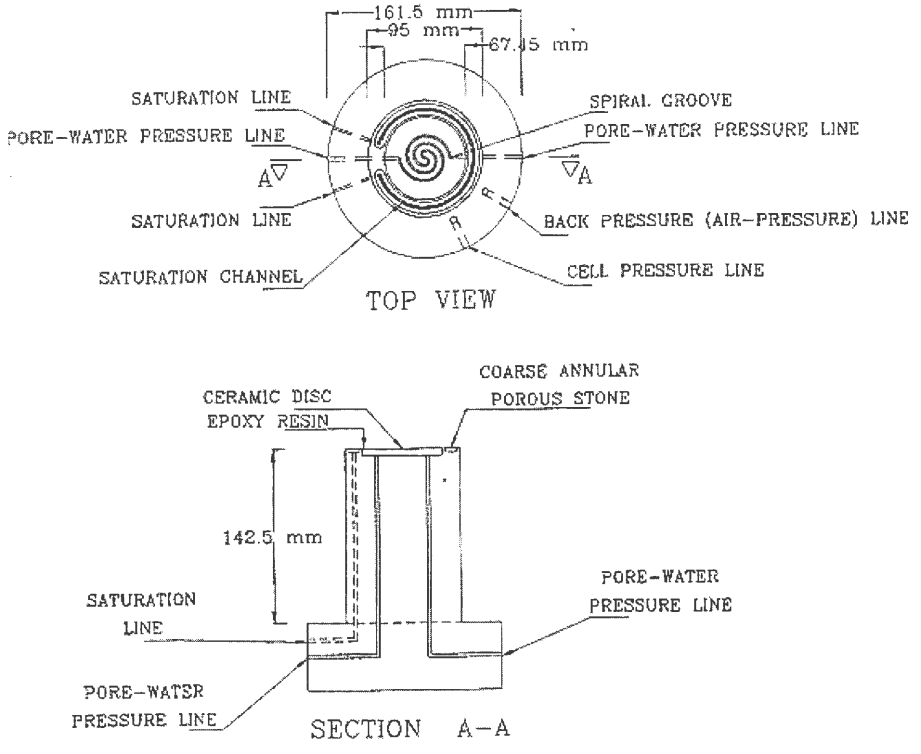

Figure 11 - Modified pedestal in triaxial cell for the measurement of changes in volume of unsaturated soil sample (after Habibagahi and Mokhberi, 1998).

permeability porous stone was used for saturating the specimen, while de-airing was done connecting two lines to the porous stone and the ceramic disk (Mokhberi, 1995). Soil specimens were prepared by compacting moist soil at pre-determined water content in a standard proctor compaction mold. The number of blows per layer of soil was chosen from pilot tests, so that the specimens had identical dry densities. The specimen was mounted on the pedestal and subjected to a cell pressure of 10 kPa until suction measured through the ceramic disk stabilized. Volume change of the soil specimen was measured by monitoring the amount of water entering the cell and noting the volume change of the system, which was measured through a calibration test at the beginning. The specimen was loaded isotropically at constant water content. The sample was saturated at different applied stress and the

amount of collapse was measured. Soil suction was measured through out the test via the ceramic disk. Saturating the soil specimens using high permeability annular porous stone reduced the suction to negligible amounts.

Field testing

Field testing is useful for identifying and characterizing collapsible soil deposits. The most important field tests for the measurement of collapse potential are plate load test, conventional field collapse test, suction monitored pressuremeter test and down-hole *in situ* collapse test.

1. Plate load test:

The plate load test (Figure 12) is conducted on the soil surface in shallow trenches (Houston *et al.* 1995 a). The soil is wetted to a considerable depth, and displacements are measured corresponding to the applied loads. In this test no stress-strain relationship is obtained but the test results can be used for the extrapolation to some prototype using modeling equation. The available modeling equations are for non-collapsible soils which may under-predict the settlement. Therefore, the plate load tests can not be used directly to measure foundation settlements. However, the wetting induced conventional plate load tests on collapsible soils are useful for their identification and for determining the degree of collapsibility.

2. Down-hole collapse test:

Down-hole collapse test is an in-situ plate load test which is conducted inside a hollow stem auger, allowing collapse testing at significant depths. These tests are particularly useful for cohesionless and gravelly soils as the extraction of samples is difficult in these soils. In the *in situ* collapse tests conducted in a borehole, load is applied to a loading plate at

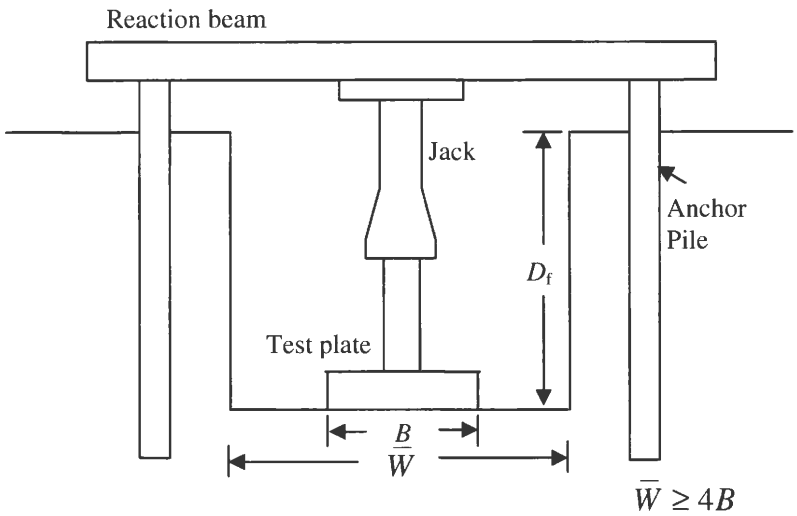

Figure 12 - Plate load test set up (after Das, 2002).

the base of the borehole. Wetting is allowed by inundation, and the load displacement response of the soil monitored. The load-displacement data are converted to stress-strain data for determining collapse potential. It has been found that the degree of wetting that occurs during the *in situ* collapse test is quite consistent with the degree of wetting observed from other field ponding tests (Houston *et al.* 1995 b). A schematic figure of down-hole collapse test is shown in Figure 13.

3. Suction monitored pressuremeter tests:

Suction monitored pressuremeter test results can also serve as a basis for identifying the collapse potential of unsaturated soils. The changes in soil properties induced by changes in suction are accounted for. A new method was proposed (Schnaid *et al.* 2004) in order to predict collapse of metastable structure material using pressuremeter test results. In this test method a borehole is drilled using prebored technique. The pressuremeter is lowered to the test level and the membrane is inflated. It is recommended that at least two tensiometers be

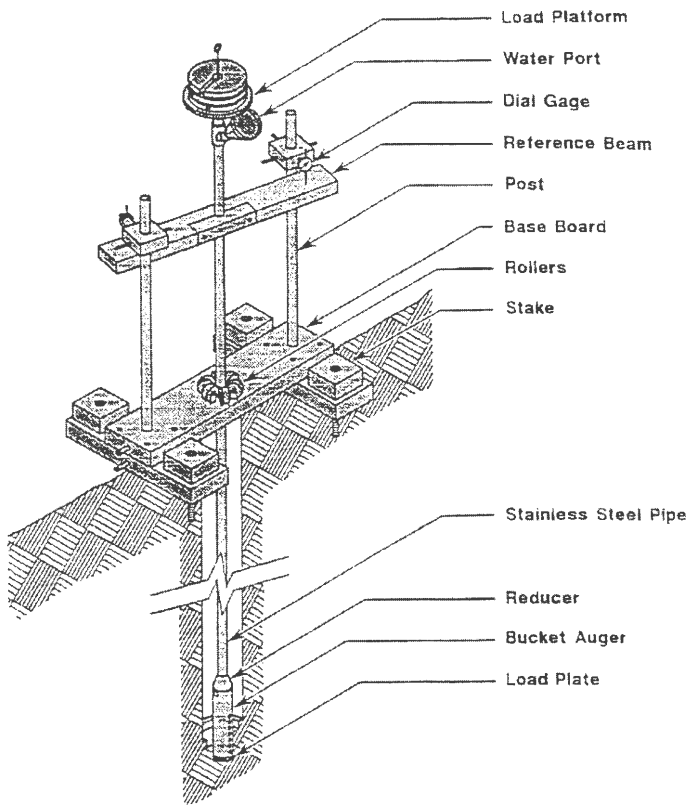

Figure 13 - Elevation of down-hole collapse test system (after Houston *et al.* 1995 b).

installed at the radial distances of 5*D* and 10*D* from the center of the probe, where *D* is the diameter of the pressuremeter probe. During expansion of the membrane the tensiometers monitor suction which remains constant. Wetting is done by filling the pressuremeter borehole with water up to the surface. During the process of wetting suction is constantly monitored through the tensiometers. Radial displacements increased at constant radial pressure during the process of wetting resulting in reduced suction. This gives a direct assessment of the collapse potential of the soils. Figure 14 shows the typical variation of cavity pressure with the radial strain (r/r_0), indicating collapse on inundation.

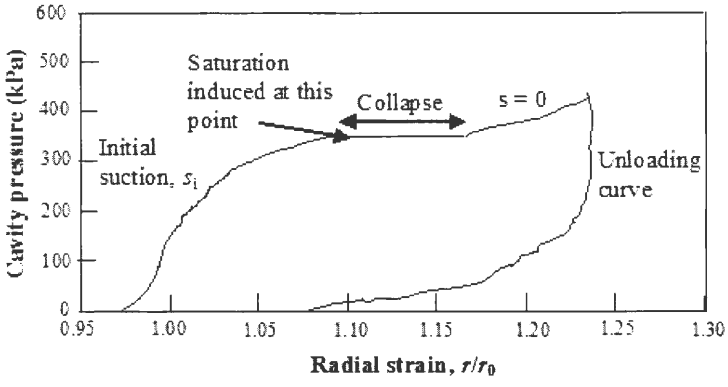

Figure 14 - Typical pressuremeter collapse test (after Schnaid *et al.* 2004).

MITIGATION ALTERNATIVES AND SITE IMPROVEMENT

Mitigation methods or techniques can be broadly defined as the design methods or measures which lessen or work out the collapse problems. Soil improvement can be taken as a subset of mitigation methods as they are used not only for collapsible soils but for other types of problematic soils also. There are many mitigation methods available for collapsible soil problems. But their applicability depends on various factors such as (a) the identification of collapse problem whether pre-construction (during investigation), during construction, or post construction, (b) the driving force for triggering collapse – overburden or structural load, (c) depth of collapsible soil deposits creating problem, (d) the possible source(s) of wetting, and (e) treatment cost including the cost of risk/liability (particularly in USA) (Houston *et al.* 2001). The mitigation alternatives for the collapsible soils are as follows (Rollins and Rogers, 1994, and Houston *et al.* 2002):

- Removal of collapsible soil
- Removal and replacement or compaction
- Dynamic compaction (under dry and wet conditions)

- Pile or pier foundations
- Prewetting (with water or sodium silicate solution)
- Differential settlement resistant foundation and structural design
- Prevention of wetting
- Controlled wetting
- Chemical stabilization
- Underpinning

Pre-construction mitigation

When the collapsible soil problem is discovered prior to construction then removal and/or re-compaction is commonly chosen as an effective remediation method. These methods are cost-efficient for collapsible soil deposits which are shallow to moderately shallow. A test program should be conducted in which samples are prepared at different values of densities and water content and a range in confining pressures and then subjected to wetting. The results from these tests can be used for selecting compaction specifications for the site (Houston *et al.* 2001). Rollins *et al.* (1998) suggested that the soil should be wetted to optimum moisture content to increase the compaction efficiency. However, for thicker and deeper fills more than one set of compaction specification are needed, with higher minimum density being used for the deeper zones (Houston at al. 2001).

Deep dynamic compaction is also recognized as an effective technique for the soil improvement. The term "deep" is used to show the effectiveness of method over roller compaction. However, the effect of dynamic compaction can be seen only up to about five meters, with the maximum improvement up to three meters (Rollins and Rogers, 1994). The

effect of dynamic compaction can be increased by dropping sufficiently large weights from great heights (Pengelly *et al.* 1997).

Grouting is also used as a soil improvement technique. Grouting improves the soil by one of the three mechanisms. These mechanisms are permeation, compaction and soil reinforcement. If grouting is done in a proper manner then the grouted zones tend to carry overburden and structural loads and thereby giving relief to the remaining loose and moisture sensitive zones between the grout bulbs (Houston *et al.* 2001). The main advantage of grouting is that it can be done even after the construction of structure. The primary disadvantage of grouting is its high initial cost over other alternatives.

The use of piles, piers, stone columns, or soil columns reduces the collapse problem effectively provided that the load is transferred below the collapsible soil layer or beyond depth of wetting. However, the cost of this alternative is much more than other alternatives for mitigation (Houston *et al.* 2001).

Prewetting is commonly used on the sites where the collapse problem is identified prior to construction. It is found to be an effective method if significant care is taken in achieving adequate degree and extent of wetting (Houston *et al.* 2002). For the shallow layers prewetting is employed with a combination of other techniques such as deep dynamic compaction or removal and recompaction to drive the collapse. Prewetting is found to be a moderately low cost alternative (Houston *et al.* 2001). Prewetting with 2% sodium silicate solution reduces the collapsibility and strengthens the soil deposits (Sokolovski and Semkin, 1984). The prewetting of soil with 2% sodium silicate not only decreases the collapsibility but it also reduces further infiltration of water into the soil (Rollins and Rogers, 1994).

Though the method is relatively expensive, it can be performed without any special equipment.

It is a good practice to design differential settlement resistant foundation and to take measures for the minimization of wetting of collapsible soil layers in addition to the mitigation techniques employed prior to construction (Houston *et al.* 2001).

Post-construction mitigation

The problem of differential settlement is most common if the severity of collapse problem is discovered after the construction of structure. The various treatment techniques employed depending on the severity of the problem are as follows: (1) controlled wetting, (2) chemical stabilization which includes grouting, and (3) underpinning. All of the three methods involve some risk and therefore, considerable care should be taken in each case. (Houston *et al.* 2001).

In controlled wetting water is introduced in a very careful manner so as to correct the tilt (Bally and Oltulesen, 1980). Controlled wetting is not used widely due to risk in its application. However, the available data from previous research shows that the cost of implementing this method is quite low (Houston *et al.* 2001). Underpinning has been in use from centuries, but it is a costly method which is comparable to grouting.

CHAPTER 3

TEST PROGRAM - DESIGN OF EXPERIMENTS, EQUIPMENT AND TESTING PROCEDURE

AIM OF THE TEST PROGRAM

Laboratory experimental program was conducted in two phases on a collapsible loess soil obtained from Turin, Western Iowa (Figure 15). The experimental program was a parametrical study aimed at studying the effect of important placement conditions of soil such as initial water content, initial dry unit weight and flooding stress (namely, the vertical compressive stress at which the soil is inundated with water) on collapse potential and other important volume change characteristics (e.g. compression index and swelling index) and shear strength characteristics of loess. These placement conditions were chosen because of their role in the collapse of a soil. The investigation comprised of:

(i) measurement of collapse potential of soil under various flooding stresses and placement conditions using single oedometer collapse test,

(ii) determination of partial saturation collapse potential of soil as a function of degree of saturation under flooding stress at various placement conditions using single oedometer collapse test,

(iii) measurement of swelling index by gradual unloading of the specimen after the application of maximum vertical compressive stress,

(iv) measurement of penetration resistance by performing Proctor needle penetration test in the soil statically compacted in Proctor's mold at different placement conditions,

(v) determination of shear strength characteristics by performing Torvane shear tests at different placement conditions,

(vi) obtaining soil water characteristic curves (SWCC) at various placement conditions by using pressure plate extractor, and

(vii) analysis of test results based on various significant parameters.

GENERAL DESCRIPTION OF THE SOIL

The loess soil used in the test program was obtained from a vertical cliff near Turin in Monona county of Western Iowa (Figure 16). This loess cliff is located along the north of Larpenteur Memorial road in Turin. The soil is a non-plastic, light-brown silty soil. It was slightly moist, and had a natural water content of 9%. It lost moisture quickly on being exposed to atmosphere.

GEOLOGICAL DESCRIPTION OF THE SITE

The loess deposits of western Iowa are wind-deposited material. These loess deposits were referred to as siliceous marl, or the Bluff Deposit in the early literature. Figure 17 shows the chief loess deposits of Iowa. Irregular-shaped nodules of calcium carbonate occur in some of Iowa's loess exposures that are formed by the irregular deposition of calcium carbonate by infiltrating water. Occasionally, tube-shaped bodies of iron-bearing minerals (once deposited by groundwater) are concentrated in loess, where plant roots were once present (Anderson, 1998).

Figure 15 - Loess hills in Turin, Iowa.

Figure 16 - Taking loess samples from loess hills in Turin, Iowa.

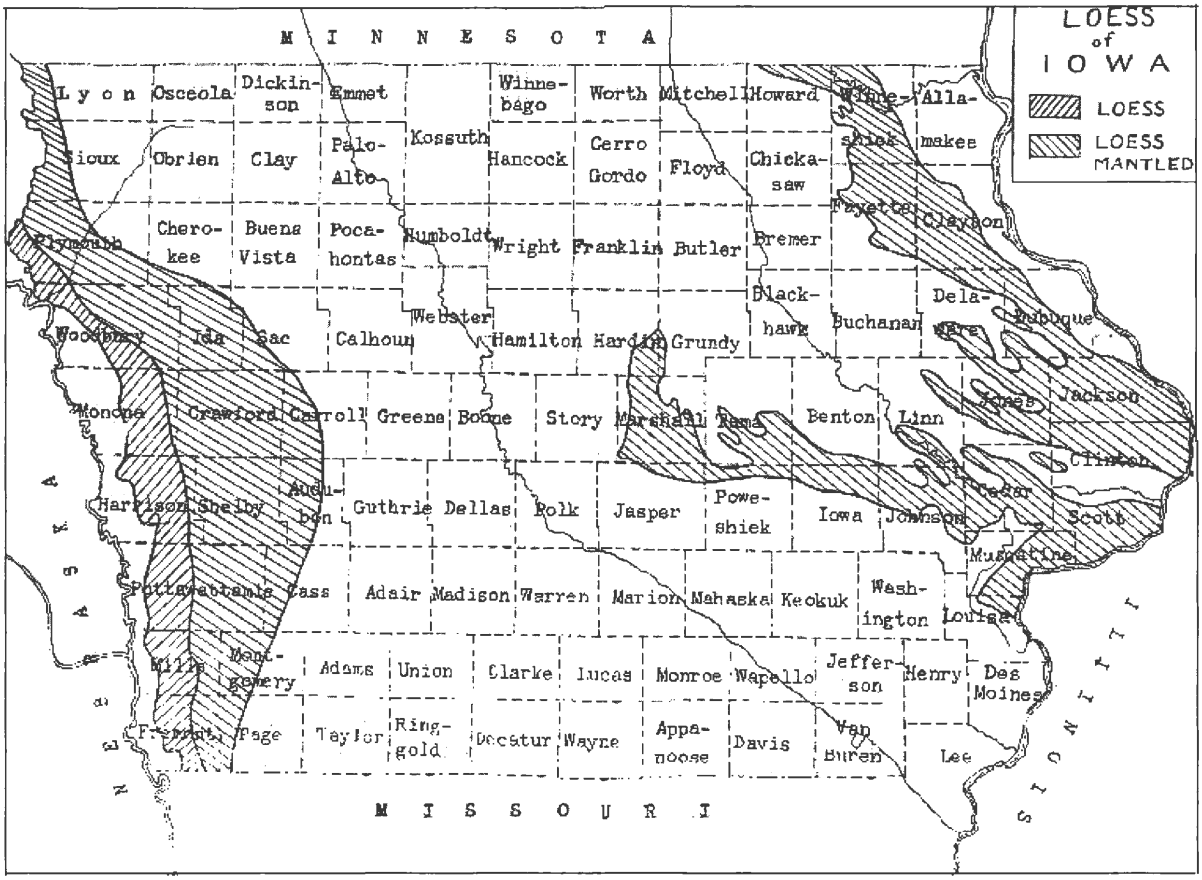

Figure 17 - Chief loess deposits of Iowa (after Kay and Apfel, 1944).

BASIC TESTS PERFORMED ON THE SOIL

The tests performed on the soil for the determination of the basic index properties are shown in Table 6. The ASTM standard for each test is indicated against the test. The procedural details of important tests are described in the subsequent sections.

Table 6 - Tests performed and ASTM designations.

Property	Standard ASTM designation
Specific gravity, G_s	ASTM D854 – 02
Natural water content, w_n(%)	ASTM D4318 – 00
Liquid limit (%)	ASTM D4318 – 00
Plastic limit (%)	ASTM D4318 – 00
Plasticity index (%)	ASTM D4318 – 00
Gravel (%) (> 6.20 – 4.75 mm)	ASTM 98 D422 – 63
Sand (%) (4.75 – 0.075 mm)	ASTM 98 D422 – 63
Silt (%) (0.075 – 0.002 mm)	ASTM 98 D422 – 63
Clay (%) (< 0.002 mm)	ASTM 98 D422 – 63
Standard Proctor Compaction test	ASTM D 5890 – 02
Modified Proctor Compaction test	ASTM D698a – 00

VARIABLES STUDIED

Volume change characteristics

The effect of the following variables on volume change characteristics such as collapse potential, partial saturation collapse potential, compression index and swelling index was studied.

- *Static compaction stress (kN/m^2)*: All the test specimens were statically compacted. The static compaction stress, denoted as *SCS* was varied as 100, 200 and 300 kN/m^2.
- *Initial water content, w_i (%)*: The tests were performed at different initial water contents of 6%, 10% and 14%. A minimum water content of 6% was chosen for convenient compaction and also for obtaining a measurable collapse potential.
- *Initial dry unit weight, γ_d (kN/m^3)*: The dry unit weight of the specimen was also changed with changing static compaction stress used for the preparation of the test specimen. The

dry unit weights for different static compaction stresses (*SCS*) of 100, 200 and 300 kPa at 6%, 10% and 14%, are given in Appendix A, respectively.

- *Flooding stress, σ_{fl} (kN/m^2)*: The vertical compressive stress, at which flooding was allowed into the one-dimensional consolidation test specimen prepared at 6% moisture content was varied as given in Table 7. However, a flooding stress value of only 100 kPa was chosen for samples prepared at 10% and 14% water content.
- *Degree of saturation, S_r (%)*: The initial void ratio of the test specimens changed on changing the static compaction stress (*SCS*) as 100, 200 and 300 kPa respectively. Hence, the initial degree of saturation also changed though the initial water content was kept constant. The values of the initial degrees of saturation for the varying *SCS* of 100, 200 and 300 kPa at 6%, 10% and 14% water contents are given in Appendix A, respectively.

Shear strength characteristics

The effect of the following variables on shear strength characteristics such as Proctor needle penetration resistance and unconfined compressive strength as obtained from Torvane shear test was studied:

- *Initial water content, w_i (%)*: The tests were performed at water contents of 6%, 10% and 14% as in the case of tests performed for the study of volume change characteristics.
- *Initial dry unit weight, γ_d (kN/m^3)*: The tests were performed on samples prepared at the same initial dry unit weights corresponding to initial moisture contents of 6%, 10% and 14% and static compaction stress of 100, 200 and 300 kPa as used for the study of volume change characteristics, respectively as shown in Appendix A.

- *Degree of saturation, S_r (%)*: The values of the initial degrees of saturation at which the samples were prepared for shear testing are the same as for volume change characteristics (see Appendix A).

Table 7 shows the independent variables used in the study of volume change and shear strength characteristics. The dependent variables such as dry unit weight and degree of saturation are provided separately in Appendix A.

Table 7 – Independent variables used in the study of volume change and shear strength characteristics.

w_i (%)	*SCS* (kPa)	σ_{fl} (kPa)
6	100	6, 12, 25, 50,100, 200, 400
6	200	50,100, 200, 400, 800
6	300	50,100, 200, 400
10	100	100
10	200	100
10	300	100
14	100	100
14	200	100
14	300	100

TESTING APPARATUS

One-dimensional consolidation apparatus

Consolidation is an important fundamental phenomenon which must be understood to gain knowledge of soil behavior in engineering applications. The test is described in many textbooks (e.g. Holtz and Kovacs, 1981; Das, 2002). Standard procedure for the test is described in ASTM D2435.

Figure 18 shows an idealized sectional view of the fixed-ring type consolidometer cell used in the test program. Three main parts can be identified in the Figure 18.

- A brass ring to hold sample laterally thus allowing strains to be considered as one-dimensional. As a result, sample volume changes can be easily calculated from any changes in the height of the sample.
- Two porous stones, made from sintered brass, are placed each at the top and bottom of the specimen. With the sample ring being impermeable, one-dimensional drainage conditions can be assumed. The double drainage condition allows the completion of consolidation of sample typically in 24 hours under any load increment.
- The base of the oedometer acts as a water container to immerse the sample and the porous stones completely when full saturation is desired.

Loads were applied to the sample by means of a rigid loading mechanism as shown in Figure 19. A high lever arm ratio of 10:1 was used in the test program allowing a maximum loading pressure of 4680 kPa on 63 mm diameter samples. The apparatus also allows making changes in the lever arm ratios to 9:1 and 11:1 in addition to 10:1 ratio, thereby minimizing loading weight requirements. The unit incorporates an integral beam support jack that eliminates the possibility of shock to the sample during load application procedures. The accurate displacement readings were recorded by an automated data logging system using linear variable displacement transducers (LVDT's) of 0 to 10 mm range. Figure 20 shows a consolidometer cell attached to an LVDT.

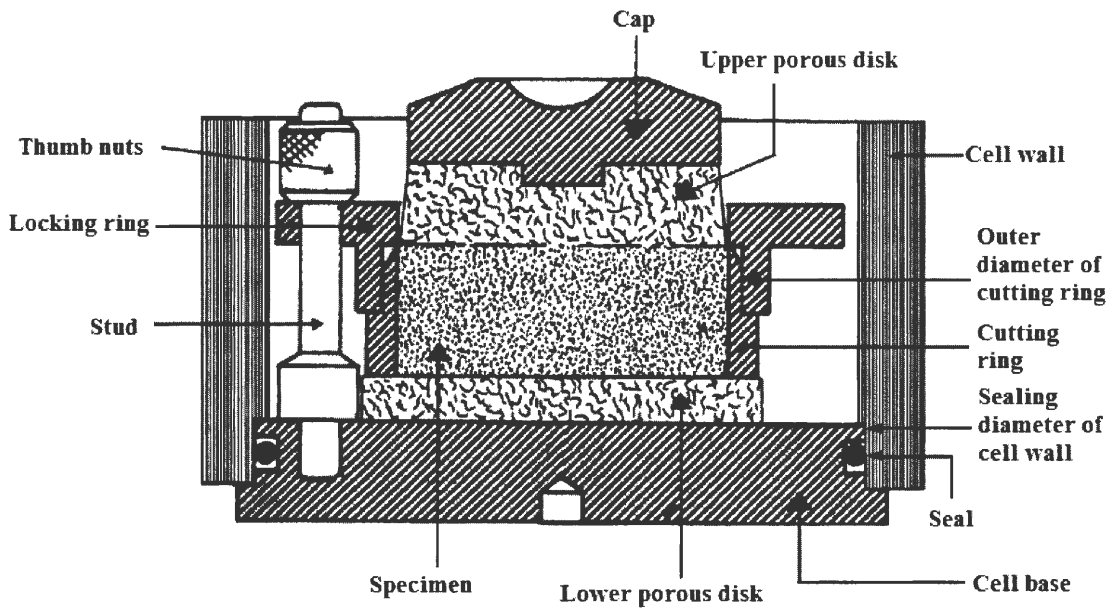

Figure 18 - Sectional view of the consolidometer cell used in the test program (from ELE International).

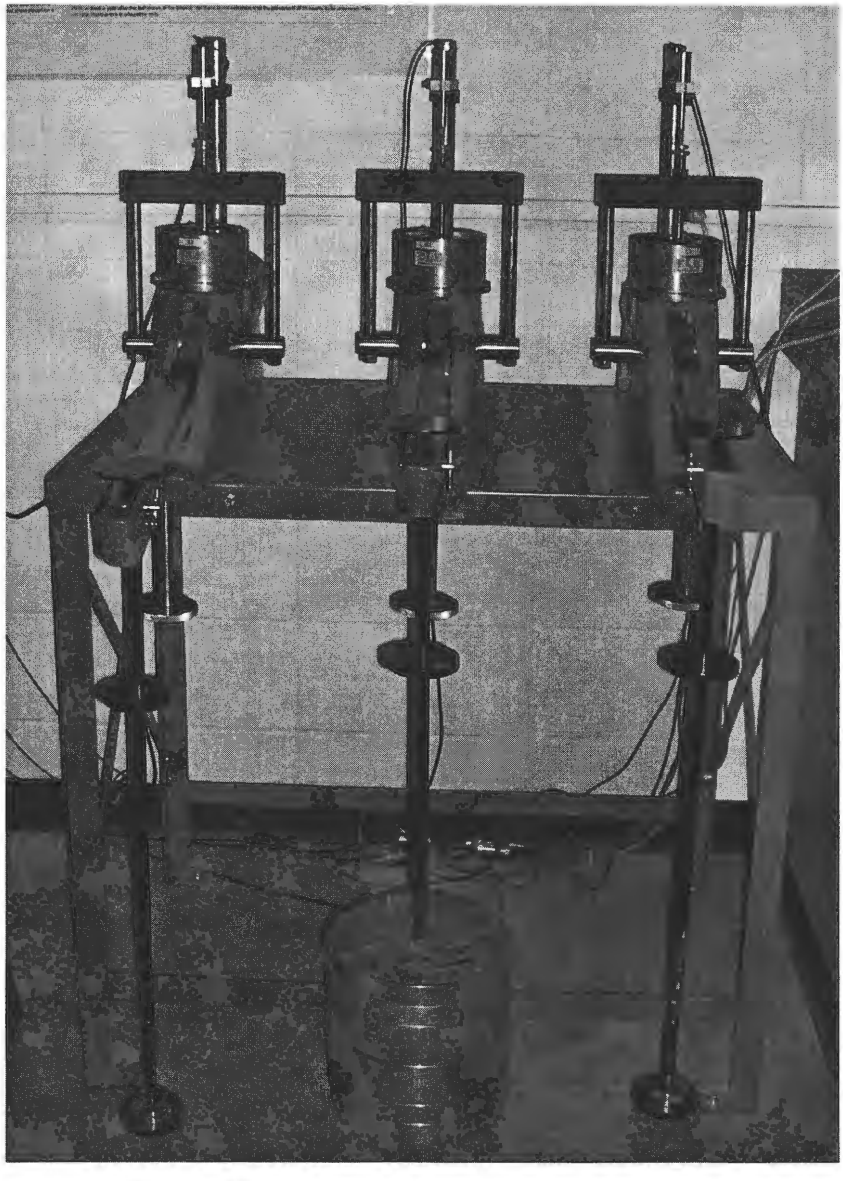

Figure 19 - Table top consolidation apparatus.

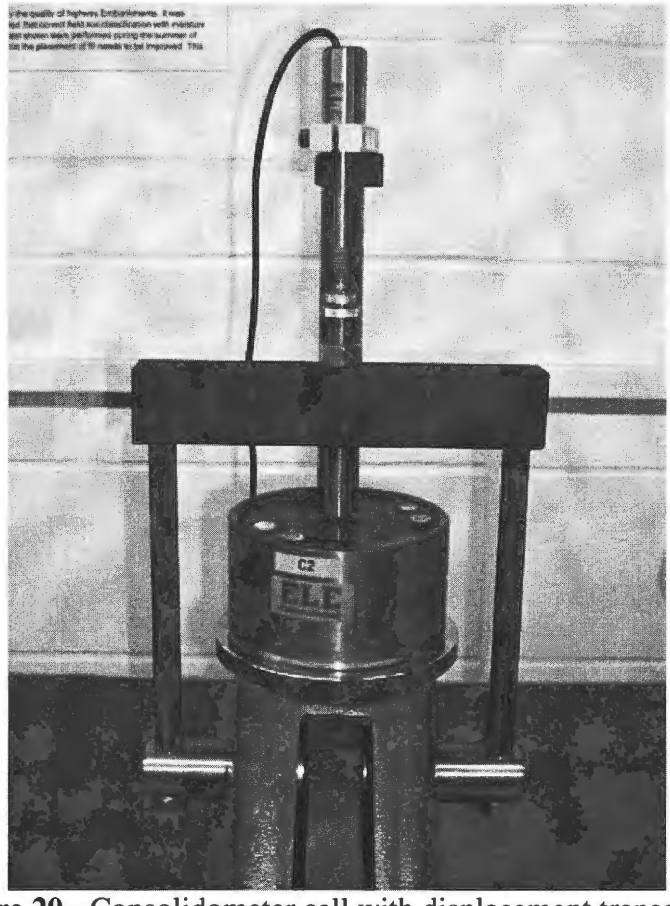

Figure 20 - Consolidometer cell with displacement transducer.

Proctor penetrometer

The Proctor penetrometer is generally used to establish a relation between moisture content, dry unit weight and penetration resistance of fine-grained soils as determined by penetration testing. The testing information is given in ASTM D-1558.

Figure 21 shows the schematic line diagram of the unit used in the test program. The unit is provided with a special calibrated spring dynamometer and a pressure-indicating scale on the stem of the handle. The maximum read out on the pressure scale is 130 lbs. A major division is located at each 10 lb. interval each divided into 10 subdivisions. Readings at the

lower side of the sliding ring on the stem indicates the maximum load obtained during the test. The set includes the penetrometer and nine needles having end areas of 1, 3/4, 1/2, 1/3, 1/5, 1/10, 1/20, 1/30 and 1/40 square inch (6.45, 4.84, 3.22, 2.15, 1.29, 0.65, 0.32, 0.21, and 0.16 cm^2). For the test program penetration needle with an end area of 1.29 cm^2 was used. Figure 22 shows the Proctor penetrometer set which includes penetrometer, nine needles and carrying case.

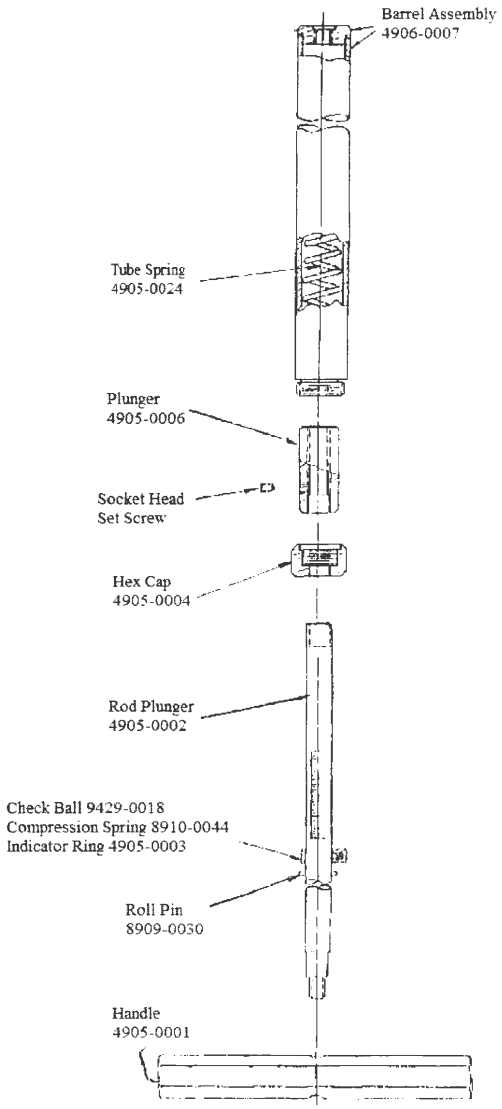

Figure 21 - Line diagram of penetrometer stem (from ELE International).

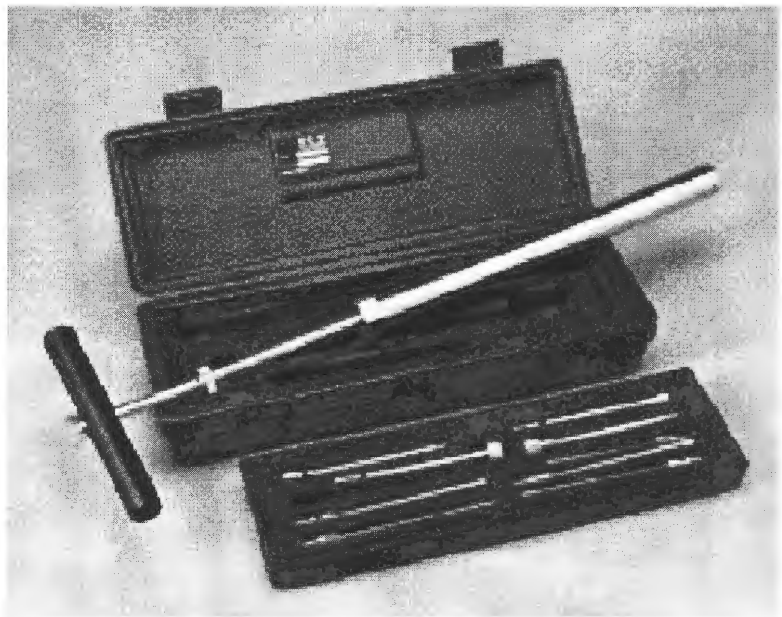

Figure 22 - Proctor penetrometer set.

Torvane shear device

A Torvane (see Figure 23) is a hand-held device for the direct measurement of shear strength of cohesive soils in tons per square foot. They are manufactured by SOILTEST, INC. (2205 Lee St., Evanston, Illinois, 60202). The calibration curve provided with the instrument compares Torvane results with values derived from unconfined and triaxial compression tests. Three interchangeable vane adapters are available which provide different ranges of operation. The curve applies only to the middle range Torvane which was used in the test program. The range of the middle range adapter is 0-1.0 tons per square foot. Since the dial on the device does not change, the Torvane shear strength must be obtained by multiplying the dial reading and the maximum capacity of the adapter.

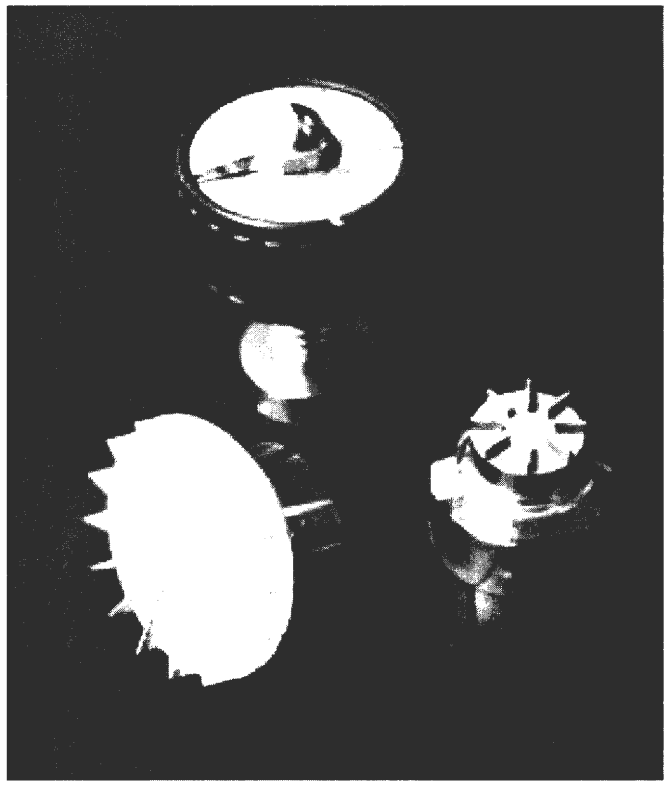

Figure 23 - Torvane shear tester (from SOILTEST, INC).

Pressure plate extractor

A pressure plate extractor is equipment used in the determination of desorption (drying) portion of a soil water characteristic curve (SWCC). The soil-water characteristic curve (SWCC) of a soil relates the volumetric water content and suction. The test procedure used is based on Method C of ASTM D6836-02. The pressure plate extractor used in this study is model A-140 15-Bar Ceramic Plate Extractor manufactured by Soilmoisture Equipment Corporation (Goleta, CA). The 15-bar porous ceramic plate extractor can be used for full-range soil moisture work. However, for the present work a 5-bar ceramic plate cell was used. This selection was based on the estimates of air-entry value of the soil used in the investigation. The model A-140 15-Bar Ceramic Plate Extractor accommodates up to 12

samples per plate. Samples are prepared in the brass rings provided by the manufacturer. Each ring is of 50 mm diameter and 10 mm height. Four valves are used in setting up the pressure plate extractor for a test as shown in Figure 24:

A. Valve between the pressure gauge and extractor vessel.

B. High pressure regulator 861– 1551 kPa (125 -225 psi).

C. Low pressure regulator 0-861 kPa (0-125 psi).

D. Valve between the air compressor and manifold (not shown in Figure 24).

A high air entry disk which is housed in the pressure plate extractor (shown with a sample placed on it in Figure 25) consists of small pores of relatively uniform size. The disk acts as a semi-permeable membrane between the air and water phases. Once the disk is saturated with water, air cannot pass through the disk due to the ability of the contractile skin to resist the flow of air. The ability of the ceramic disk to withstand the pore air pressure results from the surface tension developed by the contractile skin. The contractile skin acts like a thick membrane joining the small pores on the surface of the ceramic disk. The difference between the air pressure above the contractile skin and the water pressure below the contractile skin is defined as matric suction. The maximum matric suction that can be maintained across the surface of the disk is called its air entry value. The smaller the size of pores the larger will be air entry value.

The ability of the high air entry disk to withstand a difference between air and water pressures makes the disk suitable for the direct measurement of negative pore-water pressures in an unsaturated soil. The disk is used as an interface between the unsaturated soil and the pore-water pressure measuring system. The water in the disk acts as a link between

the pore-water in the soil and the water in the measuring system, while the air cannot pass through the high air entry disk into the measuring system.

SAMPLE PREPARATION

One of the important aspects of the test program is to measure and compare the collapse potential of soil at various flooding stresses under the same placement conditions. Thus, it is required that the results obtained in the test program should possess repeatability to ensure the validity of test results. Various techniques of compaction are available such as dynamic compaction, static compaction and kneading compaction. Of these available methods static compaction method was chosen for the sample preparation to ensure uniformity and repeatability. The dynamic compaction method was not used as it is recognized as an effective technique for improving the engineering behavior of collapsible soils.

For the sample preparation soil was initially oven-dried at 110 ^{o}C for 24 hours to remove all of the hygroscopic moisture. The soil was allowed to cool down to room temperature for one hour in a flat pan and sieved through a 425 micron sieve. A calculated amount of water was mixed with soil to achieve desired water content. The soil was kept in plastic bags for preventing moisture loss and for moisture homogenization for one hour.

Consolidation specimens

The soil was statically compacted directly into the consolidometer ring in three layers. For each layer an amount of 35 grams were taken. The surface of each layer was scarified before adding the material for the next layer. Each layer of the soil specimen was statically compacted using the unconfined compression bench as shown in Figure 26. A

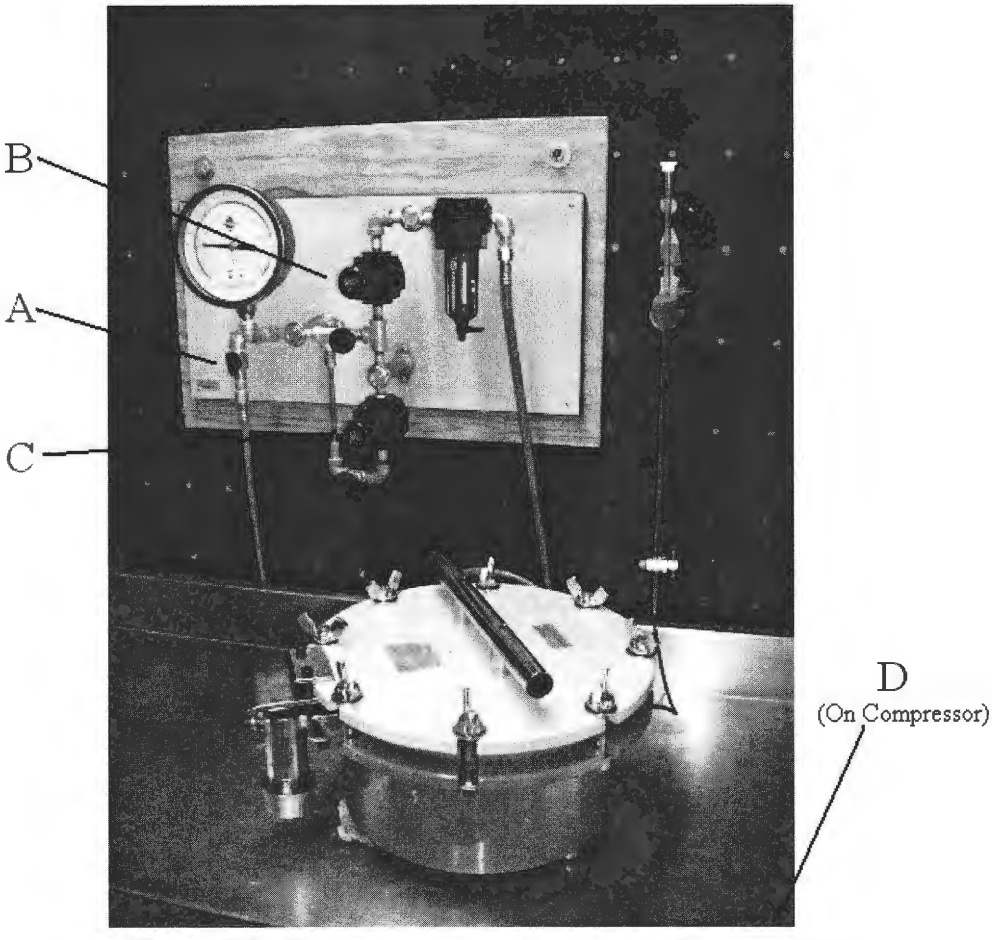

Figure 24 - Laboratory setup of pressure plate extractor.

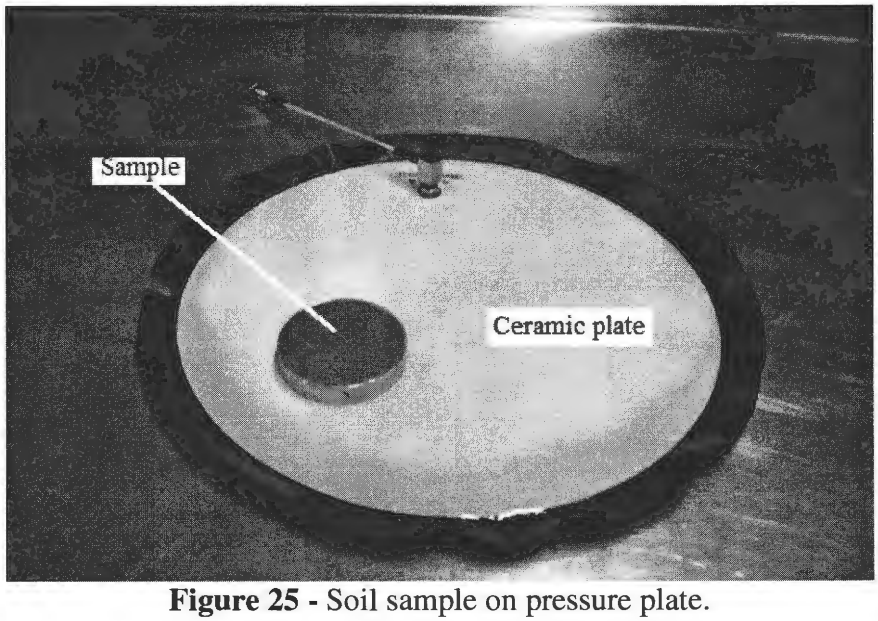

Figure 25 - Soil sample on pressure plate.

constant displacement rate of 7.4 mm/min was maintained to achieve the required static compaction stress. The reason for choosing such a high value of displacement rate was to minimize the changes in water content during compaction. The sample was trimmed on both sides after compaction. Test water content was checked.

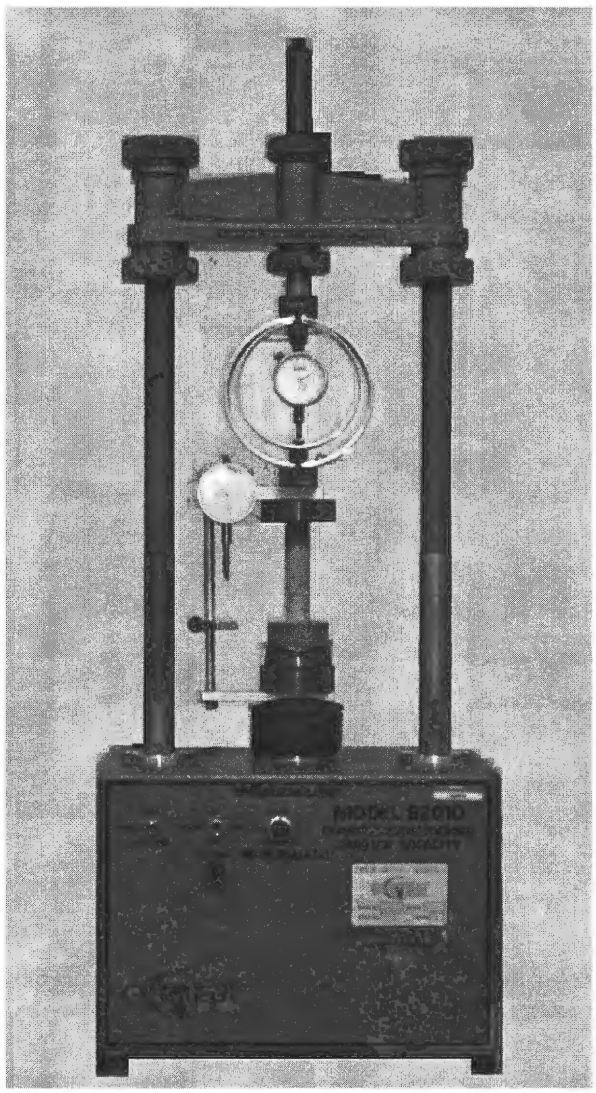

Figure 26 - Static compaction of consolidation test samples.

Proctor needle penetration specimens

The soil was statically compacted directly into the Proctor mold to achieve the same dry density as obtained in the case of consolidation specimen at the corresponding water content and static compaction stress value. The soil was compacted in three layers, each layer having the same amount of soil. The surface of each layer was scarified before adding the material for the next layer. Each layer of the soil specimen was statically compacted using a compression frame (Figure 27). The sample was trimmed after compaction. Test water content was checked.

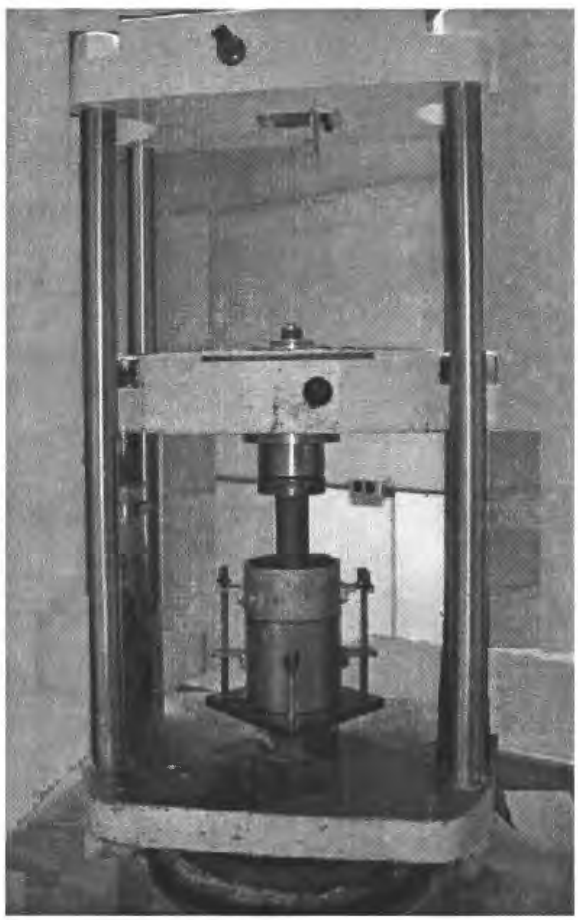

Figure 27 - Specimen preparation for Proctor needle penetration tests.

Torvane shear specimen

The soil was statically compacted directly into a cylindrical mold, 50 mm diameter and 50 mm in height, in five layers of 35 grams each as shown in Figure 28. Each layer was compacted at the same static compaction stress, and the same displacement rate of 7.4 mm/min was used as in the case of consolidation test specimens. The sample was trimmed on both sides after compaction. Test water content was checked.

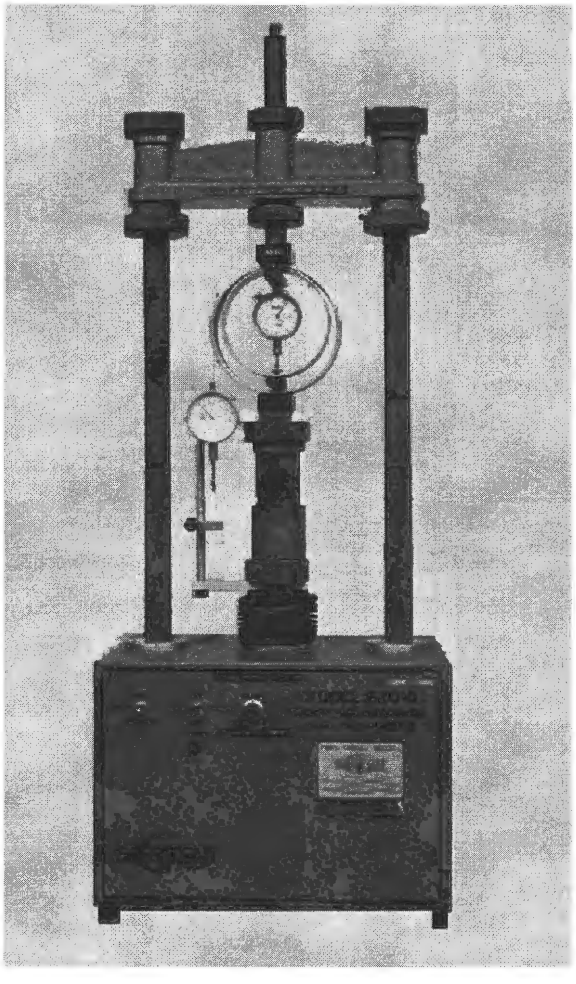

Figure 28 - Static compaction of specimens for Torvane shear tests.

Pressure plate extractor specimens

The soil was statically compacted directly into the model A-84 soil sample retaining rings of 50 mm diameter and10 mm height in a single layer of 35 gram. The soil specimens were prepared in the same way as for consolidation tests and Torvane shear tests. The samples were trimmed on both sides after compaction. Test water contents were checked.

TEST PROCEDURE FOR THE MEASUREMENT OF COLLAPSE POTENTIAL - CONVENTIONAL ONE-DIMENSIONAL CONSOLIDATION TEST

Purpose

Three series of consolidation tests were conducted in the test program. In test series No. 1, sixteen single oedometer collapse tests were performed on soil samples prepared by using static compaction stresses, namely 100 kPa, 200 kPa and 300 kPa at constant water content of 6%. The tests were performed on test specimens suddenly inundated at varying flooding stress to study the effect of initial dry unit weight, initial degree of saturation and flooding stress on collapse potential. This study helps in predicting collapse settlement *in situ* under conditions of sudden inundation.

Test series No. 2 involved nine single oedometer collapse tests at flooding stress of 100 kPa. Test specimens were prepared by varying static compaction stresses to 100 kPa, 200 kPa and 300 kPa at water contents of 6%, 10% and 14%, respectively. As the initial water content increases initial degree of saturation increases which suggests reduction in collapse potential of soil at existing vertical overburden pressure. Therefore, this test series aims at studying the variation of collapse potential with changes in initial water content of the soil at different static compaction stresses. The study also helps in identifying the initial placement

conditions in terms of water content and static compaction stress which leads to minimum collapse problem.

In the test series No. 3, partial collapse potential was measured by gradual inundation of the specimen at flooding stress (σ_{fl}) of 100 kPa, wherein a measured amount of water was allowed into the specimen till the attainment of equilibrium void ratio at that particular change of water content. Once the sample reached the equilibrium void ratio at that change in water content, next increment of water was allowed into the specimen and the procedure repeated. The tests were performed on samples prepared at a constant initial moisture content of 6%, statically compacted at 100, 200 and 300 kPa, respectively. As the void ratio changes with change in water content under flooding stress, the degree of saturation of the specimen changes. The purpose of the second series of the tests, therefore, is to study the increase in partial collapse potential with increasing degree of saturation, which helps in predicting the possible subsidence in the field triggered by increasing degree of saturation in partial wetting conditions. The study also aims at identifying a "collapse degree of saturation" which is the degree of saturation at which complete collapse takes place.

Testing procedure

Test Series1:

Porous stones were placed at each end of the sample prepared for the testing to ensure double drainage. To avoid moisture absorption, filter paper was not used. The soil sample with the porous stones and the ring was placed in the consolidometer and the loading pad was positioned centrally on the top porous stone. The consolidometer was covered with plastic wrap to minimize moisture loss. The assembly was mounted on the loading frame and the

initial adjustments were made to ensure the horizontality of the lever arm. The spindle of the compression dial gauge was kept in contact with the loading frame so that the compression of the specimen could be recorded. Vertical compressive loads were applied on the specimen starting from 6 kPa. The load was increased as 12, 25, 50, 100, 200, 400, 800 and 1600 kPa. Each load increment was applied on the specimen for two hours during the unsaturated condition. Compression of the specimen under each increment was continuously monitored till cessation of compression or attainment of equilibrium void ratio by a computer-organized data logger. Equilibrium void ratio was understood to have reached by observing the root-time versus compression dial gauge reading plot. When the plot becomes asymptotic with the X-axis, compression of the specimen under the applied load was understood to have ceased. Then the next load increment was applied, and the procedure repeated. It was observed from root time versus dial reading plot of trial tests that the time required by the specimen in unsaturated condition to reach the equilibrium void ratio was about 2 hours. Hence, time duration of 2 hours was allowed for each load increment during unsaturated condition of the specimen. However, time duration of 24 hours was allowed for the specimen to consolidate under the applied loads after flooding.

After the applied load reached the predetermined flooding stress, specimen was allowed to be compressed for two hours as usual at that particular vertical compressive stress. On the specimen reaching the equilibrium void ratio at the flooding stress in the unsaturated condition, the sample was inundated. The sample was compressed for duration of 24 hours under each load higher than the flooding load also. When the stress level reached 1600 kPa, the sample was gradually unloaded to 400, 100, 25 and 6 kPa, each decrement being maintained for 24 hours. The sample was then removed from the consolidometer ring and its

final water content measured. The initial void ratio was calculated using final water content assuming 100% degree of saturation. The collapse potential (*CP*) was calculated using Equation 1 as given by Abelev (1948) for all flooding stresses.

Test Series 2:

Test series No. 2 followed the same procedure adopted for Test series No. 1. The only difference was in the initial placement conditions of the test specimens. Test specimens were prepared at water contents of 10% and 14% in addition to water content 6% as used in case of test series No. 1 by varying static compaction stresses to 100 kPa, 200 kPa and 300 kPa. All of the specimens were inundated at a flooding stress of 100 kPa and no unloading was carried out after the application of maximum vertical compressive stress.

Test Series 3:

Test specimens were prepared in the same way as for Test Series 1. After mounting the consolidometer on the loading frame and making initial adjustments, the spindle was made to stand on the loading frame. Loading of the specimen was started with an initial vertical stress of 6 kPa incremented as 12, 25, 50 and 100 kPa. The sample was allowed to be compressed for 2 hours at each loading stage in unsaturated condition. After compressing the specimen under 100 kPa for 2 hours, partial inundation of the specimen was done by allowing a measured amount of 5 cm^3 of water into the soil. Then the root-time dial reading curve was observed. When the curve became asymptotic with the X-axis, the test was stopped. The specimen was removed from the consolidometer and its water content measured. The degree of saturation corresponding to the water content and void ratio at

equilibrium were determined. Identical specimens were prepared at the identical placement conditions and testing was done in the same way as done for the first test by adding 5 cm^3 of water at flooding stress (σ_{fl}) of 100 kPa. After the attainment of equilibrium void ratio at σ_{fl} of 100 kPa, additional 5 cm^3 of water was added to the sample and test was run till the equilibrium condition was reached. Three more tests were done in the same way by adding water to the sample in increments of 5 cm^3 at 100 kPa σ_{fl} such that the total water added to the sample becomes 15 cm^3, 20 cm^3 and 25 cm^3, respectively. Each 5 ml increment of water corresponds to an approximate increase in initial water content by 6%. The calculations were repeated to determine the degree of saturation at equilibrium at the end of each test and the calculations for partial collapse potential were done in the same way as for Test Series No. 1 and No. 2.

TEST PROCEDURE FOR THE MEASUREMENT OF SHEAR STRENGTH CHARACTERISTICS

Purpose

Two types of tests namely, Proctor penetration tests and Torvane shear tests were conducted to study the shear strength behavior of loess. The Proctor penetration test is an unconventional field test performed for the indirect measurement of shear strength, whereas the Torvane shear test is a conventional test performed both in the field and in the laboratory for the direct measurement of shear strength. In total, 18 shear tests were performed. Of these, 9 tests were performed using Proctor penetrometer device and 9 more using Torvane shear device. The test specimens were prepared by statically compacting them at compaction stresses of 100 kPa, 200 kPa and 300 kPa at corresponding water contents of 6%, 10% and

14% respectively. Torvane shear tests were conducted to obtain the undrained shear strengths of the prepared specimens. Torvane shear tests were performed because cylindrical samples prepared for unconfined compression tests did not stand in absence of any confining pressure. The purpose of performing Proctor penetration tests was to obtain a good correlation between undrained shear strength obtained from Torvane shear tests and penetration resistance. In addition to this penetration resistance from Proctor penetrometer gives an idea of the field degree of compaction (Proctor, 1933). The study aims at observing the variation of penetration resistance and undrained shear strengths with varying initial placement conditions, namely, variation of *SCS* and w_i. Also, an effort was made to prepare charts correlating penetration resistance and collapse potential for different water contents. These charts may be useful in predicting field collapse potential from penetration resistance and field moisture content for a particular collapsible soil.

Proctor needle penetration test

Penetration resistance of the loess soil, indicative of its shear strength, was determined using the Proctor's needle. The amount of resistance offered by the soil to penetration of the needle reflects the shear strength of the soil. The test samples were prepared in the Proctor's mold by statically compacting it at water contents of 6%, 10% and 14% and at dry unit weights corresponding to the static compaction stresses of 100, 200 and 300 kPa (as in the case of samples prepared for 1-D consolidation testing). After the compaction was over, the Proctor needle to which a shoe of 12.8 mm diameter was attached was kept vertically on the soil surface and pushed into the soil up to a depth of 75 mm, and the penetration force reading, as indicated by the sliding ring on the stem of the apparatus

was noted. Three penetration force readings were taken and the average penetration force was determined.

Torvane shear test

Unconfined compression tests were performed to obtain undrained shear strength. About three unconfined compression tests were attempted on the samples prepared by static compaction. But due to low static compaction energies and low water contents used in the preparation of the samples, a great difficulty was experienced in conducting the unconfined compression tests on prepared samples, as the samples did not stand in the absence of any confining pressure. However, as Torvane shear strength can be converted to unconfined compressive strength using strength correlation curve provided by the manufacturer, Torvane shear tests were performed on soil specimens for measuring undrained shear strength instead of unconfined compression tests. Samples were statically compacted at water contents of 6%, 10% and 14% at dry unit weights corresponding to 100, 200, 300 kPa in an open-end container of 50 mm thickness and 50 mm diameter in five layers taking 35 grams of soil for each layer. Both the surfaces were trimmed flat. The cylindrical test specimens were placed on a hard and smooth surface. Torvane was pressed carefully into the soil specimen up to the full depth of the vanes or blades. The knob of the Torvane was rotated at a constant speed maintaining a constant vertical load by finger pressure to generate torque on the Torvane till the failure. At failure, Torvane shear strength readings were taken on the dial head. After the test was over, the reading indicator was returned to zero and the test was performed on the other side of the specimen also. If both the values come comparable, average value was taken.

TEST PROCEDURE FOR OBTAINING SOIL WATER CHARACTERISTIC CURVES

Purpose

Nine soil water characteristic curves were developed to study the unsaturated behavior of loess. The pressure plate is a simple and accurate way of measuring suction on both the undisturbed and laboratory compacted samples. In general, at least five tests were performed to obtain data points for each single SWCC. Additional tests were performed based on the need of extra data points on the respective SWCC. The suction range used in the testing was 10-400 kPa. The test specimens were prepared by statically compacting them at compaction stresses of 100 kPa, 200 kPa and 300 kPa at corresponding water contents of 6%, 10% and 14%, respectively. The purpose of performing pressure plate tests is to study the impact of sample placement conditions such as initial water content and static compaction stress on the developed SWCCs. The study also aims at observing the variation in collapse potential with varying initial soil suction corresponding to initial water content obtained using respective SWCC.

Test procedure

Soil water characteristic curves (desorption) to study the unsaturated behavior of loess soil were developed using pressure plate apparatus. Duplicate samples were used to obtain each data point on SWCC. Prior to placing of the samples, the nylon tube and rubber sleeve were connected to the outlet stem on the pressure plate cell. Group of the soil samples with retaining rings were placed on the ceramic plate. The samples were allowed to stand for one hour with an excess of water on the plate. When the samples were ready for the

extractor, the excess water was removed from the ceramic plates with a syringe, the cells were mounted in the extractor and the outflow tubes were connected by making sure that the triangular support kept at the bottom of the vessel. The "O" ring was kept in its place, the lid mounted and clamping bolts screwed down. The outflow tube was connected to the tip of a burette with a piece of small diameter tubing to determine whether the equilibrium has reached or not. Through this small tube diffusing gas through the ceramic plate passed continuously in small bubbles and the extracted liquid was transported to the burette. The approach of equilibrium was followed by reading the burette periodically. When no measurable amount of change in the burette reading was observed over a period of many hours or days, equilibrium was assumed to have attained. The pressure was build up slowly in the extractor to the equilibrium value. The samples were removed when reading on the outflow burette indicated that the flow has stopped and equilibrium attained. The hydraulic equilibrium was attained within 24 hours. At the end of a run, before releasing the air pressure in the extractor, the external tube running from the outflow tube was removed to prevent backflow of water to the samples after the pressure was released. The pressure regulator was then shut off and the pressure exhausted from the extractor. The clamping bolts and lid were removed immediately.

The samples along with rings were taken out carefully in plates and their weights were measured. A scale with accuracy to 0.01 of a gram was used. The plates with samples and rings were kept for ovendrying for 24 hours. After ovendrying, the samples were weighed with the plate and ring. Samples were kept in air for one hour for cooling. Weight of the samples with plate and ring were taken again. The molten wax was then poured into the samples in the rings and leveled off. The weight of the samples with plate, ring and wax were

recorded. The weight of the wax in the individual rings was calculated. The change in volume of each sample after the application of suction was calculated by dividing the weight of the poured wax poured over the samples in the individual rings by the density of the wax. The density of the wax was obtained by pouring the molten wax into a ring of known volume and by measuring the weight of poured and leveled wax in the ring.

CHAPTER 4

ANALYSIS OF RESULTS

This chapter presents the results obtained in the test program and also a discussion thereof.

SOIL CLASSIFICATION & MOISTURE – DRY UNIT WEIGHT RELATIONSHIPS

Table 8 shows the index properties of the soil tested. Based on the index properties, the soil can be classified as ML, according to the USCS classification (ASTM D 2487). It is a non-plastic silt-sized soil with a natural moisture content of 9%, which is less than its plastic limit. Figure 29 shows the gradation analysis of the soil.

Table 8 - Index properties.

Property		Value
Specific gravity, G_s		2.62
Natural water content, w_n(%)		9.0
Liquid limit (%)		29
Plastic limit (%)		23
Plasticity index (%)		6
Grain size:	Gravel (%) (>6.20 – 4.75 mm)	0.04
	Sand (%) (4.75 – 0.075 mm)	3.16
	Silt (%) (0.075 – 0.002 mm)	91.43
	Clay (%) (<0.002 mm)	5.37

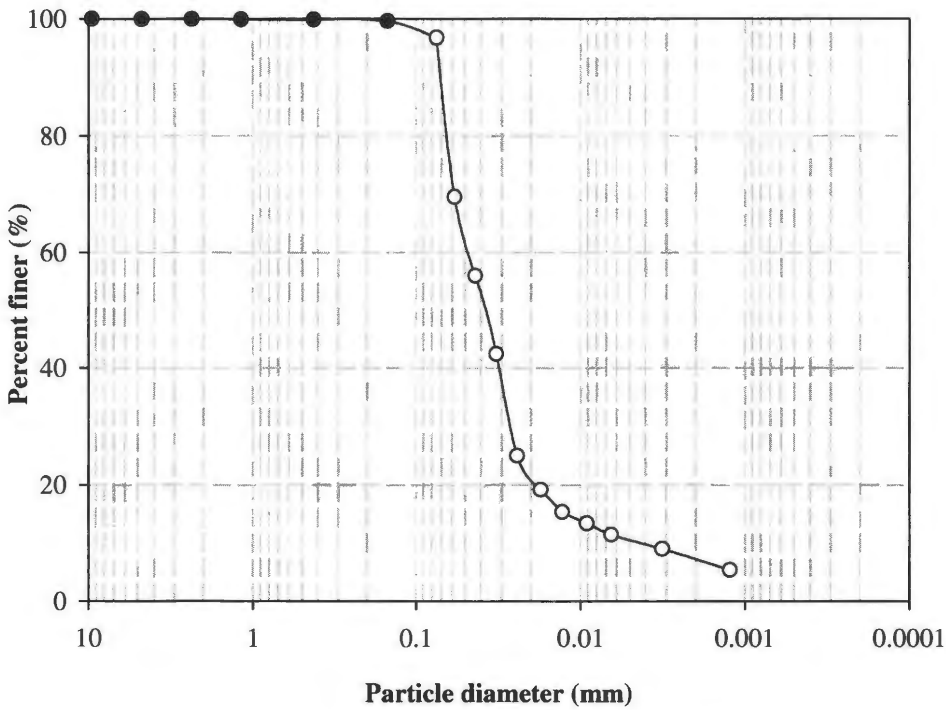

Figure 29 - Grain-size distribution curve.

Standard Proctor and modified Proctor compaction tests were performed to obtain the moisture-dry unit weight relationships. The maximum dry unit weights and optimum moisture contents are given in Table 9, and the moisture-dry unit weight relationships for the two compaction efforts are shown in Figure 30.

Table 9 - Maximum dry unit weights and optimum moisture contents.

Test type	w_{opt} (%)	$\gamma_{d\ max}$ (kN/m^3)
Standard proctor compaction test	17.5	16.8
Modified proctor compaction test	13.1	17.2

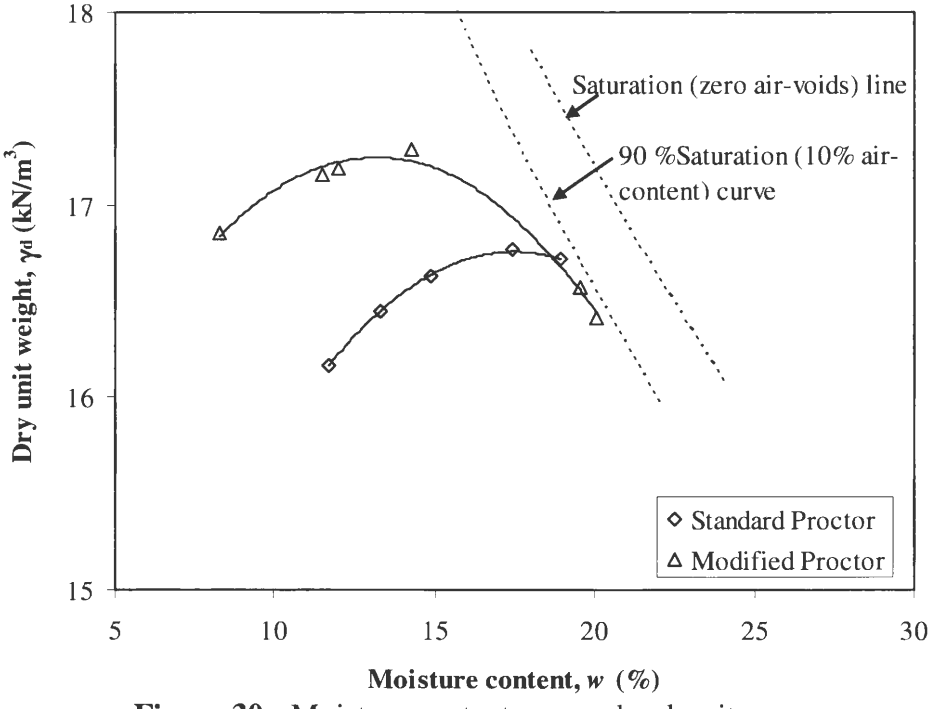

Figure 30 - Moisture content versus dry density curves.

SINGLE OEDOMETER COLLAPSE TESTS

Test series No. 1: Influence of flooding stress on collapse potential

Figure 31 shows three parts of the e versus log σ_v curve, namely A, B and C which are plotted as separate figures for the test results obtained in Test series No. 1. The variation in void ratio, e with vertical stress, σ_v prior to inundation is shown by Part A. In this curve the sample is in unsaturated condition with the same water content as the placement water content. While, Part B and Part C of the e - log σ_v curve show the variation of void ratio at constant flooding stress, σ_{fl} and subsequent loading and unloading of sample at and after σ_{fl}, respectively.

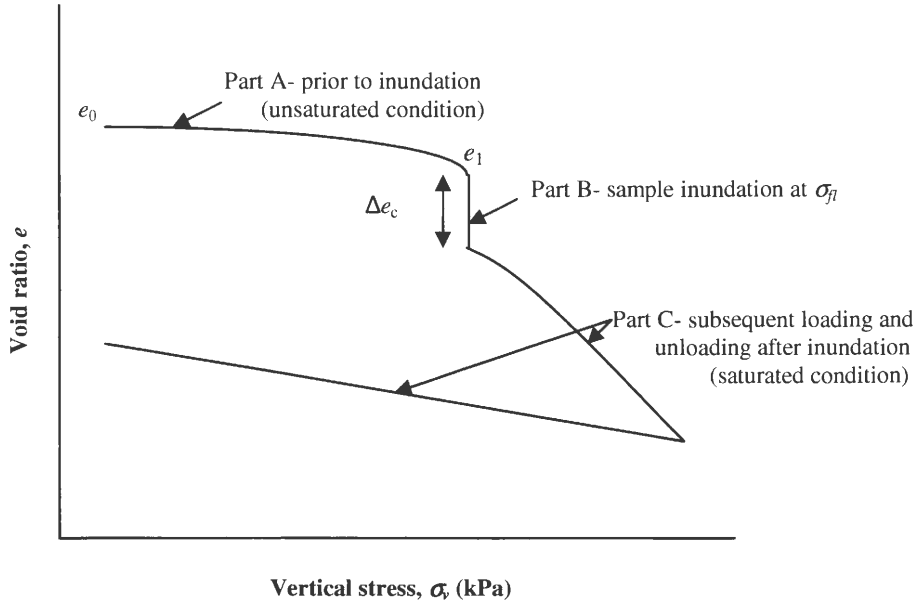

Figure 31 - Typical e versus log σ_v curve in a single oedometer collapse test.

The tests were carried out at constant water content of 6% and by varying flooding stress and static compaction stress values. Test results for Test series No. 1 are presented in the following three subsections.

(i) Constants: w_i = 6%; SCS = 100 kPa;

Variables: σ_{fl} = 6 kPa, 12 kPa, 25 kPa, 55 kPa, 100 kPa, 200 kPa, 400 kPa

From Figure 32, the maximum decrease in void ratio from equilibrium void ratio, e_0 (at 6 kPa) on loading from 6 kPa to 100 kPa is found to be 0.043, which is a negligible value. However, there is a significant decrease in the void ratio on increasing the vertical stress beyond 100 kPa. The maximum decrease in void ratio on loading from 100 kPa to 400 kPa was 0.20. Using Casagrande (1936) graphic construction to determine the preconsolidation pressure, the preconsolidation pressure, σ_{uc} from unsaturated portion of the e-log σ_v curve is approximately 120 kPa as shown in Figure 33. It seems that the samples started yielding beyond preconsolidation pressure, σ_{uc}.

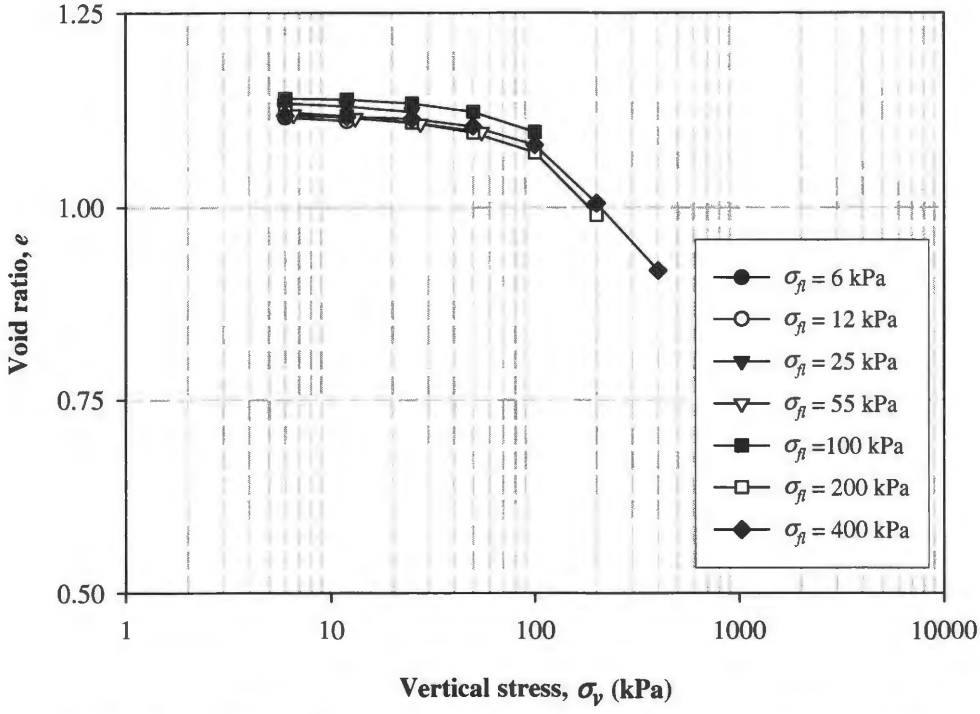

Figure 32 - Part A of e versus log σ_v curve (SCS = 100 kPa; w_i = 6%).

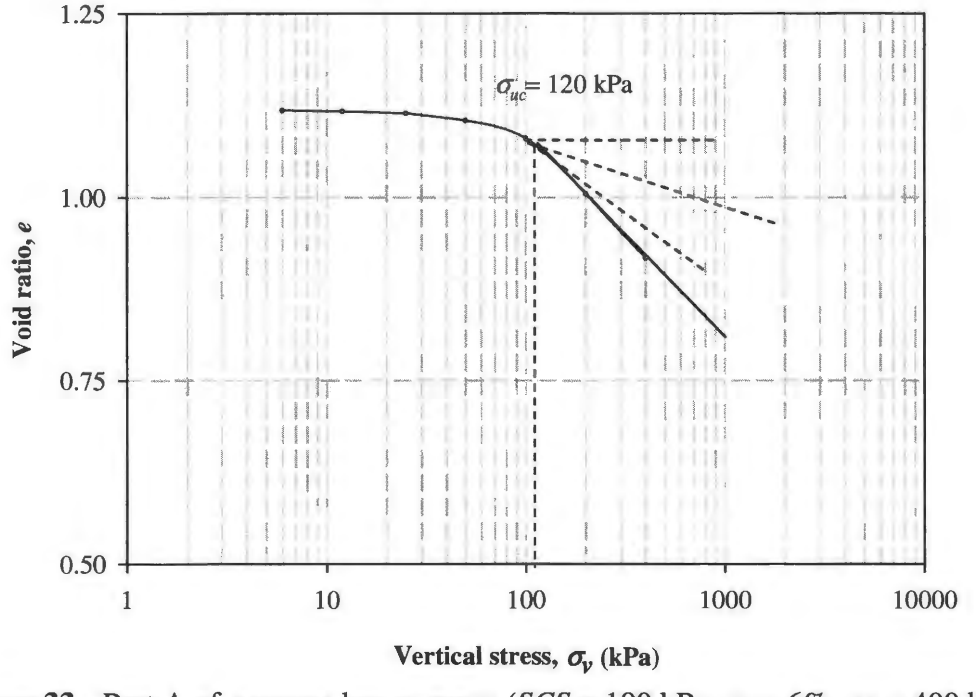

Figure 33 - Part A of e versus log σ_v curve (SCS = 100 kPa; w_i = 6%; σ_{fl} = 400 kPa).

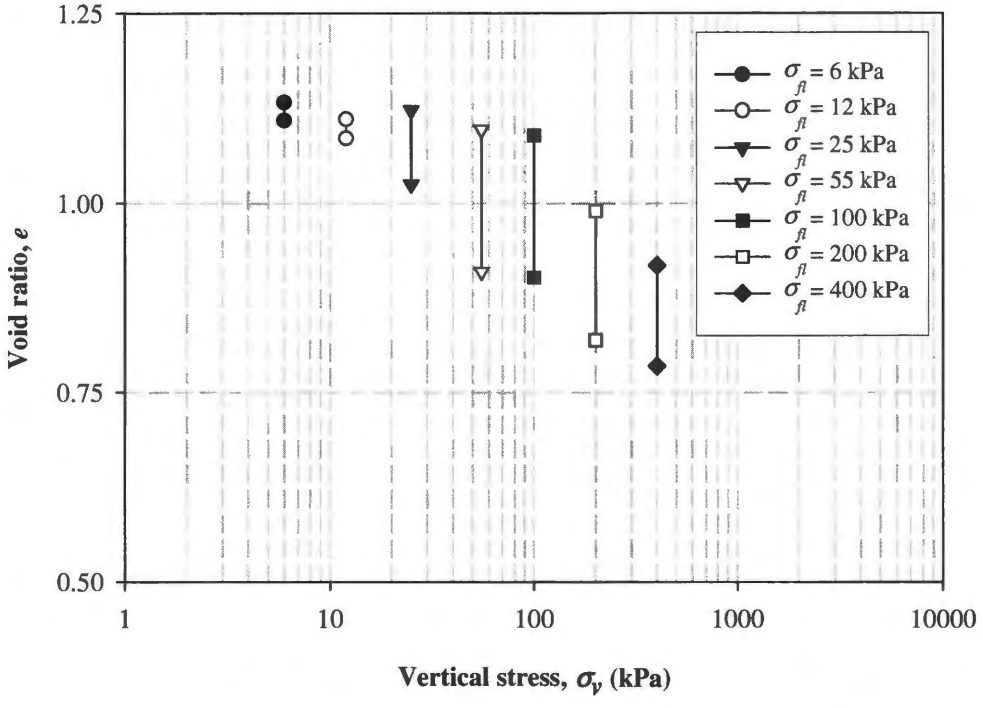

Figure 34 - Part B of e versus log σ_v curve (SCS = 100 kPa; w_i = 6%).

An estimate of collapse potential values at various flooding stresses, σ_{fl} can be made from Figure 34, which shows an increase in collapse potential values with increasing σ_{fl} values from 6 kPa to 55 kPa. Between 55 kPa and 200 kPa the soil collapsed to the maximum extent. After 200 kPa σ_{fl}, however, the collapse potential started decreasing. Hence, 55 kPa can be said to be the critical value of collapse potential for the soil used for the given placement conditions (w_i = 6% and SCS = 100 kPa). It is worth noting that, with increasing vertical stress in unsaturated condition followed by flooding, the collapse potential decreased after a certain value of vertical stress. This phenomenon suggests that the soil was already compressed to a large extent in the unsaturated condition prior to flooding. This means that the higher the values of overburden pressures (vertical stress) lower the value of collapse potential. Table 10 summarizes the values of collapse potential at varying flooding stresses.

Table 10 - Collapse potential and compression index values at different vertical stresses at inundation (w_i = 6%; SCS = 100 kPa).

Flooding stress, σ_{fl} (kPa)	Collapse potential, CP (%)	Compression index, C_c
6	1.11	0.19
12	1.21	0.19
25	4.60	0.20
55	8.96	0.17
100	8.98	0.18
200	8.59	0.19
400	6.90	0.22

Figure 35 shows the change in void ratio with the change in vertical stress after the application of flooding stress on specimens. The slopes of virgin compression curves show that compression index, C_c is almost the same for all values of flooding stresses. The C_c values are given in Table 10. The slopes of rebound curves in Figure 35 are relatively flat, showing a negligible value of swelling index for the three oedometer tests. The average value of swelling index is 0.018. It appears from the curves that even after the collapse, the soil exists in a "loose" state, namely, at high void ratio with respect to the applied vertical stress.

Part A of the e - log σ_v curve for the flooding stress equal to 400 kPa and the curve joining the void ratios just prior to inundation at varying flooding stresses are provided in Figure 36. The overlapping of these two curves shows the repeatability of the sample preparation procedure.

Figure 37 shows the variation in void ratio at various flooding stresses with root time starting from the time at which inundation was allowed. From Figure 37, it seems that the full collapse of the sample takes place only within 1-1.5 hours after the sample inundation for all

the values of flooding stresses. As the equilibrium void ratio is attained only within few hours after inundation, it is not mandatory to keep the sample under loading for 24 hours.

Figure 38 shows the influence of flooding stress on collapse potential. The figure suggests that collapse potential is dependent on the flooding stress. This trend was observed by previous researchers also (Feda, 1964; Kezdi, 1974; Lutenegger and Saber, 1988). The results in Figure 38 indicate an initial increase in collapse potential up to flooding stress value of 55 kPa. At a flooding stress of 55 kPa, collapse potential reached the maximum value, and thereafter remained constant up to flooding stress of 200 kPa. It is interesting to note that after a flooding stress of 200 kPa, collapse potential decreased. This reduction in collapse potential from the maximum value may, possibly, be due to the yielding of the soil prior to inundation. Feda (1966) also noted the same pattern of increasing collapse followed by decreasing collapse as the flooding stress values were incremented.

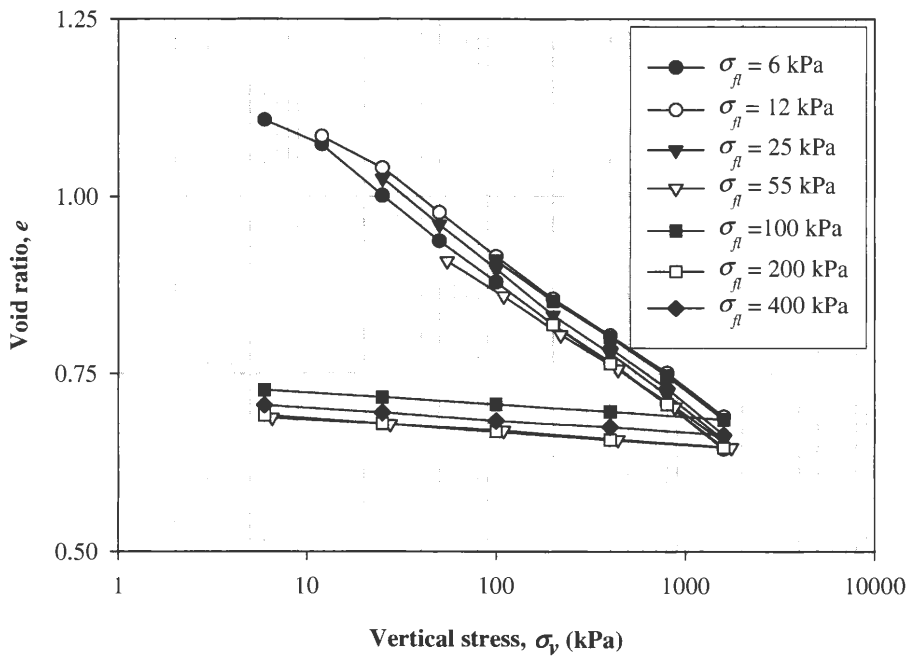

Figure 35 - Part C of e versus log σ_v curve (SCS = 100 kPa; w_i = 6%).

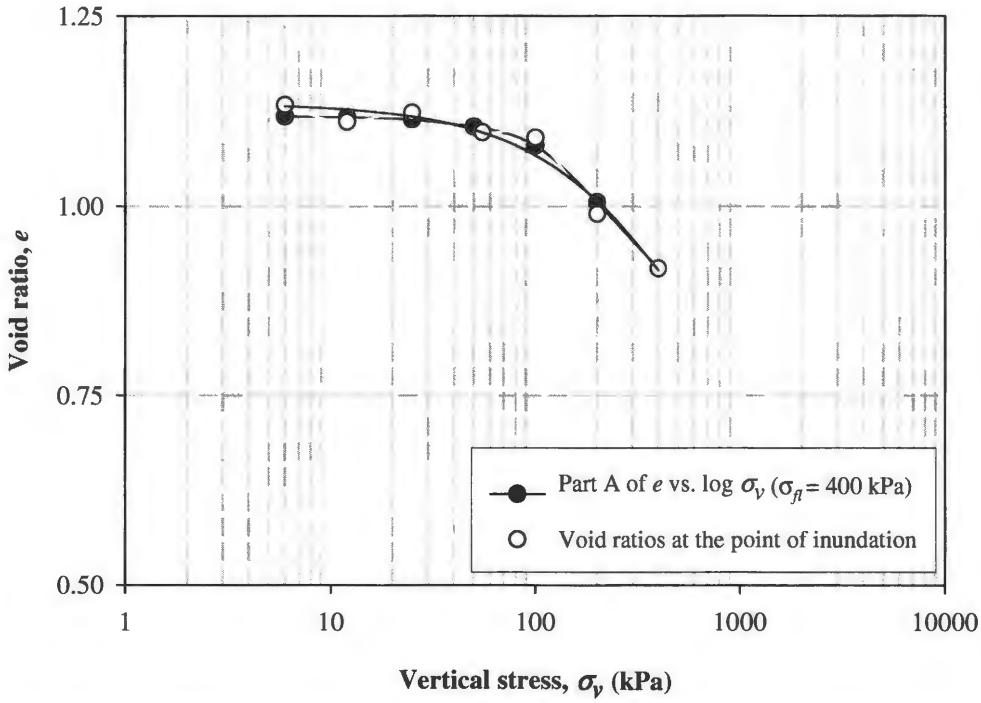

Figure 36 - Comparison of Part A of e versus log σ_v curve (SCS = 100 kPa; w_i = 6%; σ_{fl} = 400 kPa) and the equilibrium void ratios at the point of inundation at varying flooding stresses.

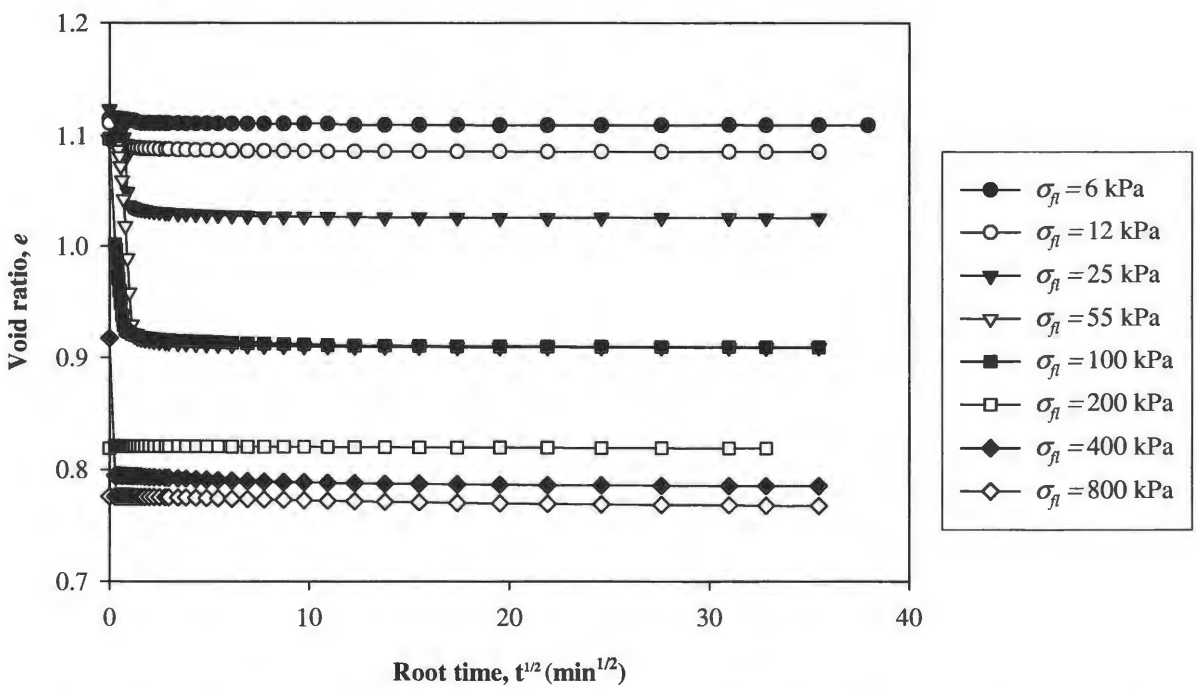

Figure 37 - Variation in void ratio at various flooding stresses with root time (SCS = 100 kPa; w_i = 6%).

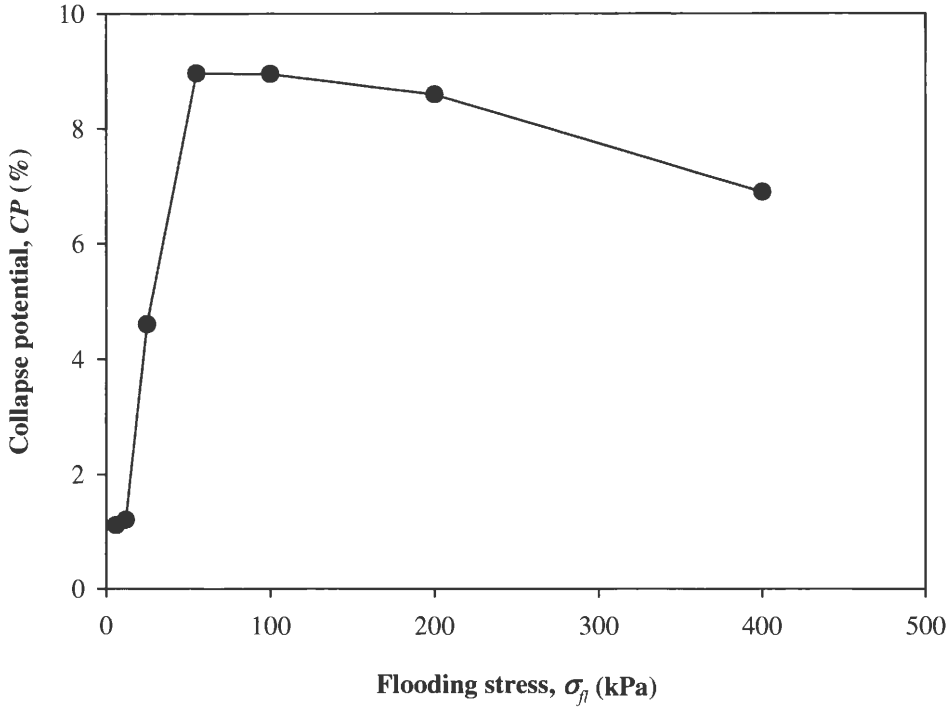

Figure 38 - Collapse potential versus flooding stress (SCS = 100 kPa; w_i = 6%).

(ii) Constants: w_i = 6%; SCS = 200 kPa;

Variables: σ_{fl} = 50 kPa, 100 kPa, 200 kPa, 400 kPa, 800 kPa

From Figure 39, the variations in void ratio, e_o, appear to be negligible on increasing the value of vertical stress from 6 kPa to 50 kPa. However, as the vertical stress increased beyond 50 kPa, a significant fall in the values of void ratios was observed. From Figure 40, the preconsolidation pressure, σ_{uc} from unsaturated portion of the e-log σ_v curve is approximately 60 kPa. It can be seen that the samples started yielding after the preconsolidation pressure, σ_{uc}. Therefore, 50 kPa can be considered as a critical value of vertical stress in the given partially saturated condition. A noticeable decrease in the void ratio values with the increase in vertical stress from 50 kPa to 800 kPa shows that the soil started yielding after 50 kPa.

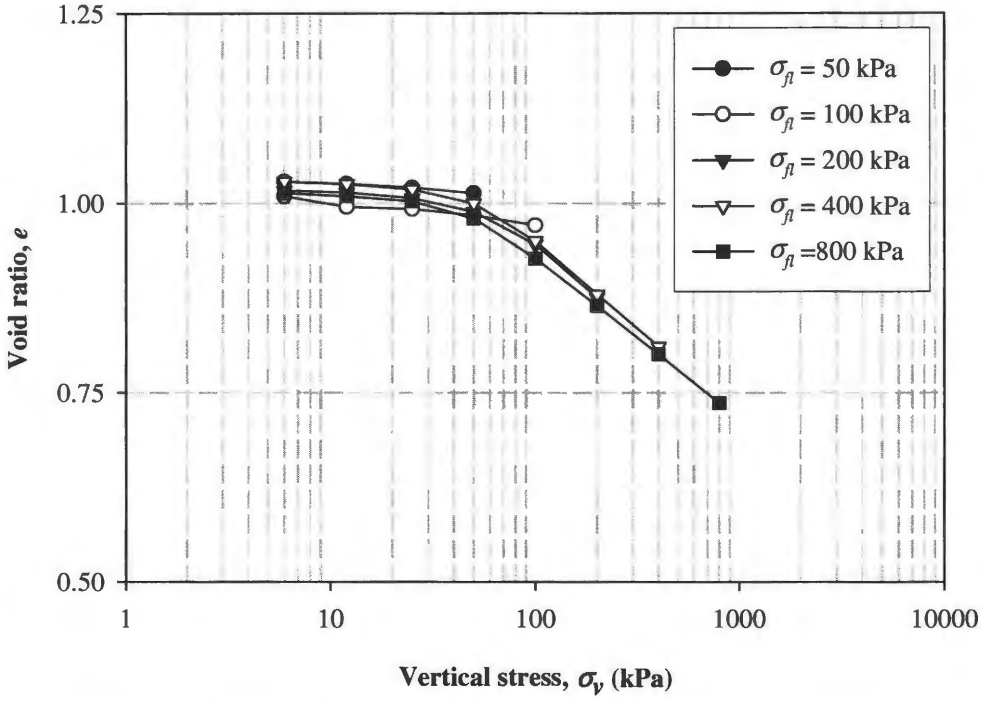

Figure 39 - Part A of e versus log σ_v curve (SCS = 200 kPa; w_i = 6%).

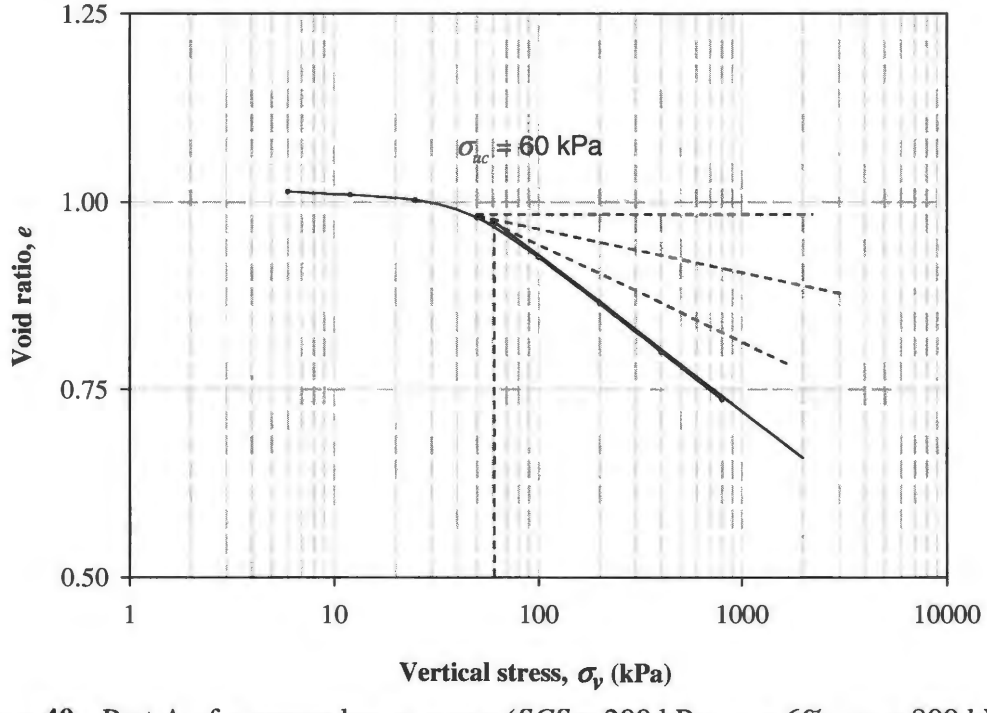

Figure 40 - Part A of e versus log σ_v curve (SCS = 200 kPa; w_i = 6%; σ_{fl} = 800 kPa).

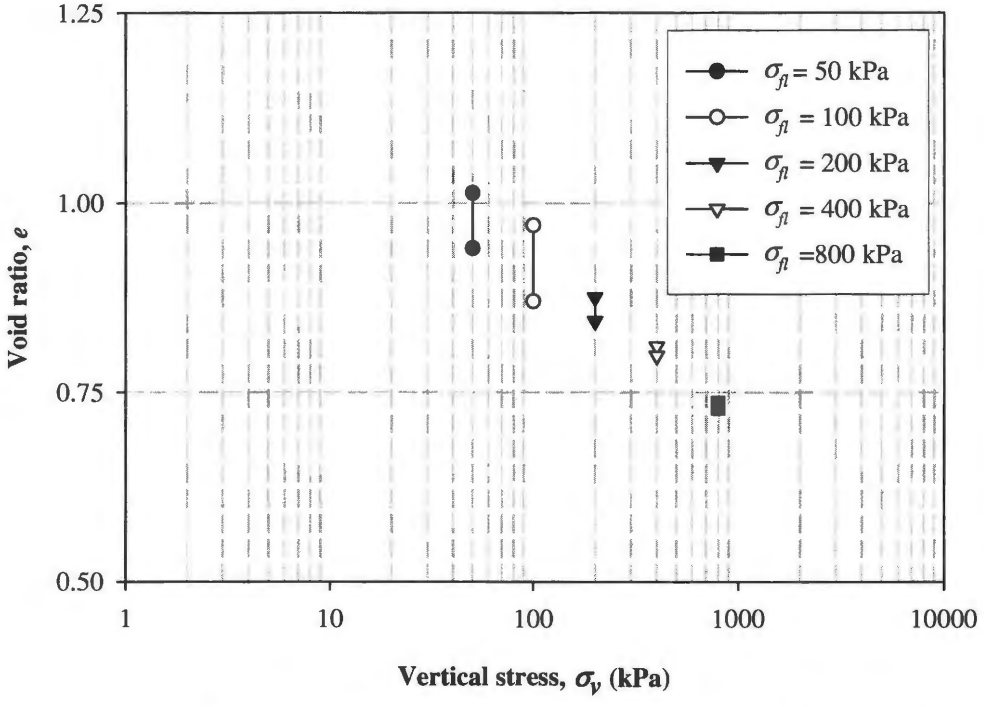

Figure 41 - Part B of e versus log σ_v curve (SCS = 200 kPa; w_i = 6%).

Figure 41, shows the collapse potential of soil at varying flooding stresses, σ_{fl}. An initial increase in collapse potential was observed on increasing σ_{fl} value from 50 kPa to 100 kPa. This is followed by a decrease in collapse potential values as the σ_{fl} increased beyond 100 kPa. Therefore 100 kPa can be considered as the critical vertical stress causing the maximum collapse potential for the given placement conditions (w_i = 6% and SCS = 200 kPa). The decrease in collapse potential on increasing σ_{fl} value above 100 kPa, indicates that the soil was already compressed to a greater extent in unsaturated condition prior to the application of that particular value of σ_{fl}.

The summarized values of collapse potential and compression index at varying vertical stresses at inundation are given in Table 11.

Table 11 - Collapse potential values at different flooding stress (w_i = 6%; SCS = 200 kPa).

Flooding stress, σ_{fl} (kPa)	Collapse potential, CP (%)	Compression index, C_c
50	3.65	0.19
100	5.13	0.20
200	2.19	0.20
400	0.68	0.22
800	0.43	0.23

Part C of the e - log σ_v curves for all the samples at given placement condition is shown in Figure 42. The variation in compression index with varying flooding stress is given in Table 11. The slopes of the rebound curves are relatively flat showing a negligible value (close to zero) of swelling index. From calculations the average value of swelling index is 0.023. From the curves it appears that even after collapse, the soil exists in a "loose" state exhibiting large void ratio. However, the loose state of the soil disappeared as σ_{fl} increased.

Figure 43 shows that the full collapse of the sample has taken place within 1 hour after inundation. The equilibrium void ratio was attained only within an hour after inundation and therefore, the sample must be kept under the flooding stress only for that duration and subsequent loading could be applied to the sample after that.

Figure 44 shows the influence of flooding stress on collapse potential. An initial increase in collapse potential was noted as the flooding stress increased from 50 kPa to 100 kPa. At σ_{fl} = 100 kPa, collapse potential reached the maximum value. After the maximum value of collapse, a sharp reduction in the amount of collapse was noted. This trend continued till σ_{fl} was increased up to 400 kPa. Thereafter, collapse potential remained almost constant which suggests that maximum possible yielding could take place at a σ_{fl} value of 400 kPa prior to inundation.

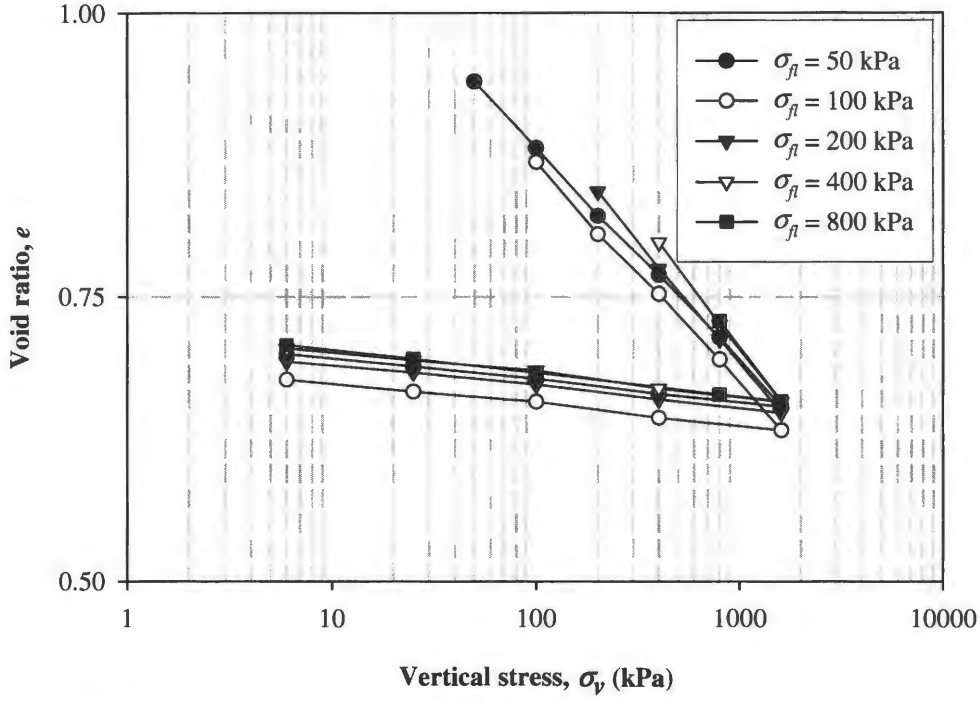

Figure 42 - Part C of e versus log σ_v curve (SCS = 200 kPa; w_i = 6%).

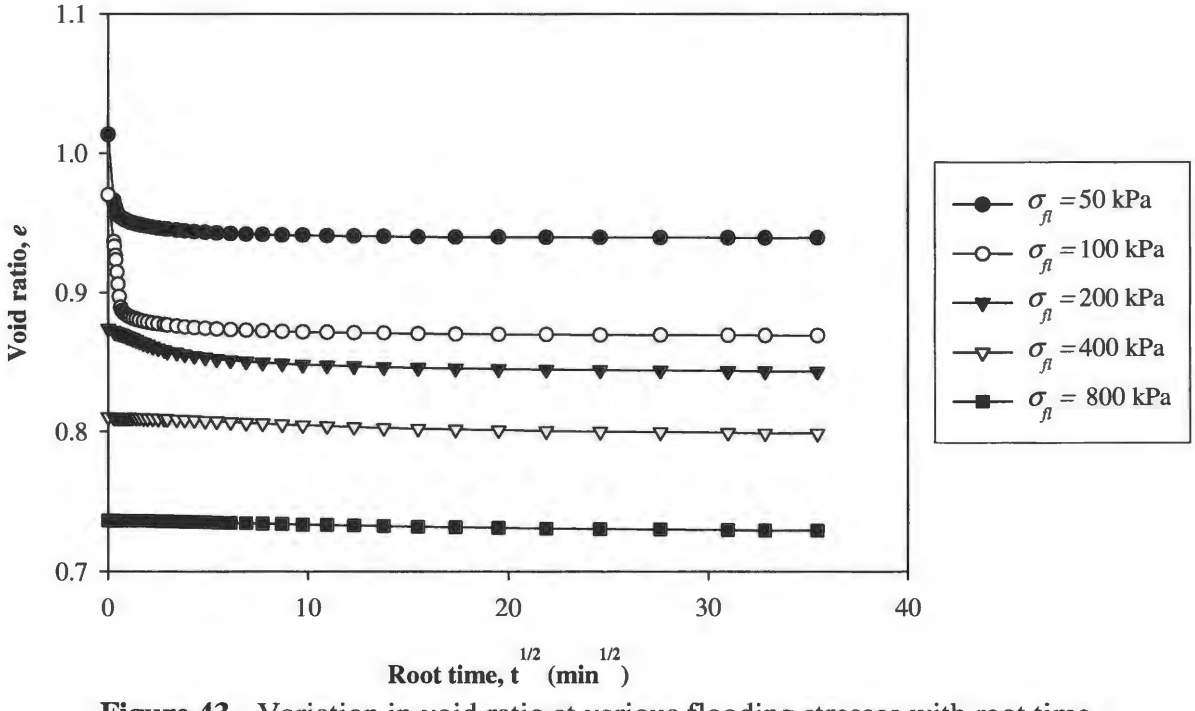

Figure 43 - Variation in void ratio at various flooding stresses with root time (SCS = 200 kPa; w_i = 6%).

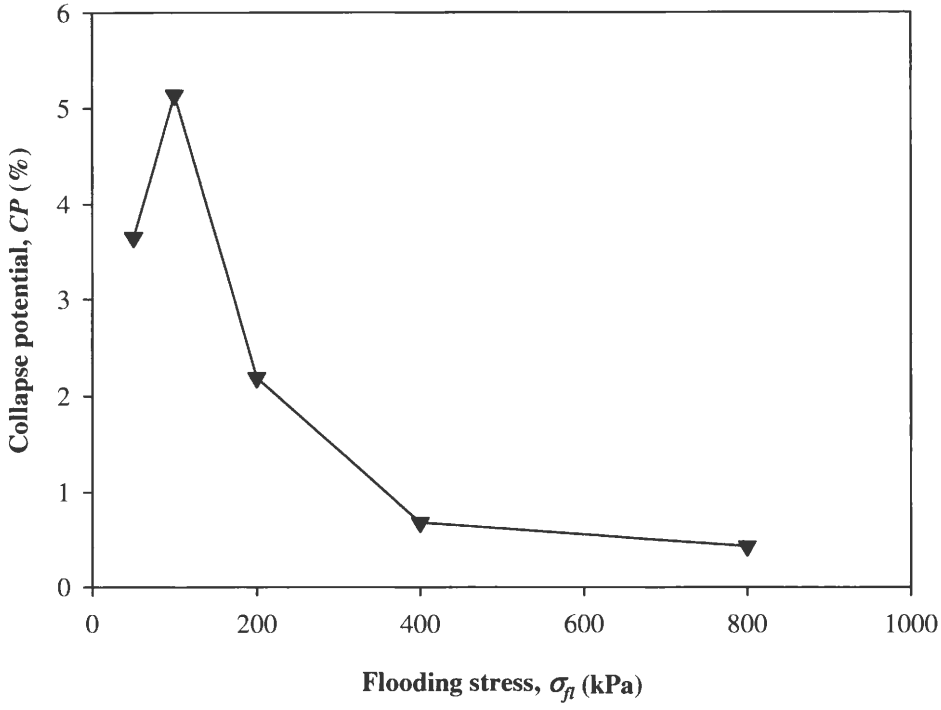

Figure 44 - Collapse potential versus flooding stress (*SCS* = 200 kPa; w_i = 6%).

(iii) Constants: w_i = 6%; *SCS* = 300 kPa;

Variables: σ_{fl} = 50 kPa, 100 kPa, 200 kPa, 400 kPa

Figure 45 shows the part A of the e - log σ_v curve. The variations in void ratios from void ratio, e_o appear to be negligible as the value of vertical stress is increased from 6 kPa to 100 kPa. As the vertical stress increased beyond 100 kPa, a significant reduction in the void ratios was observed. Also, the approximate value of preconsolidation pressure, σ_{uc} from Figure 46 is found out to be 90 kPa. Therefore, 90 kPa can be considered as a critical value of vertical stress in the given unsaturated condition. A noticeable decrease in the void ratio values with the increase in vertical stress from 90 kPa to 400 kPa show that yielding of soil started after 90 kPa.

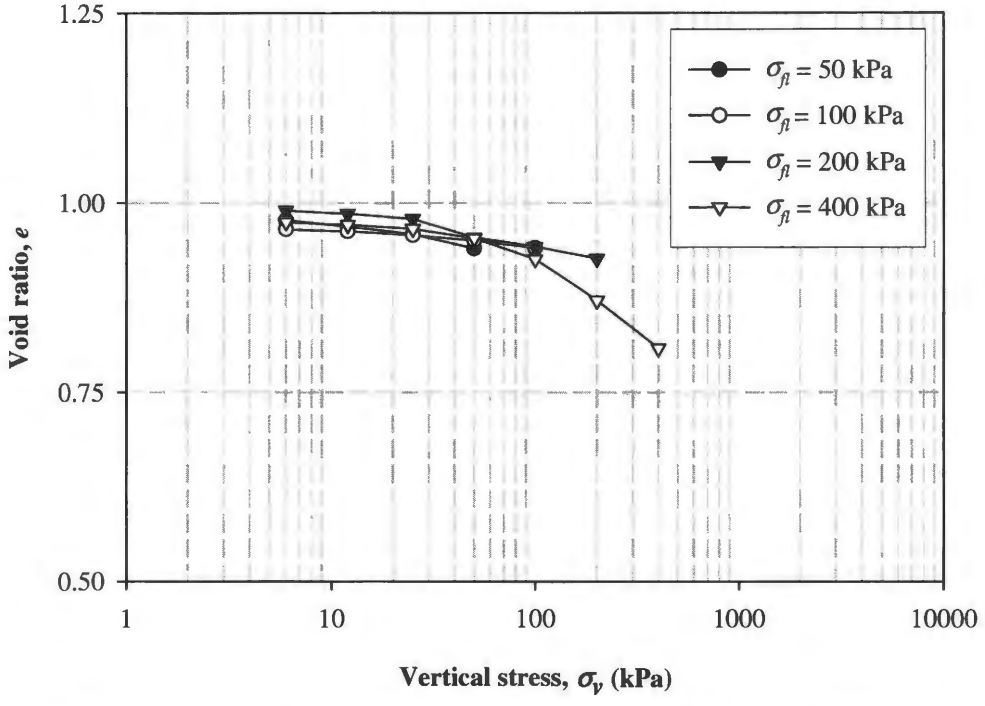

Figure 45 - Part A of e versus log σ_v curve (SCS = 300 kPa; w_i = 6%).

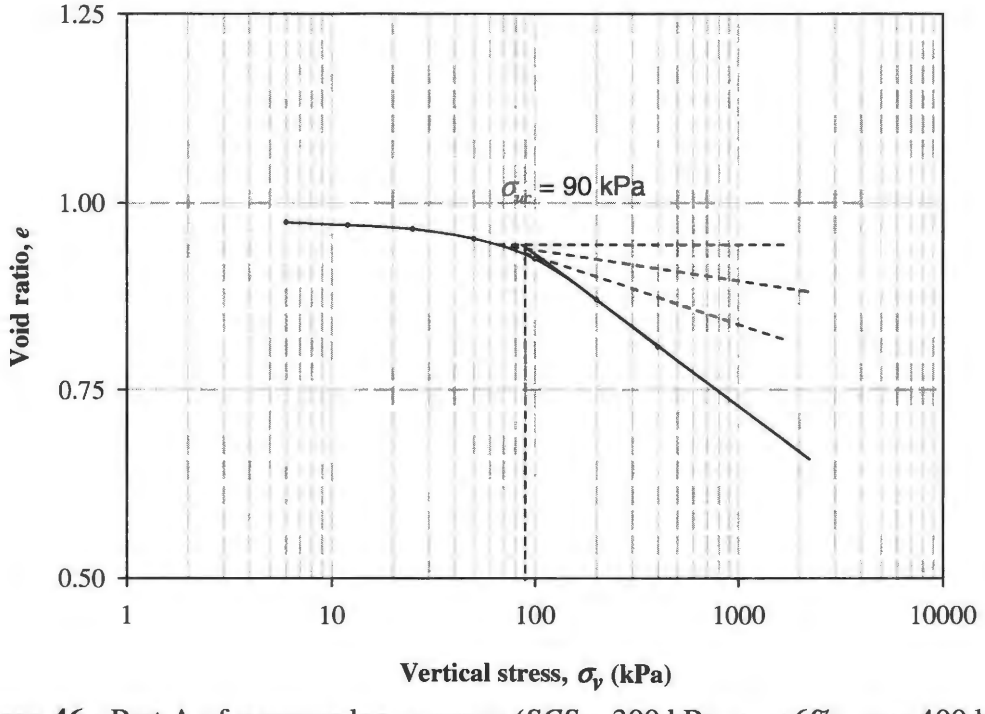

Figure 46 - Part A of e versus log σ_v curve (SCS = 300 kPa; w_i = 6%; σ_{fl} = 400 kPa).

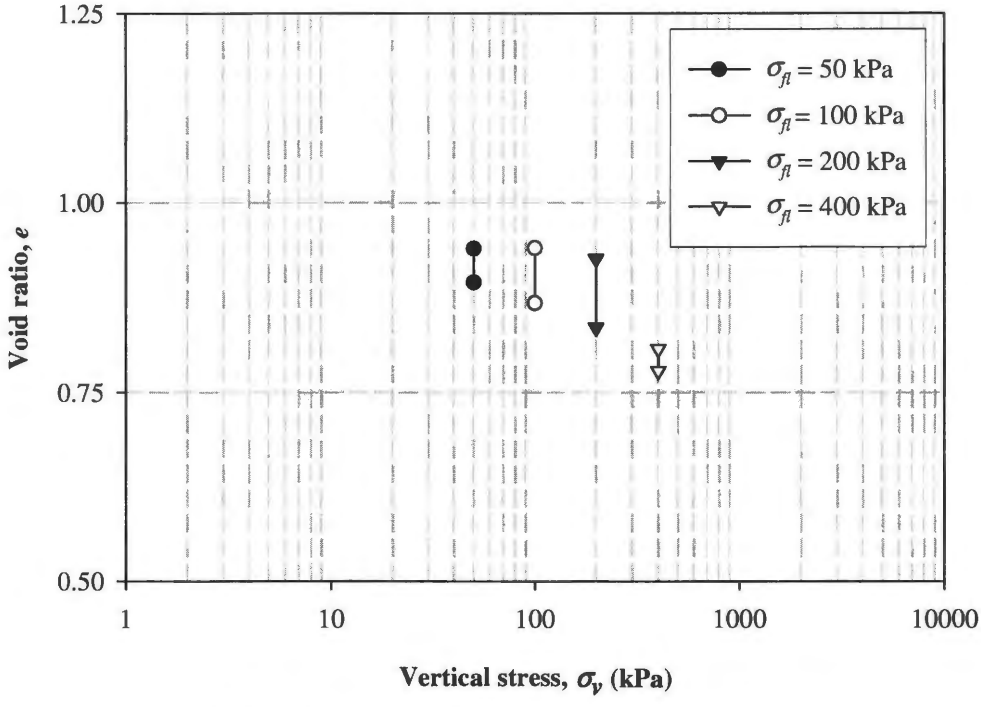

Figure 47 - Part B of e versus log σ_v curve (SCS = 300 kPa; w_i = 6%).

Figure 47, shows the variation in collapse potential of soil with the applied flooding stresses (σ_{fl}). An initial increase in collapse potential was observed on increasing σ_{fl} from 50 kPa to 200 kPa, which is followed by a reduction in collapse potential as σ_{fl} further increased from 200 kPa to 400 kPa. Therefore, 200 kPa can be considered as the critical vertical stress showing the maximum collapse potential for the given placement conditions (w_i = 6% and SCS = 300 kPa). The reduction in collapse potential suggests the compression of soil to a greater extent in unsaturated conditions on applying vertical stresses less than or equal to 400 kPa prior to inundation.

The summarized values of collapse potential at varying flooding stresses are provided in Table 12.

Table 12 - Collapse potential values at different flooding stresses (w_i = 6%; *SCS* = 300 kPa).

Flooding stress, σ_{fl} (kPa)	Collapse potential, *CP* (%)	Compression index, C_c
50	2.28	0.19
100	3.70	0.19
200	4.67	0.19
400	1.61	0.22

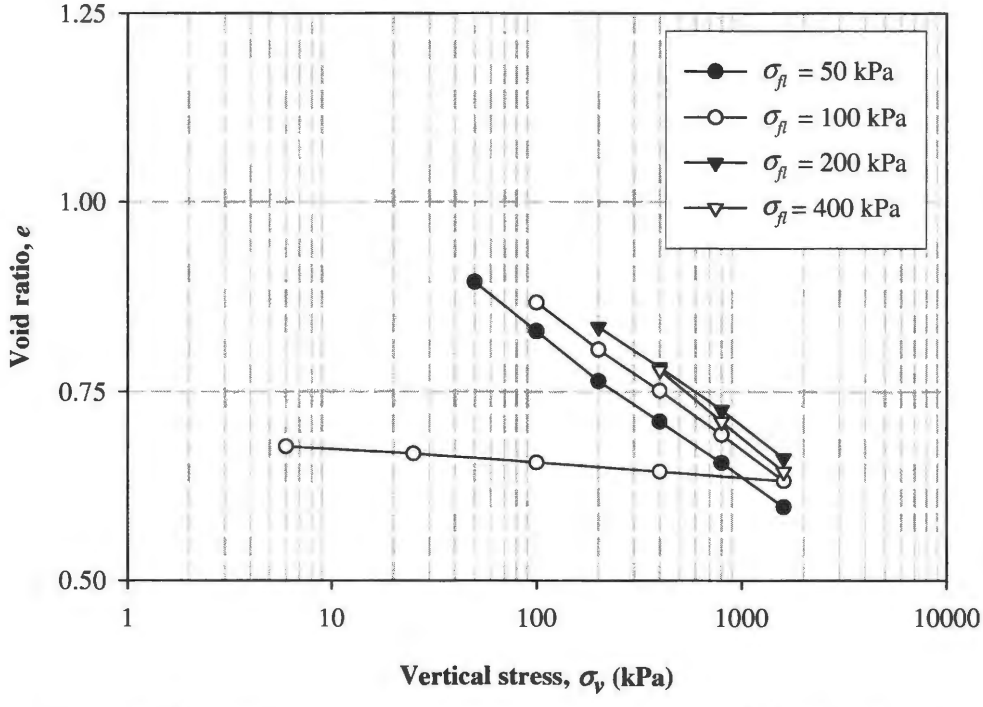

Figure 48 - Part C of *e* versus log σ_v curve (*SCS* = 300 kPa; w_i = 6%).

Figure 48 shows Part C of the *e* - log σ_v curves for all the samples at the given placement conditions. The slopes of virgin compression curves show the same value of compression index for all values of vertical stresses at inundation, σ_{fl} except for σ_{fl} = 400kPa (see Table 12). The slope of the rebound curve for the test sample with σ_{fl} value equal to 100 kPa is relatively flat showing a very small value (close to zero) of swelling index. The value of swelling index from calculations is 0.02. From the curves it appears that, even after the

collapse, the soil exists in a "loose" state, having high void ratios with respect to the applied vertical stress. However, the loose state of the soil disappeared as the σ_{fl} increased.

Figure 49 shows the variation in void ratios at various vertical stresses at inundation with root time. The equilibrium void ratio was attained only within one hour after inundation, which suggests that the sample needs to be kept under the flooding stress only for an hour prior to the application of next increment of load in an oedometer test.

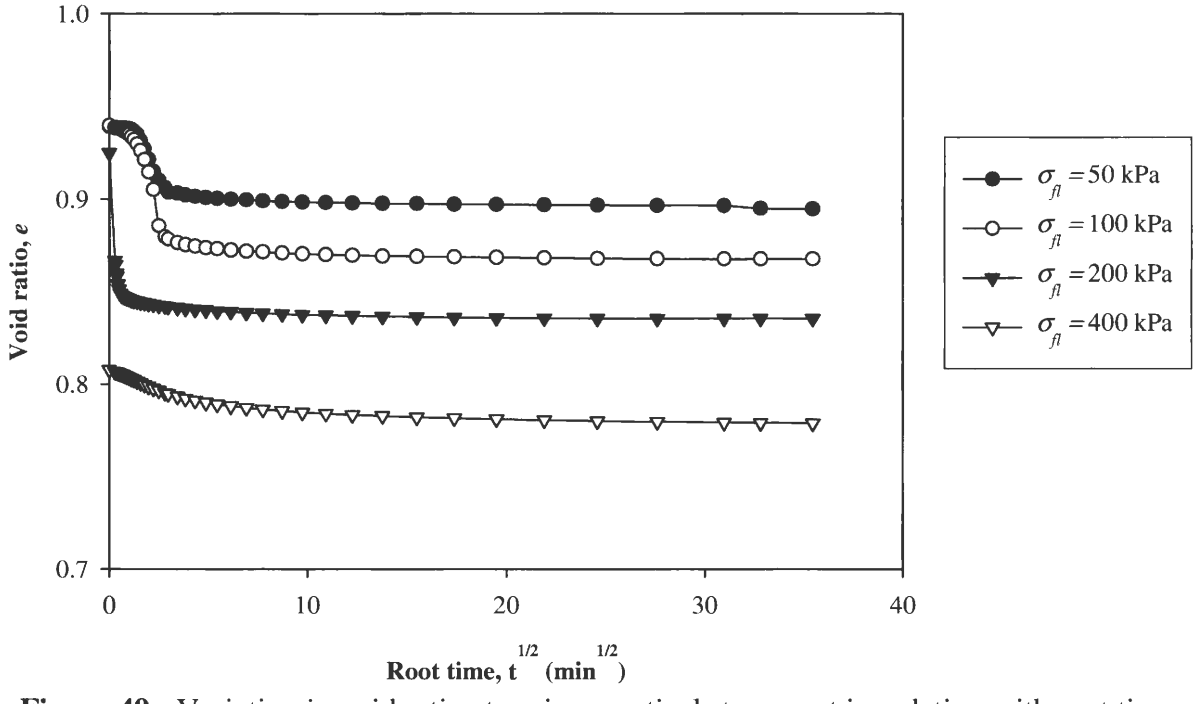

Figure 49 - Variation in void ratio at various vertical stresses at inundation with root time (*SCS* = 300 kPa; w_i = 6%).

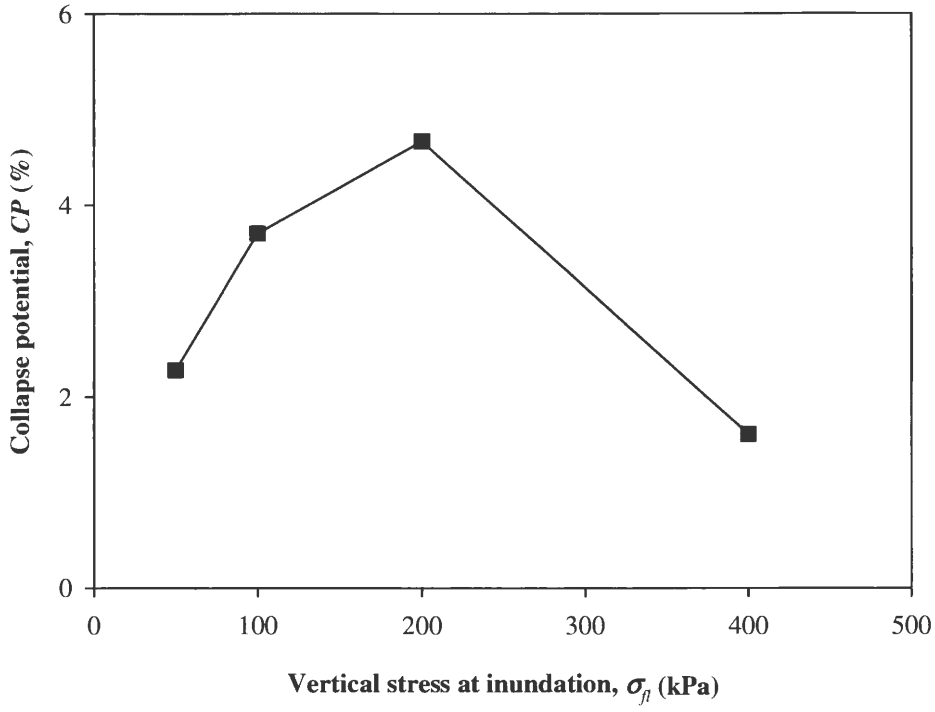

Figure 50 - Collapse potential versus flooding stress (SCS = 300 kPa; w_i = 6%).

Figure 50 shows the influence of flooding stress on collapse potential. The results (Figure 50) indicate an initial increase in collapse potential as the flooding stress value is increased from 50 kPa to 200 kPa. Collapse potential reached the maximum value at a vertical stress of 200 kPa at inundation. After σ_{fl} reached 200 kPa, a sharp reduction in the amount of collapse was noted as σ_{fl} was increased up to 400 kPa. This indicates the possible yielding or particle crushing of soil at a σ_{fl} of 400 kPa prior to inundation.

Figure 51 provides a summary of the variation in collapse potential with flooding stress for all of the static compaction stress values used in the test program. The critical or limiting value of flooding stress increased with increasing static compaction stress. A summary of the limiting vertical stresses at inundation for varying static compaction stresses

is given in Table 13. Also, the collapsibility of soil decreased as the static compaction effort used for the compaction of soil specimens increased.

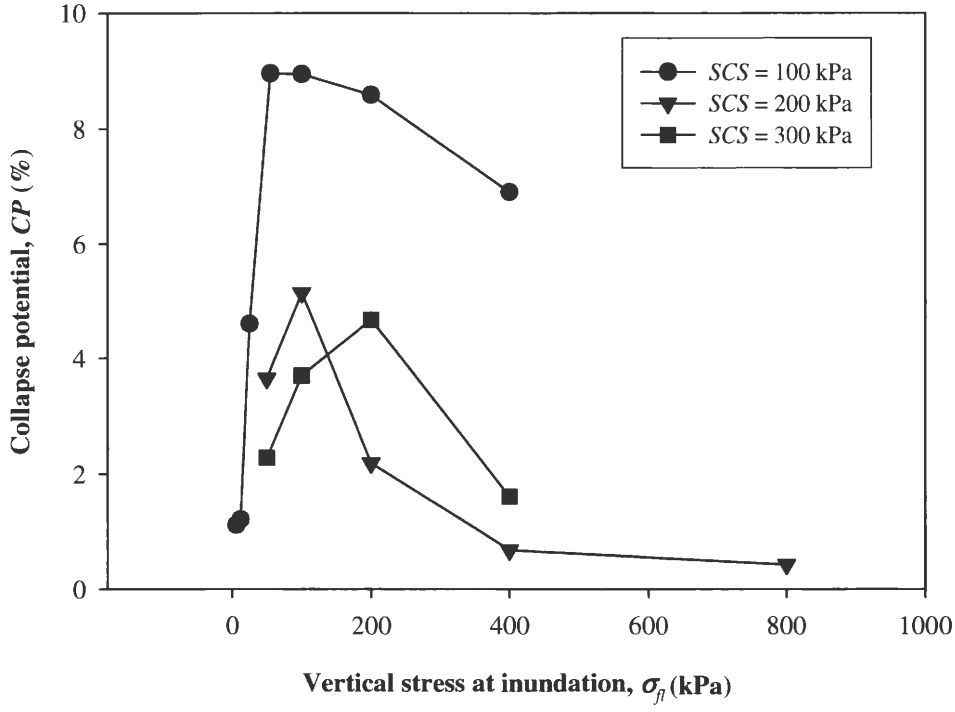

Figure 51 - Collapse potential versus flooding stress (w_i = 6%).

Table 13 - Variation in limiting values of vertical stresses at inundation with varying static compaction stresses.

Static compaction stress	Limiting flooding stress (kPa)
100	55
200	100
300	200

Test series No. 2: Influence of initial water content on collapse potential

The tests were done at a constant flooding stress of 100 kPa with variation of initial water content and static compaction stress values. Test results are shown in the form of *e* -

log σ_v curve, plotted based on the static compaction stress values. Three curves are plotted in each figure showing the effect of variation of initial water content on collapse potential. In general, from Figure 52, Figure 53 and Figure 54 it can be seen that the collapse potential decreased with increasing initial water contents.

Figure 52 shows the yielding of soil for initial water content (w_i) of 14% prior to the flooding stress i.e., between 25 kPa and 50 kPa. However, no yielding was observed in unsaturated condition for w_i values of 6% and 10% prior to 100 kPa. The compression index, C_c for all three w_i's is found to be a constant value of 0.18. From Figure 53, no yielding of soil was observed for all three initial water contents prior to inundation. Also, the compression index, C_c for all three w_i's is found to be a constant value of 0.19. A significant drop in collapse potential on increasing initial water content can be seen from Figure 54. No yielding of soil was observed for all three initial water contents prior to inundation at 100 kPa. The compression index, C_c for all three w_i's is found to be 0.19.

Figure 55 shows the variation of collapse potential with initial water content for static compaction stresses (*SCS*) of 100, 200 and 300 kPa. From Figure 55, for all the values of static compaction stresses, collapse potential value decreased linearly when water content increased from 6% to 14%, which can be described in terms of increase in both the degree of saturation and increase in dry density with increasing initial water content.

It can be seen from Figure 55 that collapse potential decreases linearly with increasing static compaction stress (*SCS*). However, the percentage reduction in collapse potential when *SCS* changed from 100 kPa to 200 kPa, is much higher than the reduction in collapse potential when *SCS* changed from 200 kPa to 300 kPa. This may be due to the fact

that increase in dry density when *SCS* changed from 100 kPa to 200 kPa is much higher than the increase in dry density when *SCS* changed 200 kPa to 300 kPa.

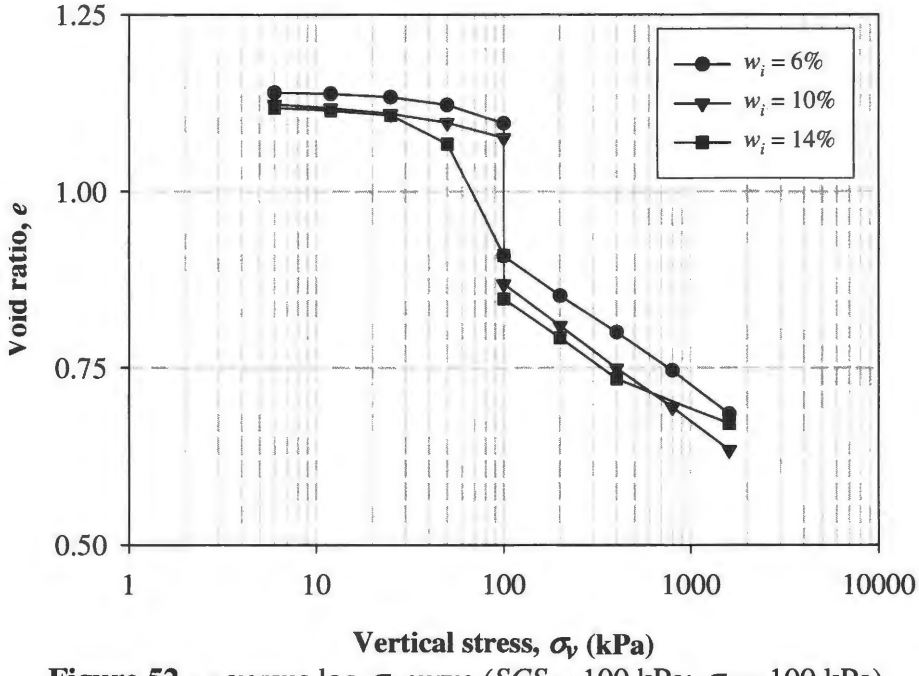

Figure 52 - *e* versus log σ_v curve (*SCS* = 100 kPa; σ_{fl} = 100 kPa).

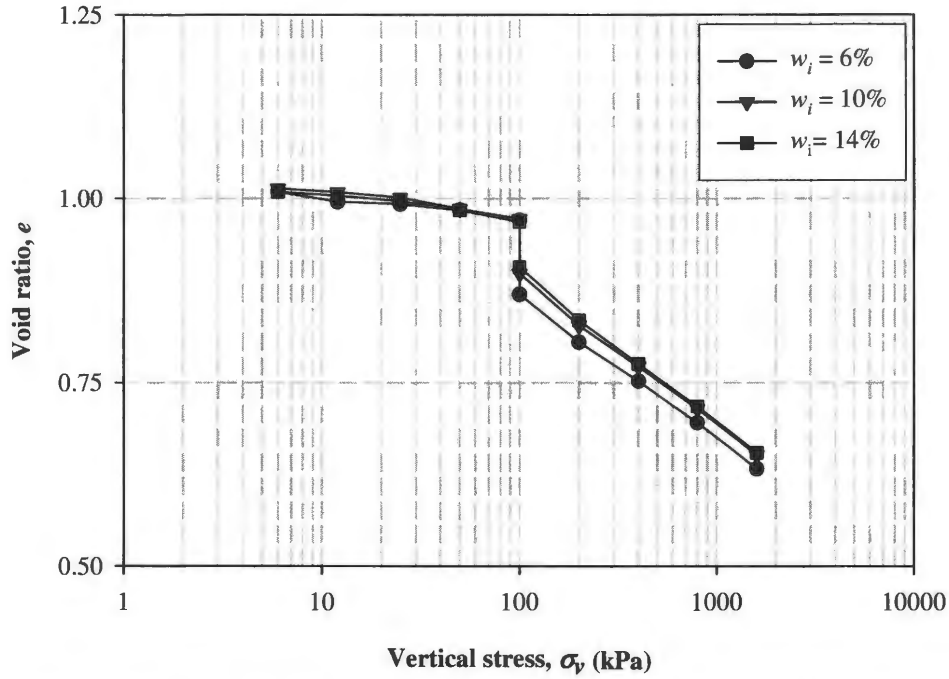

Figure 53 - *e* versus log σ_v curve (*SCS* = 200 kPa; σ_{fl} = 100 kPa).

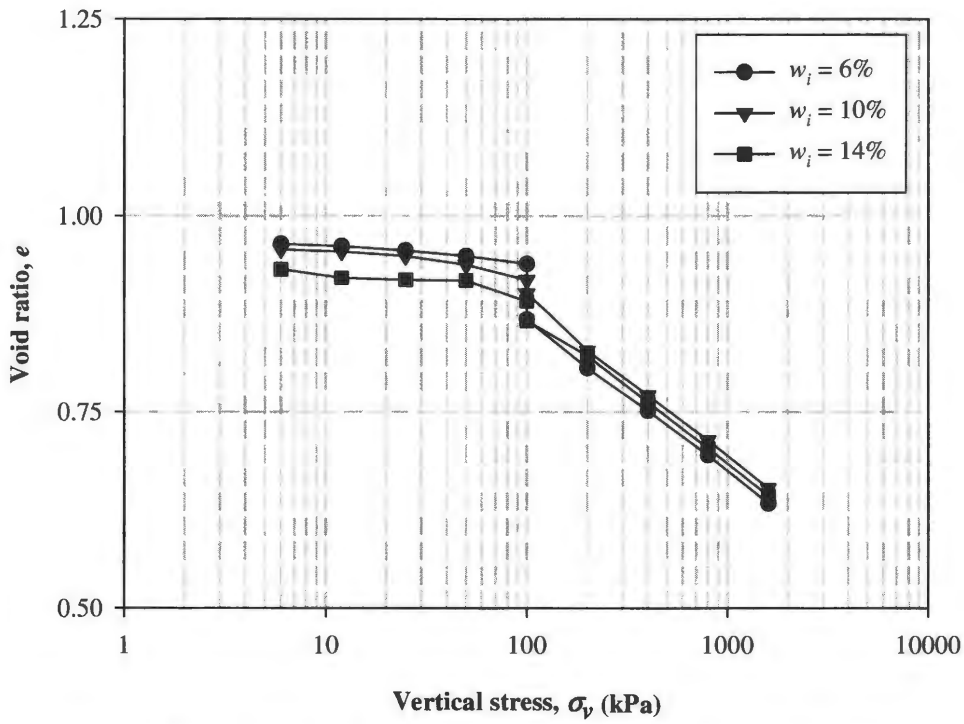

Figure 54 - *e* versus log σ_v curve (*SCS* = 300 kPa; σ_{fl} = 100 kPa).

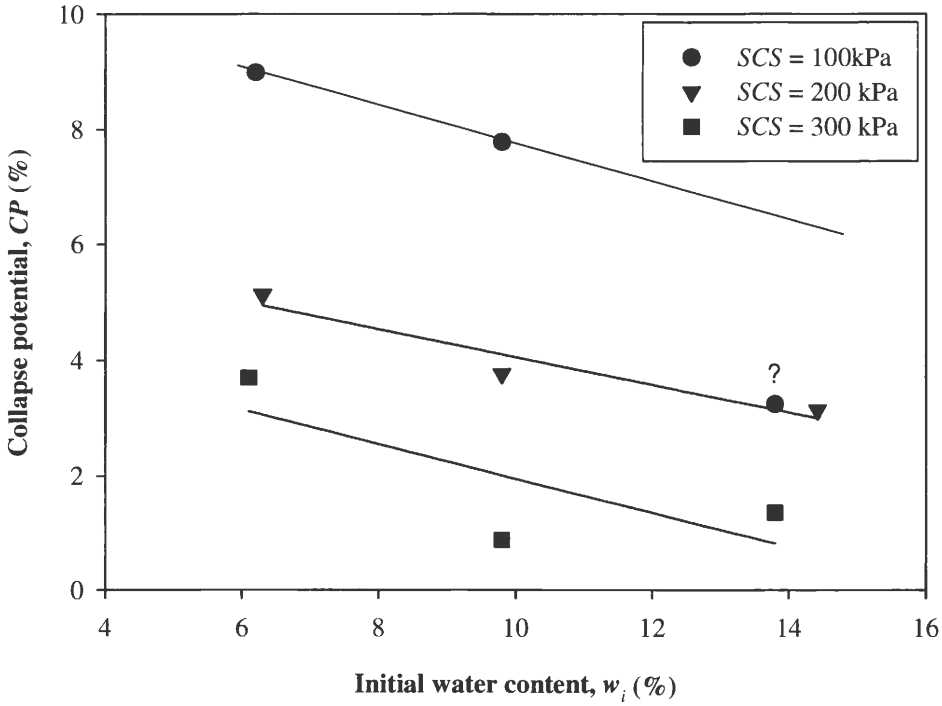

Figure 55 - Summarized collapse potential versus initial water content (σ_{fl} = 100 kPa).

Test series No.3: Staged inundation

Figure 56 shows the four stages of partial collapse of identical soil samples prepared using static compaction stress value of 100 kPa, in which variable amounts of water were added gradually to the sample, i.e. 5 ml of water at a time and the full collapse of the sample on complete inundation at a time. The legend shows the corresponding increase in water content in each stage with respect to the final water content attained in the previous stage. For stage 1 the increase in water content was calculated by subtracting the final water content from the initial water content. A very small variation in the initial void ratio from Figure 56 ensures the validity of the preparation of identical samples. It is evident from Figure 56 that collapse potential increased with increasing degree of saturation at a constant value of

flooding stress. Figures 57 and 58 also show similar trends for samples compacted using static compaction stress values of 200 kPa and 300 kPa.

Figure 59 shows the variation of partial collapse expressed as the ratio of partial saturation collapse potential and full collapse potential with the varying degree of saturation that was achieved by adding different amounts of water gradually at a constant value of flooding stress, i.e. 100 kPa. It can be seen from Figure 59 that the amount of collapse is increasing with increasing degree of saturation at the same value of vertical stress. However, different trends are obtained for different values of static compaction stresses used in the sample preparation. From Figure 59, the collapse degree of saturation for SCS = 100 kPa is somewhere between 78% and 100 %. The collapse degree of saturation for static compaction stresses 200 kPa and 300 kPa are 87% and 85% respectively, from Figure 59.

As obserevd by El-Ehwany and Houston (1990) and others, in wetting conditions well below 100% degree of saturation, collapse is only a fraction of that obtained in fully inundated laboratory specimens. The extent to which wetting occurs in the field also varies with depth. Hence, settlement calculations must be done considering the variation of degree of saturation with depth. Therefore, partial collapse curves are very useful in explaining the observed field settlements in partial wetting conditions.

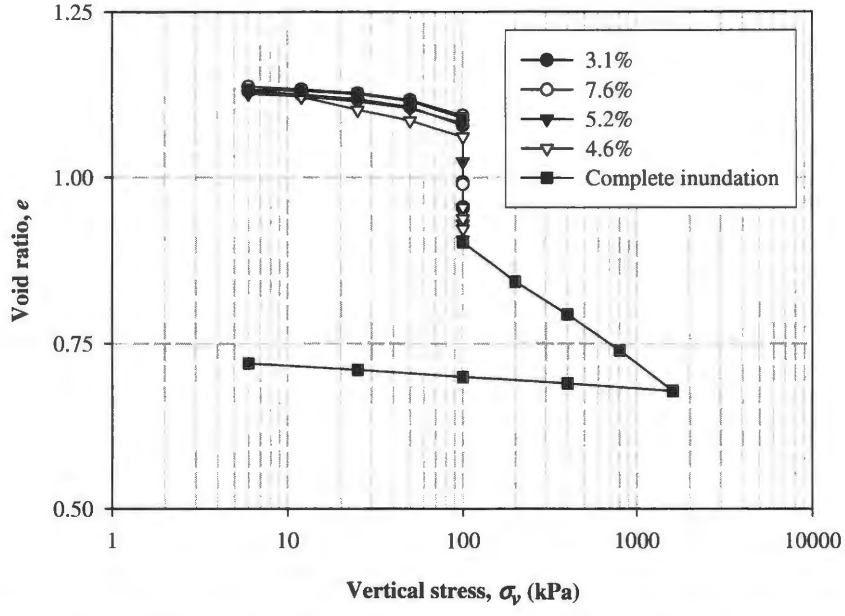

Figure 56 - e versus log σ_v curve – staged inundation (w_i = 6%; SCS = 100 kPa; σ_{fl} = 100 kPa).

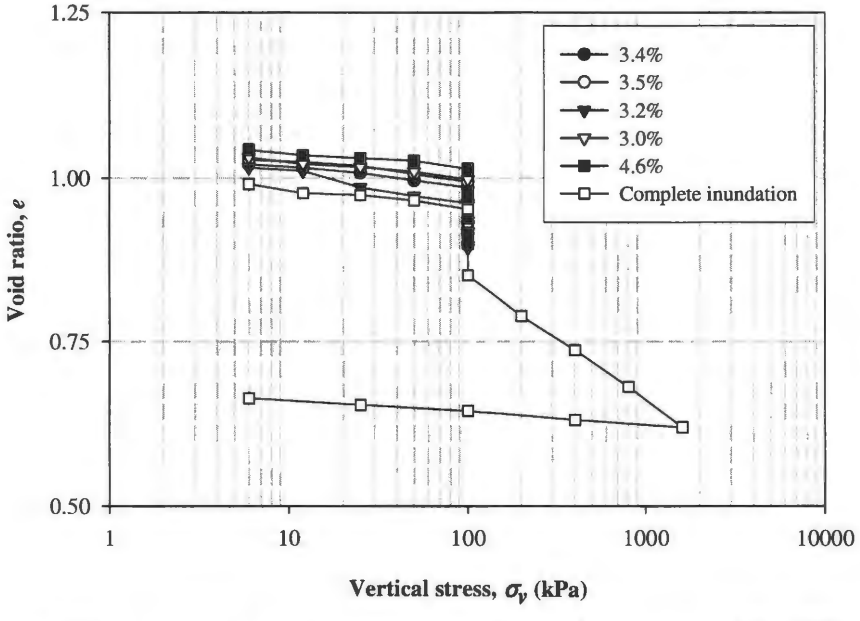

Figure 57 - e versus log σ_v curve – staged inundation (w_i = 6%; SCS = 200 kPa; σ_{fl} = 100 kPa).

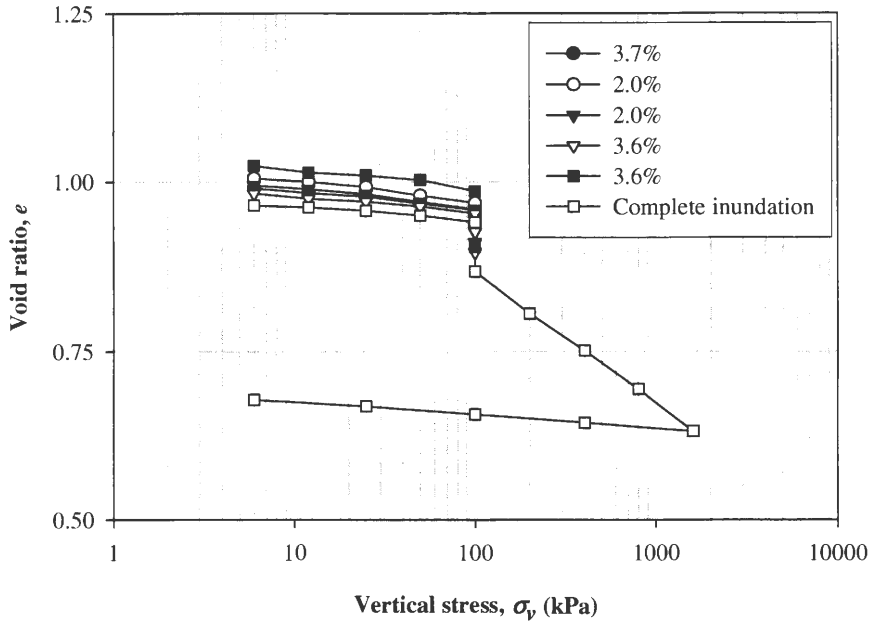

Figure 58 - e versus log σ_v curve - staged inundation (w_i = 6%; SCS = 300 kPa; σ_{fl} = 100 kPa).

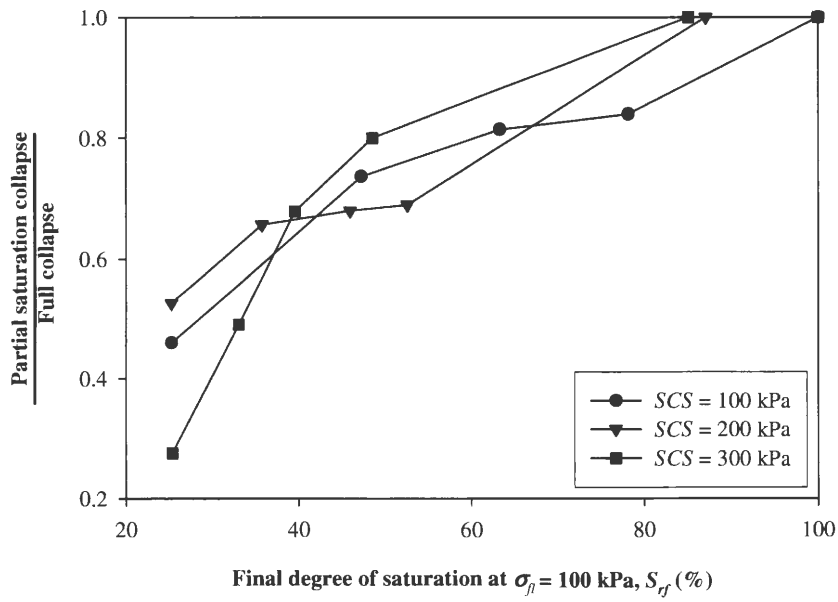

Figure 59 - Partial collapse curves (w_i = 6%; σ_{fl} = 100 kPa).

SHEAR STRENGTH TESTS

Proctor needle penetration tests

Figure 60 shows the variation of penetration resistance with static compaction stress and water content. The penetration resistance increased initially with increasing water content. However, it showed a decrease when water content reached higher values for all three compaction stress values used for preparing the samples. The initial increase in penetration resistance can be explained in terms of increasing dry density with increasing water content which increases the undrained shear strength also. Dry density increased from $w_i = 6\%$ to $w_i = 10\%$ and thereafter decreased. Therefore, the penetration resistance remained nearly constant with small changes in dry density. However, the penetration resistance increased with the increase in static compaction stress level for all water contents.

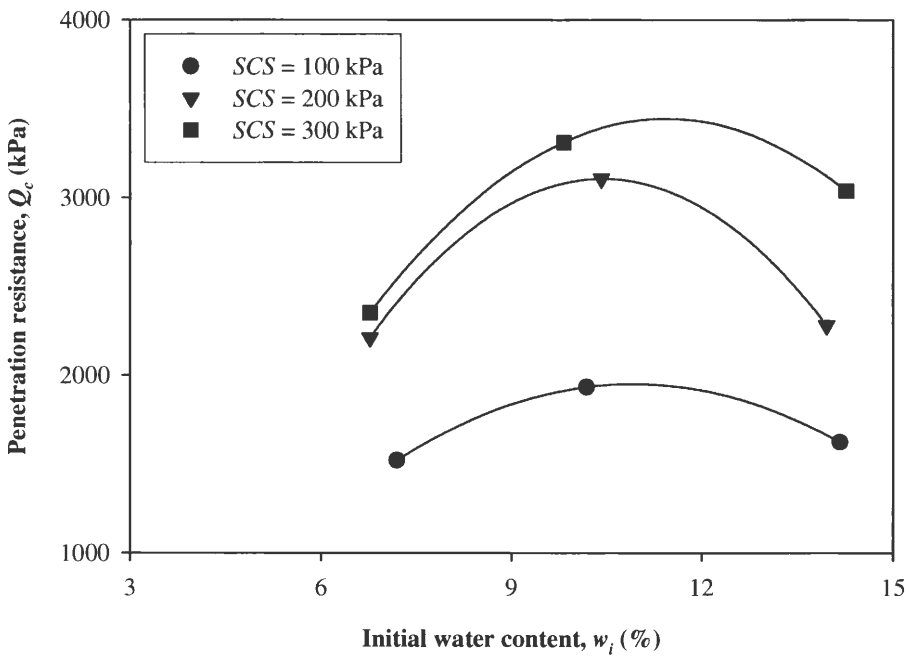

Figure 60 - Variation of penetration resistance with static compaction stress and water content.

Torvane shear tests

Figure 61 shows the variation of undrained shear strength, c_u obtained from Torvane shear tests at predetermined static compaction stress and water content. The c_u values increased initially with increasing water content. However, c_u decreased from the peak value with further increase in water content for all three compaction stress values used for preparing the test samples. However, c_u increased with increasing static compaction stress for all water contents except for static compaction stress of 300 kPa at 6%. The c_u for SCS = 300 kPa and w_i = 6% is smaller than the c_u for SCS = 200 kPa and w_i = 6%.

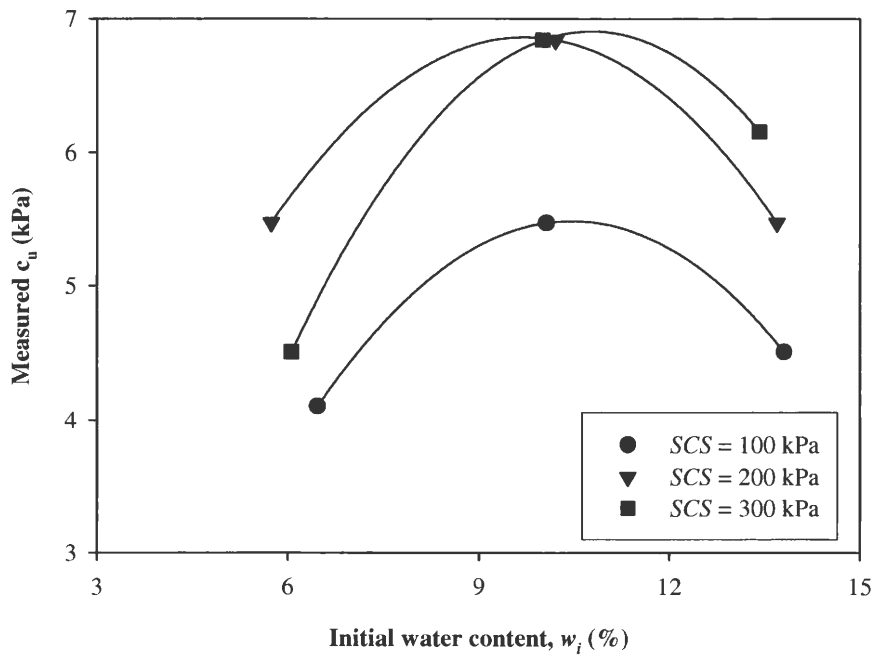

Figure 61 - Variation of measured c_u with static compaction stress and water content.

Prediction of c_u from penetration resistance

A relationship between the penetration resistance and c_u was proposed by Sanglerat (1972), given as follows:

$$Q_c = N_k c_u + P_o \tag{4}$$

where, Q_c = penetration resistance; c_u = undrained cohesion; P_o = total overburden pressure; and N_k = penetration constant.

From Equation 4, values of c_u can be predicted if the penetration resistance value is known. The measured values of c_u from Torvane shear tests are compared with the values of c_u predicted from the measured penetration resistance. The penetration resistance, Q_c was measured using a Proctor needle. As the Proctor needle tests were conducted in small molds, the overburden pressure, P_o in the Equation 4 was neglected. Similar study was done by Phani Kumar and Sharma (2004) to determine the penetration resistance of the soil mixed with fly ash by using a proctor needle with a shoe diameter 20 mm.

Different values of penetration constant, N_k were assumed corresponding to different static compaction stresses *(SCS)* used for the sample preparation as shown in Table 14. Figure 62 shows a linear relationship between static compaction stress, *SCS* and penetration constant, N_k.

Table 14 - Penetration resistance values for different static compaction stresses.

SCS (kPa)	N_k
100	350
200	425
300	500

A comparison of measured values of c_u obtained from Torvane shear test and valued of c_u predicted from penetration resistance is shown in Figure 63. An excellent correlation between c_u (measured) and c_u (predicted) is evident from Figure 63. Therefore, it can be said that the Equation 4 holds good for predicting c_u values for samples prepared using different compaction stress values.

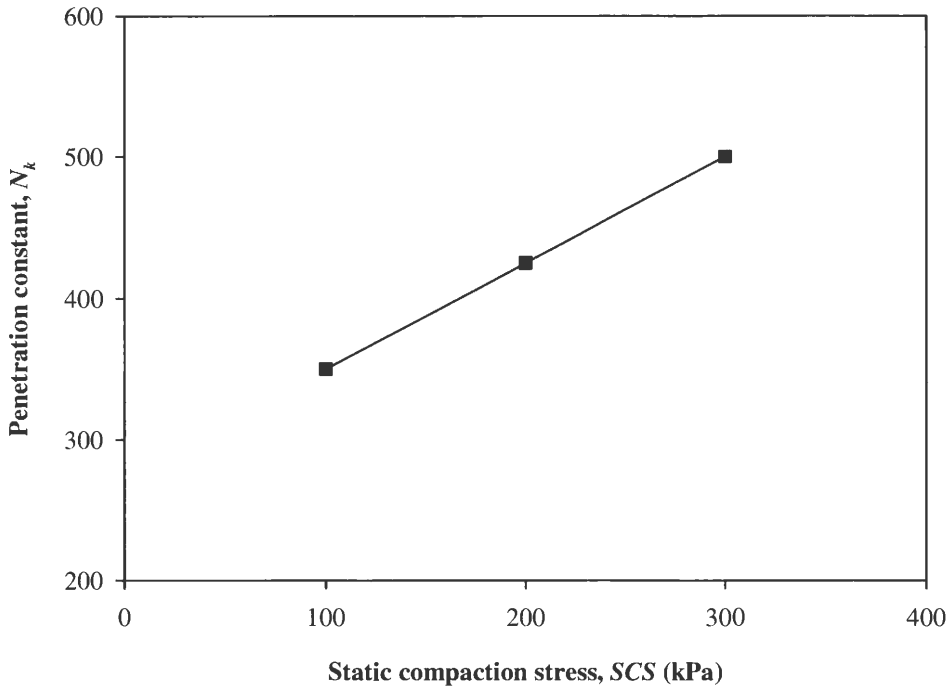

Figure 62 - Penetration resistance versus static compaction stress.

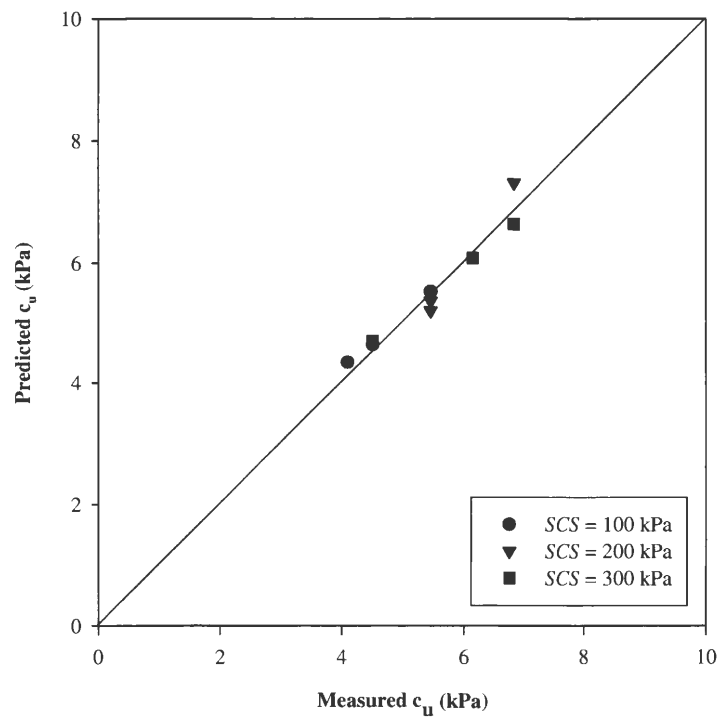

Figure 63 - Correlation between penetration resistances and shear strengths from Torvane shear test.

ESTIMATION OF COLLAPSE FROM PENETRATION RESISTANCE

Figure 64 shows the correlation between penetration resistance, collapse potential and field water content. The linear fit lines for collapse potential versus initial water content from Figure 55 and the parabolic fit for penetration resistance versus initial water content from Figure 60 are used in developing Figure 64. The proposed correlation can be used in estimating field collapse potential if penetration resistance and field water content is known. For example, if the field water content is 9% and penetration resistance is 2000 kPa then from Figure 64, the estimated value of collapse potential is 1% (as shown by point P in Figure 64). In addition to this Figure 64 also gives an estimation of the degree of compaction. However, the correlation is not validated as no field tests were conducted.

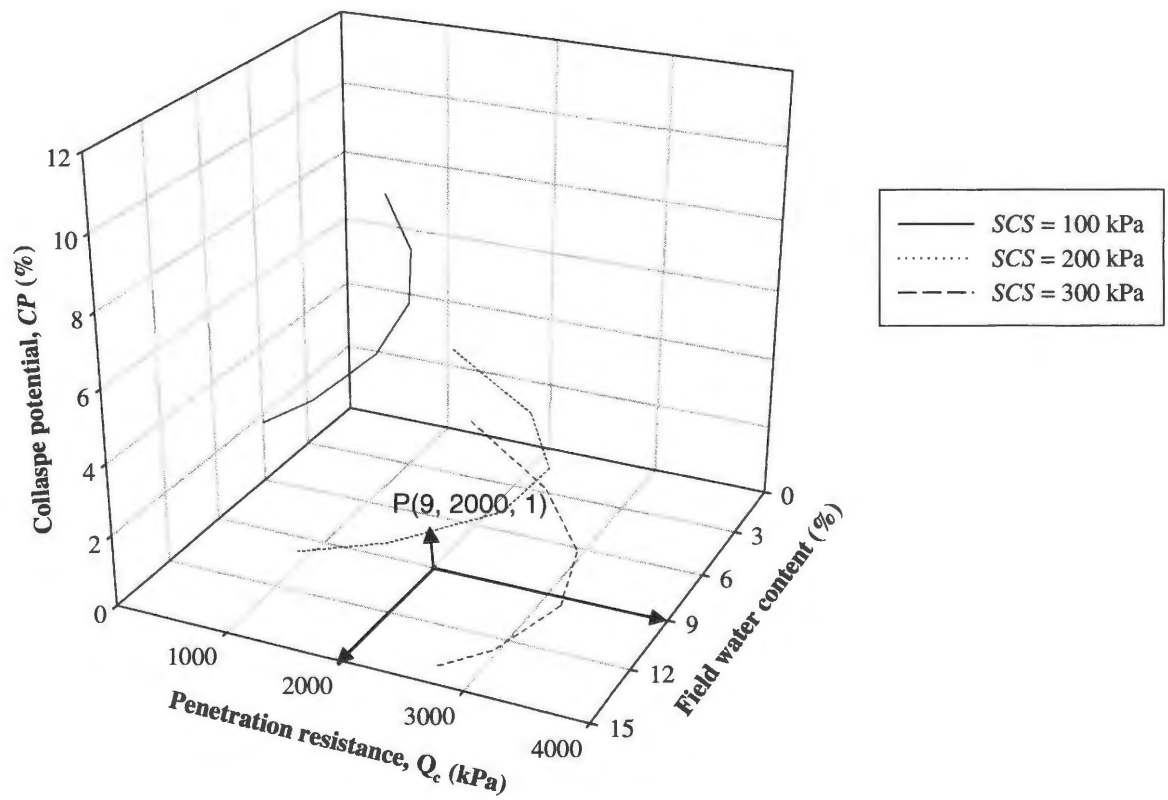

Figure 64 - Correlation between penetration resistance, collapse potential and field water content.

CHAPTER 5

SUCTION STUDY & CORRELATIONS WITH COLLAPSE POTENTIAL

SOIL WATER CHARACTERISTIC CURVES

A soil-water characteristic curve (SWCC) defines the relationship between water content and suction for a soil. The water content which defines the amount of water contained within the pores of the soil is commonly expressed using any one of the parameters such as gravimetric water content, w, volumetric water content, θ_w or degree of saturation, S_r. The relationship between volumetric water content, degree of saturation and gravimetric water content is given by:

$$\theta_w(1+e) = S_r e = wG_s \tag{5}$$

where, G_s is the specific gravity of soil solids.

A normalized form of water content can also be used using residual water content as the reference water content (Fredlund and Xing, 1994). The residual water content is the water content where a large change in suction is required to remove additional water from the soil. The residual water content refers to the residual state condition when the water phase is discontinuous and isolated with thin films of water surrounding the soil and air (Vanapalli *et al.* 1998). A typical plot of a soil-water characteristic curve for a silty soil is shown in Figure 65, along with some of its key characteristics. Figure 65 shows a consistent way to define the

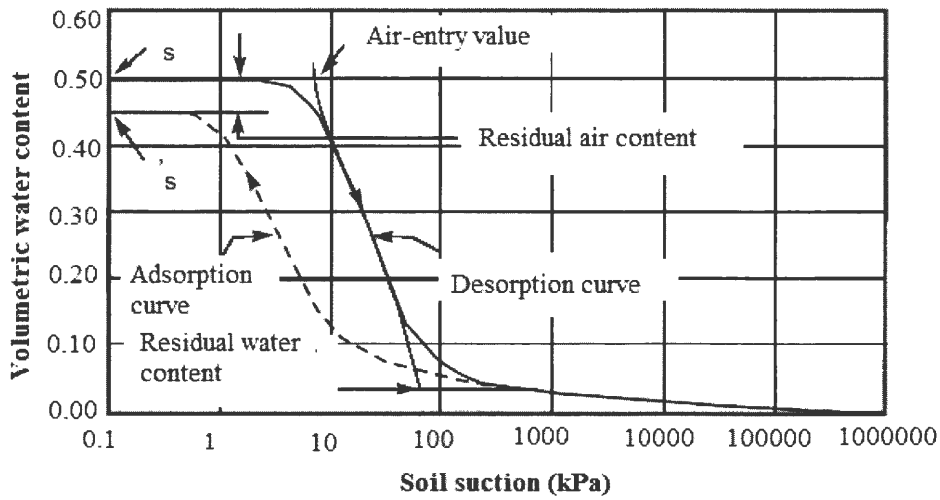

Figure 65 - Typical soil water characteristic curve for a silty soil (after Fredlund and Xing, 1994).

residual water content. A tangent line is drawn from the inflection point in an SWCC and the curve in the high-suction range is approximated by another line. The ordinate of the point at which the two lines intersect represents the approximate value of residual water content θ_r as shown in Figure 65 (Fredlund and Xing, 1994). However, as the soil-water characteristic curve is a continuous function and there is no specific point on the SWCC that can be called the residual water content. Therefore, most researchers consider residual water content as a fitting parameter with no real physical significance (Vanapalli *et al.* 1998; van Genuchten, 1991; van Genuchten, 1980), or avoid the controversy by using a correction factor (Fredlund and Xing, 1994). The air-entry value of the soil (i.e., bubbling pressure) as shown in Figure 65 is the matric suction where air starts to enter the largest pores in the soil.

Matric suction ($(u_a - u_w)$, where u_a is the pore-air pressure and u_w is the pore-water pressure) is usually used for the SWCC. However, total suction (matric plus osmotic suction) is also used, though occasionally (Fredlund and Xing, 1994; Zapata *et al.* 2000). SWCCs for

soils with low suction range are often presented using an arithmetic scale. However, SWCCs over the entire suction range are often plotted using a logarithmic scale.

The main curve in Figure 65 is a desorption curve. The adsorption (wetting) curve differs from the desorption curve (drying) as a result of hysteresis. The end point of the adsorption curve may differ from the starting point of the desorption curve because of air entrapment in the soil (Fredlund and Xing, 1994). The hysteretic nature of the soil-water characteristic curve is reported by many authors including Croney (1952). As a result of "hydraulic hysteresis" the wetting and the drying paths possess different degrees of saturation at a given value of suction, as illustrated schematically in Figure 65. A significant effect of hysteresis is in the transition between saturated and unsaturated conditions, which occurs at different values of suction on drying and wetting path (Wheeler *et al.* 2003). On drying curve, a saturated soil remains saturated until the suction exceeds air entry value (Bishop *et al.* 1975). In contrast, on wetting curve the degree of saturation remains significantly below unity on lowering down suction values even up to zero (Sharma, 1998; Sivakumar, 1993; Wheeler *et al.* 2003).

IMPORTANCE OF SOIL WATER CHARACTERISTIC CURVES

A relationship between the soil-water characteristic curve for a particular soil and the properties of unsaturated soil has been found from laboratory studies (Fredlund and Rahardjo, 1993; Fredlund and Xing, 1994). For example, experimental evidence supported a significant influence of both soil suction and degree of saturation on stress-strain behavior of an unsaturated soil (Wheeler *et al.* 2003; Gallipoli *et al.* 2003). Similarly, by examining the nature of the relationship between matric suction and degree of saturation under cycles of

drying and wetting, the effects of fluctuations of groundwater table on LNAPL(light non-aqueous phase liquids) distribution can be analyzed and quantified (Sharma and Mohamed, 2003a & b). The determination of permeability function for an unsaturated soil by using the saturated coefficient of permeability and the soil-water characteristic curve has become a common practice now (Marshall 1958; Mualem 1986; University of Saskatchewan 1984). Also, various procedures have been suggested to determine the shear strength properties of unsaturated soils (Fredlund and Rahardjo, 1993). In this chapter the soil-water characteristic curve is used as a basis for the prediction of collapse behavior of a collapsible soil by coupling the suction-saturation relationship for a collapsible soil with collapse potential.

DETERMINATION OF SOIL WATER CHARACTERISTIC CURVES

Tests were conducted using pressure plate apparatus to determine desorption (drying) portion of the soil water characteristic curves (SWCC) using a pressure plate extractor. The unsaturated soil behavior was studied by using SWCCs for nine different conditions produced by varying initial water contents and static compaction stresses. The range of suction used in the testing was 10 - 400 kPa and hence, the resulting conclusions should be limited to this range only. Soil-water characteristic curves are plotted over the entire suction range (10 - 400 kPa) by using a logarithmic scale. As the soil samples were compacted using different initial water contents and different static compaction stress levels, the soil samples can be considered as different soils based on the soil fabric though the mineralogical composition, plasticity and texture of the soil is same (Vanapalli *et al.* 1996).

Saturation volumetric water contents, θ_s for the first six tests performed at initial water contents of 6% and 10% and compacted at SCS values of 100 kPa, 200 kPa and 300

kPa, respectively were determined by measuring the weight of water in soil samples by oven drying after application of the lowest value of suction that could be applied (as the degree of saturation was found out to be 100%) and final volume of the samples. The final volume of the soil samples were determined by deducting the volume of the poured wax over the sample in the ring from the volume of the ring. For the tests conducted at 14% initial water content, the saturation volumetric water content was calculated theoretically from the initial volume of the soil samples and the volume of soil solids in the compacted specimens. Due to the lack of measured SWCC data in the high-suction range, the value of residual water content (θ_r) could not be determined. However, an estimation of residual water content (θ_r) based on the extrapolated SWCC.

Curve fitting of the experimental data for SWCCs is done by using van Genuchten (1980) model which is expressed as

$$\frac{\theta - \theta_r}{\theta_s - \theta_r} = \frac{1}{\left[1 + \left(\frac{s}{\alpha}\right)^n\right]^m} \tag{6}$$

where, s is the suction, θ is the corresponding volumetric water content on the drying curve and θ_r, α, n, and m are the optimized parameters. To improve the stability of the curve fitting process the parameter m is set to $1 - n^{-1}$ (van Genuchten *et al.* 1991). The parameter α is directly proportional to the air entry value and is the pivot point of the SWCC curve. The slope of the SWCC about the pivot point is controlled by the parameter n, which occurs at normalized volumetric water content (Θ) of 0.5, where:

$$\Theta = \frac{(\theta - \theta_r)}{(\theta_s - \theta_r)} \tag{7}$$

As n increases, the slope of the SWCC between s_a and the knee (the point of inflection at the lower portion of the curve as it becomes asymptotic) becomes steeper. The rotation of the sloping portion of the curve is controlled by the parameter m. With an increase in m, the range of the SWCC between s_a and the knee becomes narrower (Leong and Rahardjo, 1997).

The curve fitting parameters for all nine SWCCs from van Genuchten model are given in Table 15. The fitting parameters were calculated based on the minimum sum of the squared residual (SSR) defined as

$$SSR = \sum_{i=1}^{n} w_i(\theta_i - \theta_{ci})^2 \tag{8}$$

where, w_i = weighing factor; θ_i = measured water content at a certain pressure level; and θ_{ci} = calculated water content from van Genuchten model at the same pressure level. The best fit was assumed to be the one that resulted in the minimum SSR value. The value of weighing factor was chosen as 1 by assuming the equal significance of all the data points. The SSR values for each of the fitted SWCC are provided in Table 15. The experimental and fitted values of volumetric water content corresponding to their suction values are given in Appendix B.

The soil water characteristic curves obtained using van Genuchten model are shown in Figure 66 to Figure 74 corresponding to their initial placement conditions. Figure 75 shows the typical soil water characteristic curve for a clay soil. On comparing the obtained SWCCs for loess with that of clay, it can be seen that the SWCCs for loess are to the left of the SWCC for clay. Also, the air-entry value, residual volumetric water content and saturated

volumetric water content for loess which is a silty soil are smaller than that for clay. In all cases, the SSR is less than 10^{-3}.

In general less the plasticity of a soil, the less the amount of water available for removal at higher suction levels say from 100 to 1,000 kPa as the more significant fraction of moisture was removed in the 0-100 kPa pressure range (Miller *et al.* 2002). Therefore, for low plasticity or non-plastic soils, the slope of the SWCC will be almost flat at these suction levels as the release of water is smallest for the given change in suction. This trend can be seen for all the obtained SWCCs for loess which is a silty soil.

Table 15 - Soil water characteristic curve fit parameters for van Genuchten model.

	$w_i = 6\%$			$w_i = 10\%$			$w_i = 14\%$		
***SCS* (kPa)**	100	200	300	100	200	300	100	200	300
α (kPa x 10^2)	0.38	0.38	0.27	0.29	0.35	0.26	0.07	0.06	0.07
n	6.70	6.80	17.00	6.17	5.40	11.40	2.20	2.00	2.00
m_r	0.85	0.85	0.94	0.84	0.81	0.91	0.55	0.47	0.44
θ_r	0.12	0.12	0.12	0.13	0.12	0.13	0.14	0.14	0.15
SSR	1.9E-04	3.0E-04	6.5E-03	4.3E-04	8.1E-04	3.4E-03	1.4E-04	8.0E-04	8.4E-04

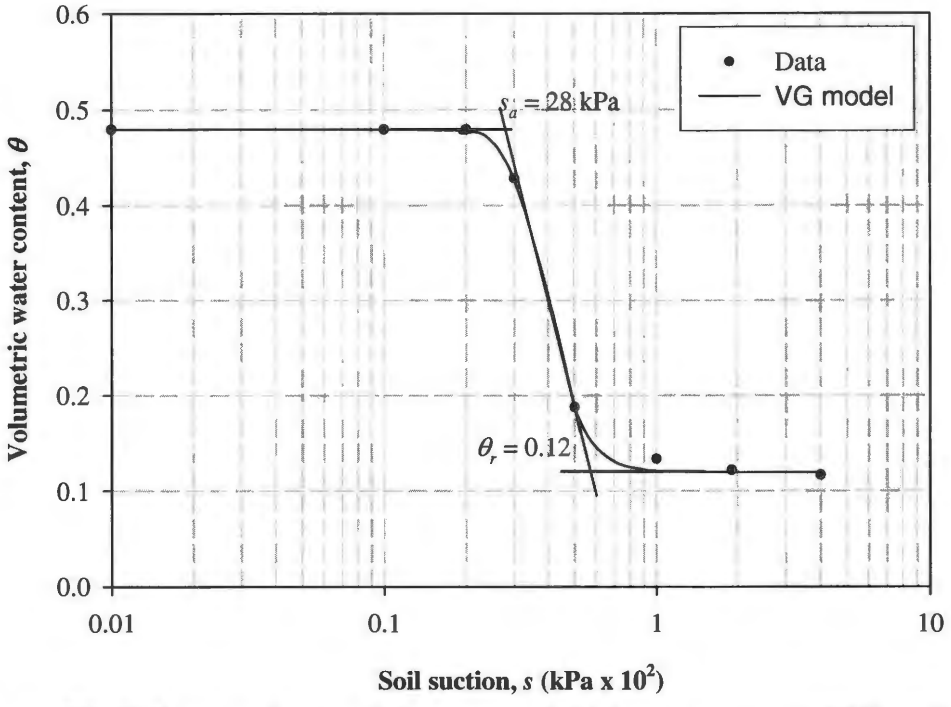

Figure 66 - Soil water characteristic curve at initial water content of 6% and static compaction stress of 100 kPa.

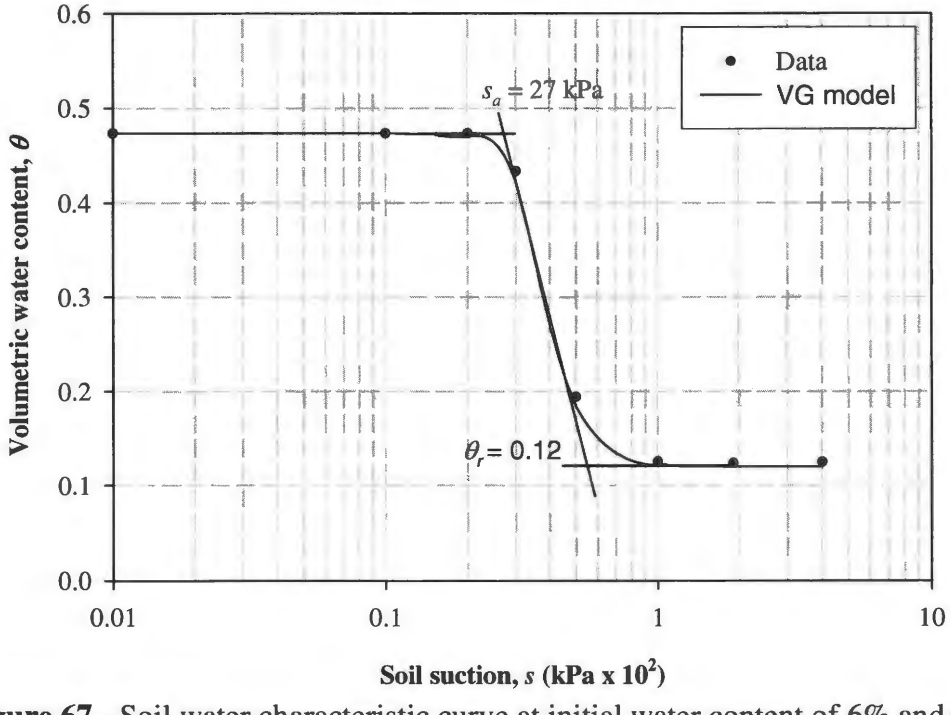

Figure 67 - Soil water characteristic curve at initial water content of 6% and static compaction stress 200 kPa.

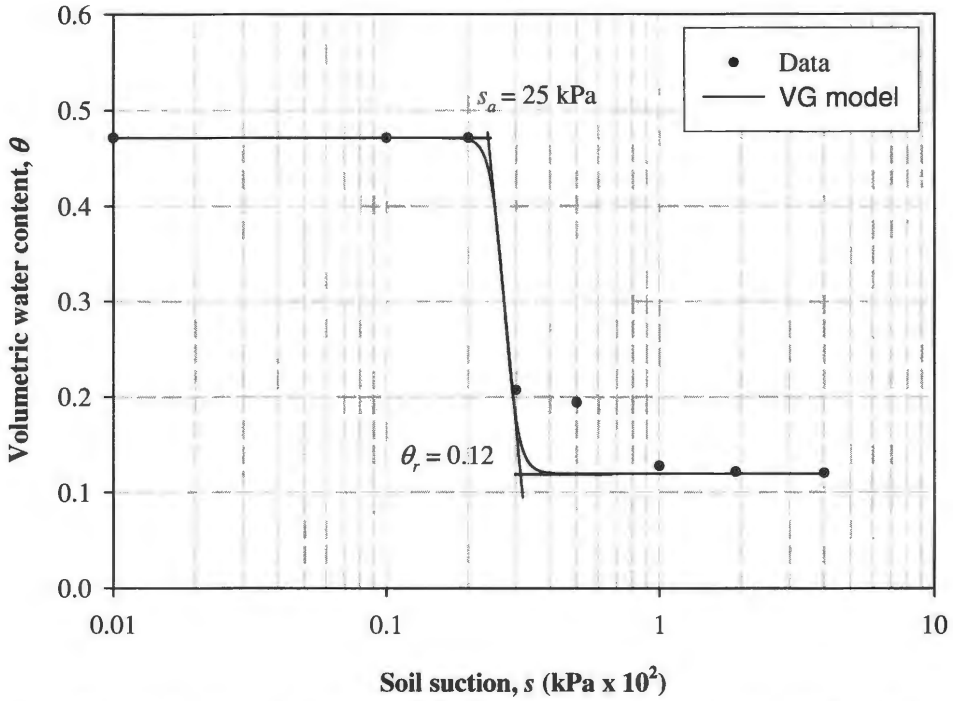

Figure 68 - Soil water characteristic curve at initial water content of 6% and static compaction stress 300 kPa.

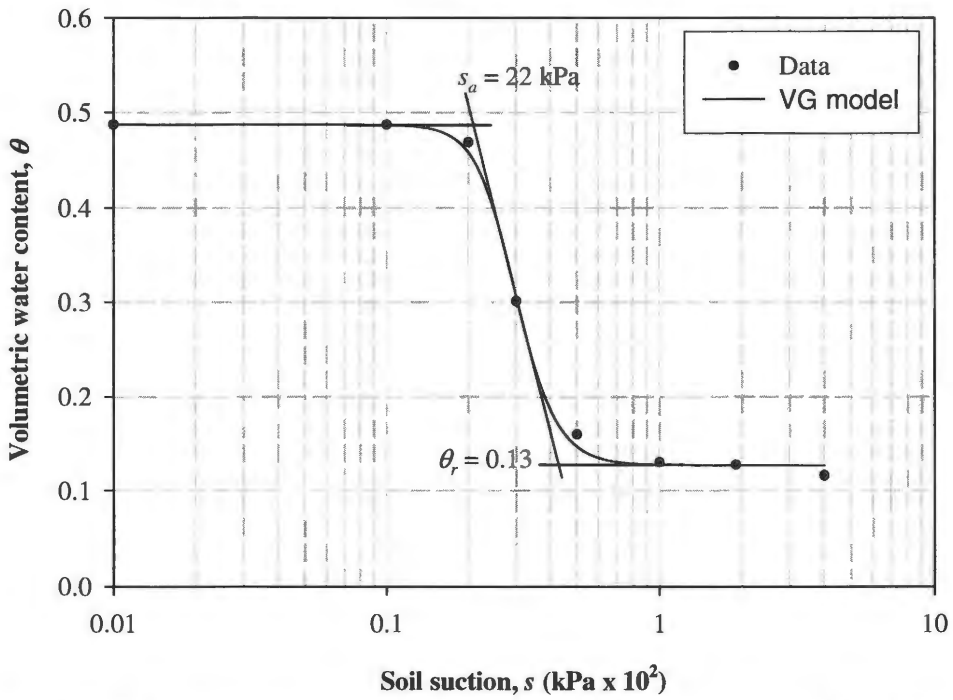

Figure 69 - Soil water characteristic curve at initial water content of 10% and static compaction stress of 100 kPa.

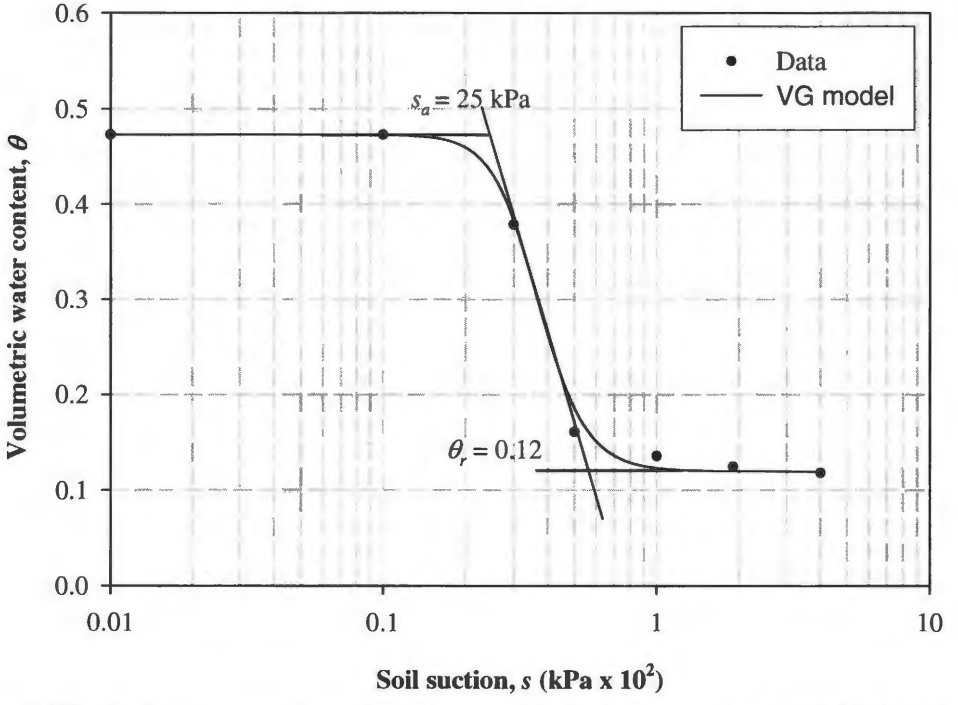

Figure 70 - Soil water characteristic curve at initial water content of 10% and static compaction stress of 200 kPa.

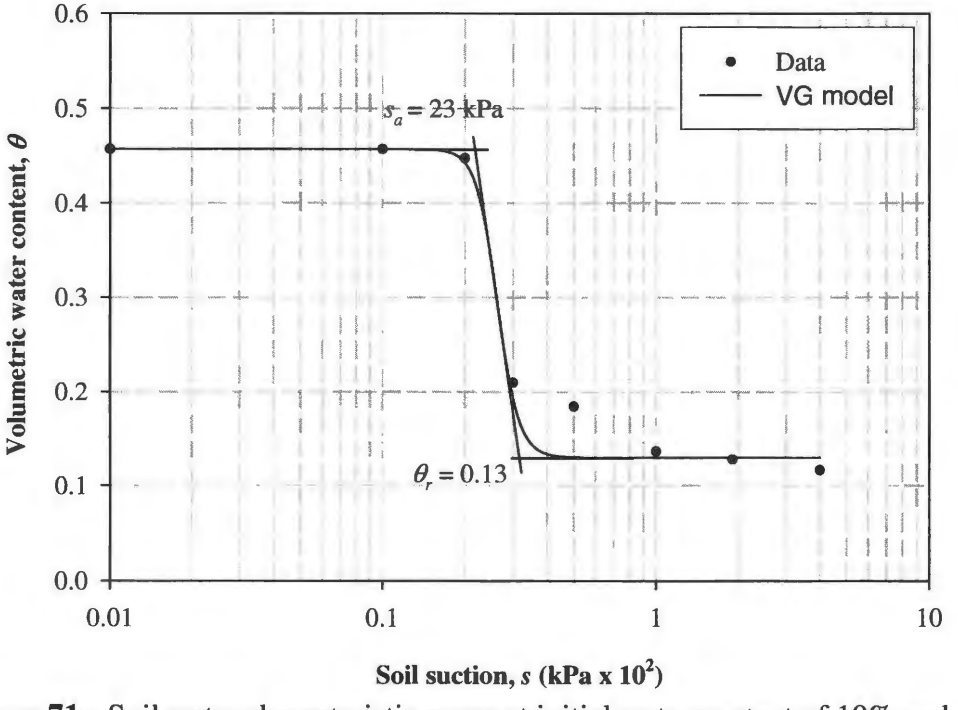

Figure 71 - Soil water characteristic curve at initial water content of 10% and static compaction stress of 300 kPa.

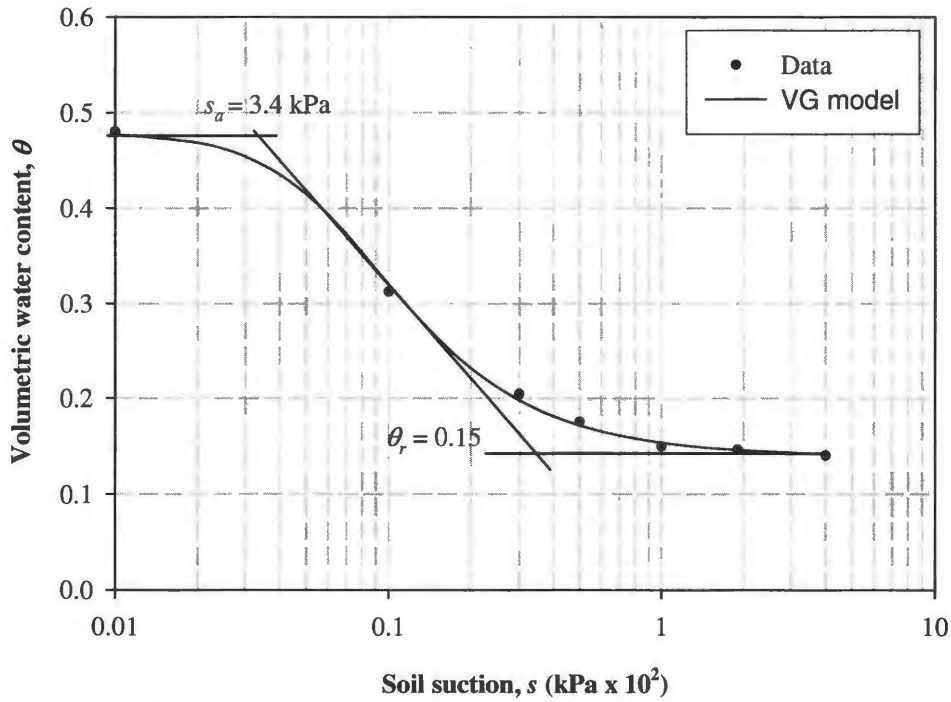

Figure 72 - Soil water characteristic curve at initial water content of 14% and static compaction stress of 100 kPa.

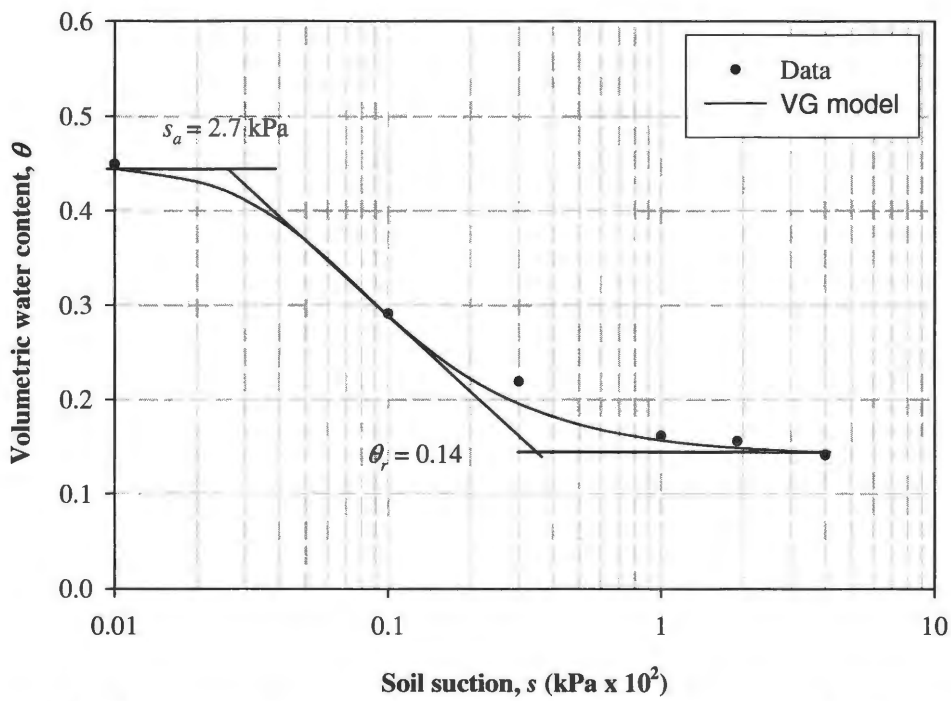

Figure 73 - Soil water characteristic curve at initial water content of 14% and static compaction stress of 200 kPa.

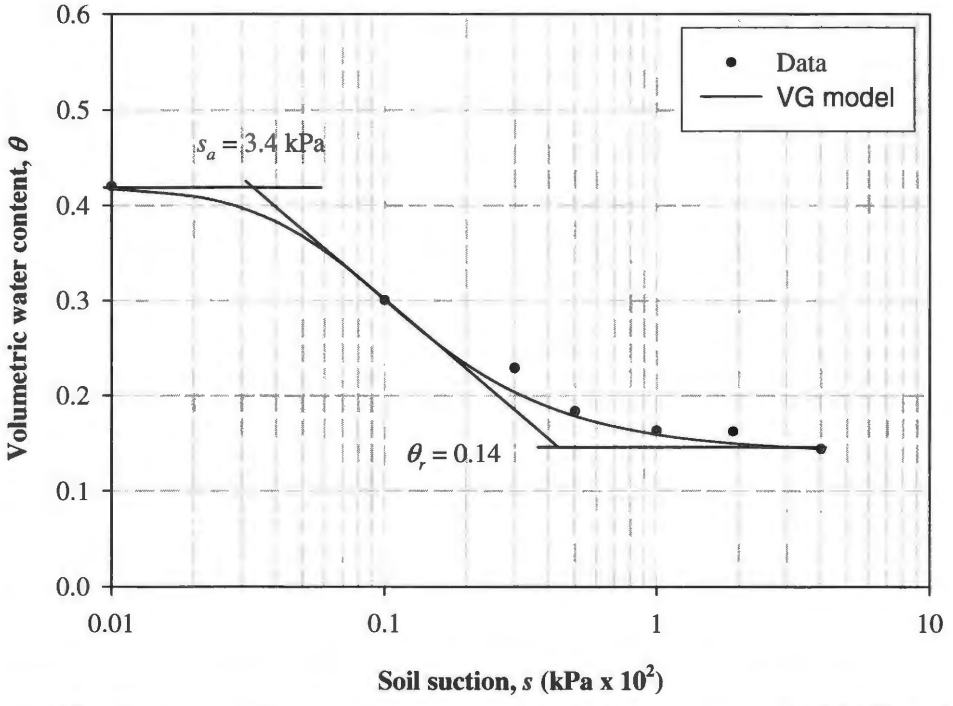

Figure 74 - Soil water characteristic curve at initial water content of 14% and static compaction stress of 300 kPa.

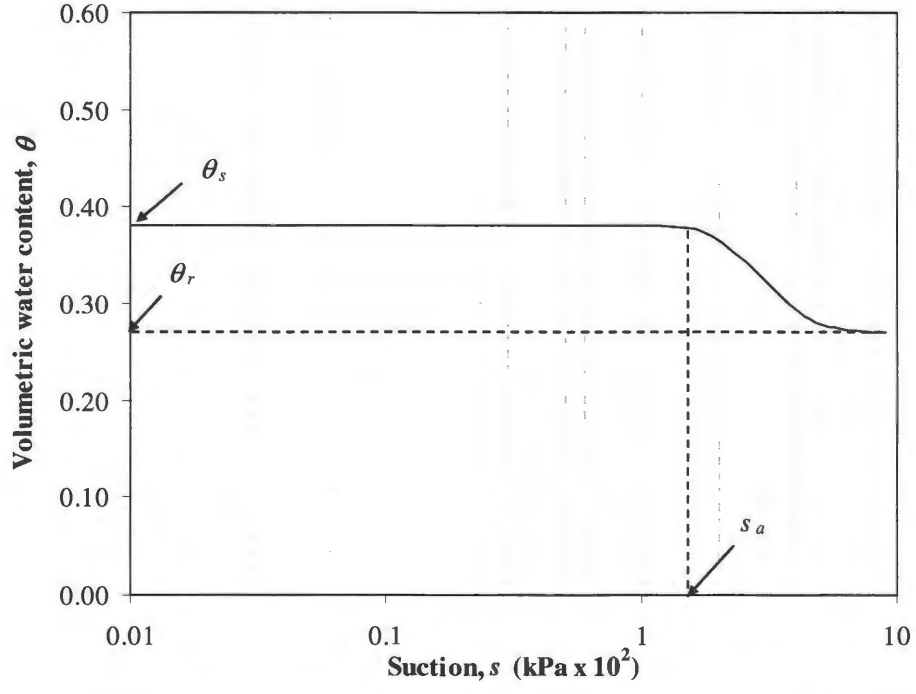

Figure 75 - Typical soil water characteristic curve for a clay soil (after Miller *et al.* 2002).

Variation of soil water characteristic curves with compaction conditions

In general, the SWCCs for higher-compaction efforts lie above the SWCCs for lower-compaction efforts for the same initial water content. The pore size of the soil samples decreases with increase in compaction efforts for the same water content. The decrease in pore sizes leads to an increase in pore water suctions. A link can be made between pore radius and the radius of curvature. As the pore radius decreases the radius of curvature also decreases. The matric suction, s is related to the radius of curvature of the meniscus, R_s by the following equation:

$$s = \frac{2T}{R_s} \tag{5}$$

where, T is the surface tension of water. The effect of varying compaction effort on matric suction varies with plasticity of the soils. This effect is more significant for a high-plasticity soil than for a low plasticity soil. In high-plasticity soils, the increase in compaction efforts lead to the largest percentage change in unit weight and hence, in void ratio. The large range of variation in unit weight with varying compaction efforts in high-plasticity soils leads to a more pronounced variation in the respective locations of the SWCC curves (Miller *et al.* 2002).

From Figure 76, it can be seen that there is not much effect of varying static compaction stress on the residual water contents (θ_r) for initial water content of 6%. However, there is a small decrease in the air entry values (s_a) as the static compaction stress is increased. A summary of approximate air entry values determined from the SWCCs is given in Table 16. No specific conclusions can be drawn from Table 16. From Figure 77 and Figure 78, the saturation volumetric water content is decreasing as the compaction effort is

increasing at constant water content. Figure 78 shows that the air entry values (s_a) for all the three curves lies below 10 kPa suction which is the minimum suction level that could be maintained using the available pressure plate apparatus. As θ_r is more dependent on the type of soil than the soil structure, the residual water content seems to be fairly constant for all three compaction stress values used for all three moisture contents 6%, 10% and 14%. However, the exact values of θ_r could not be confirmed due to the lack of experimental data.

Table 16 - Air entry value and saturation volumetric water content from SWCCs.

	$w_i = 6\%$		$w_i = 10\%$		$w_i = 14\%$	
***SCS* (kPa)**	s_a	θ_s	s_a	θ_s	s_a	θ_s
100	28	0.48	22	0.49	3.4	0.48
200	27	0.47	25	0.47	2.7	0.45
300	25	0.47	23	0.46	3.4	0.42

A crossover in SWCCs for different compaction efforts can be seen in Figure 77 and Figure 78, except for *SCS* = 300 kPa in Figure 77. At the crossover point a reversal in the relative positions of the curves occurs. The reason for this cross over is the largest value of θ_s (see Table 16) for the least compacted soil. However, on increasing suction after the cross over value less water content available is for any associated suction for the least compacted as compared to more compacted soils. This crossover occurs at approximately 20 kPa suction, which is also the approximate value of the air-entry suction for SWCC 10% initial water content. Nothing could be said about Figure 78 due to the lack of the data points below 10 kPa suction. However, at higher suction range of 100 kPa - 400 kPa the SWCCs for all the static compaction stress values were found to converge to a same value of residual water content of 0.14.

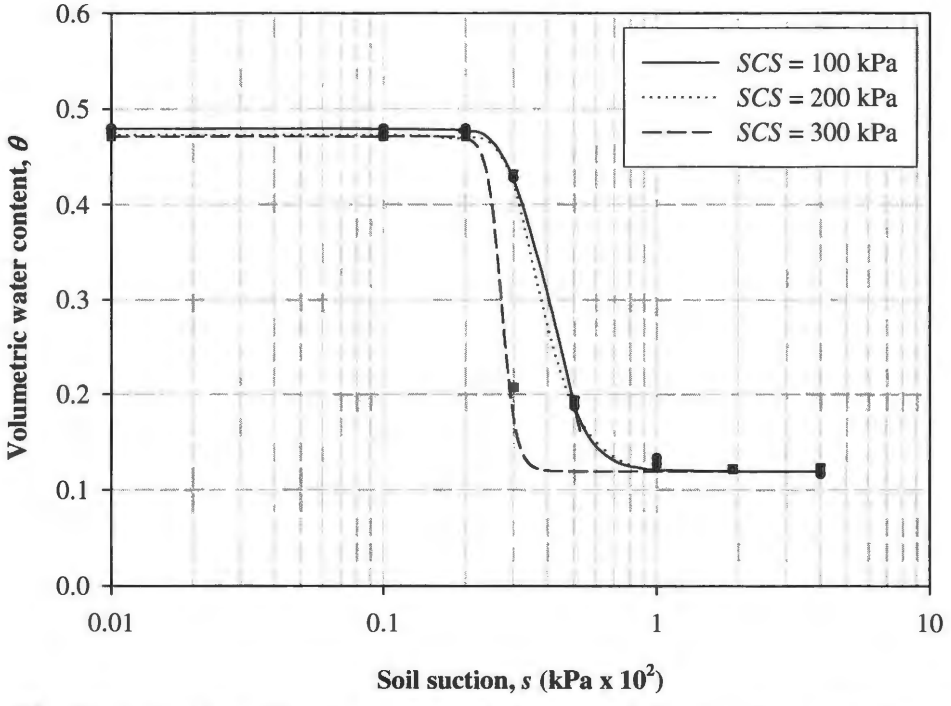

Figure 76 - Variation in soil water characteristic curve behavior due to static compaction effort at w_i = 6%.

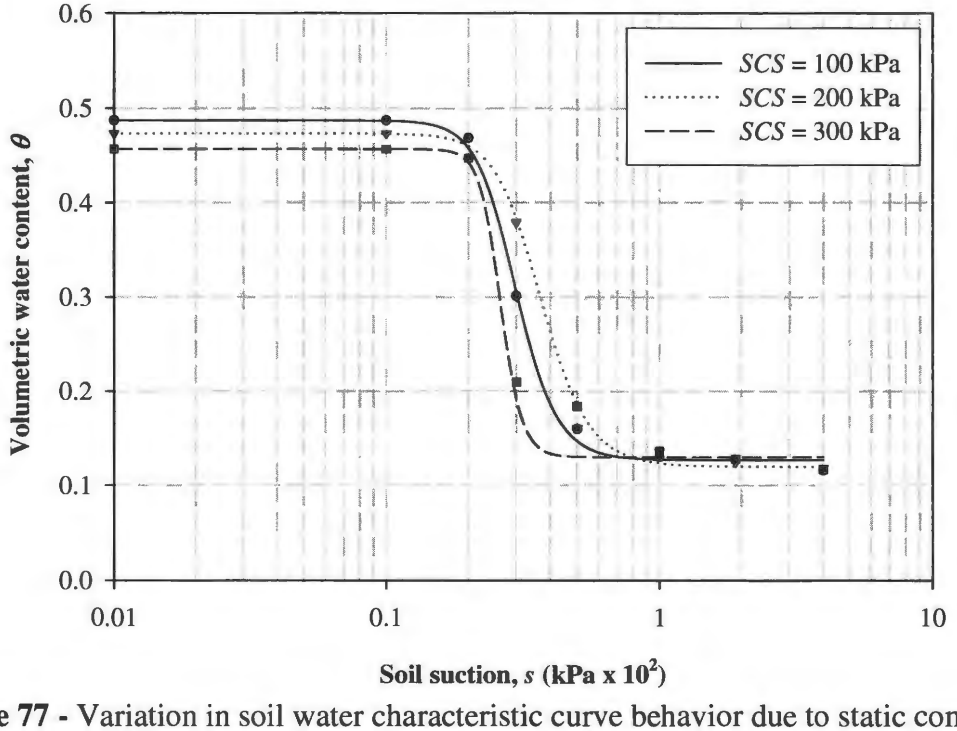

Figure 77 - Variation in soil water characteristic curve behavior due to static compaction effort at w_i = 10%.

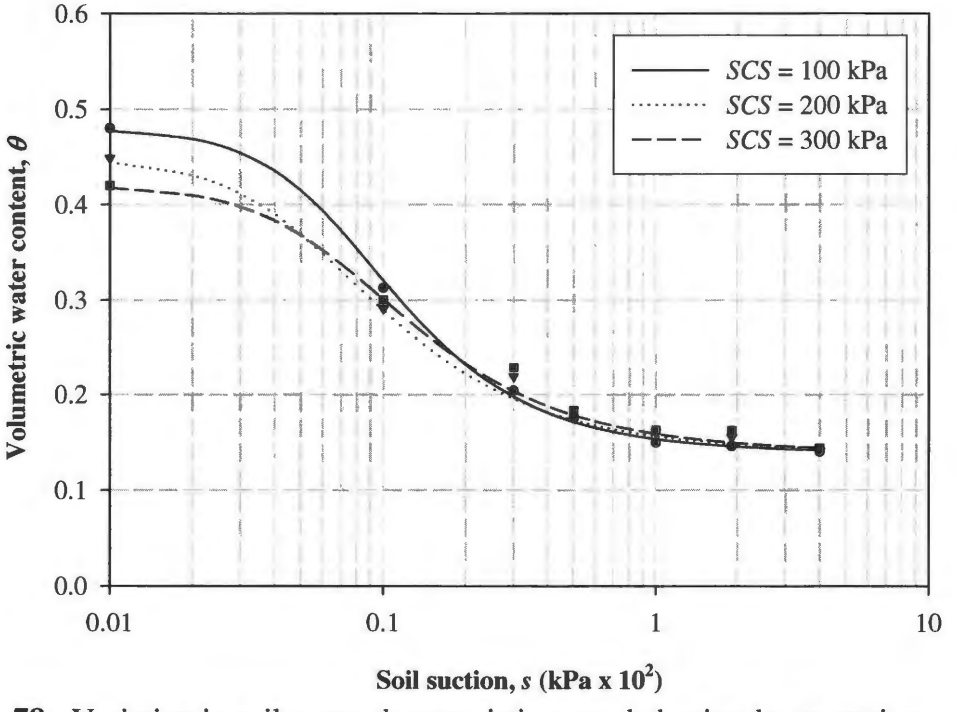

Figure 78 - Variation in soil water characteristic curve behavior due to static compaction effort at w_i = 14%.

Variation of soil water characteristic curves with initial water contents

From Figures 79, 80 and 81, the variation in compaction water content resulted in a significant variation in the resulting SWCC. The data of Marinho and Chandler (1993) and Miller *et al.* (2002) indicate that the SWCCs were essentially independent of the compaction water content. However, from Table 15, an increase in the residual water content values was observed with increasing initial water content. The values of parameter α also indicate that the air entry suction values reduced as the initial water content increased. This can be observed in the Figures 79, 80 and 81 also.

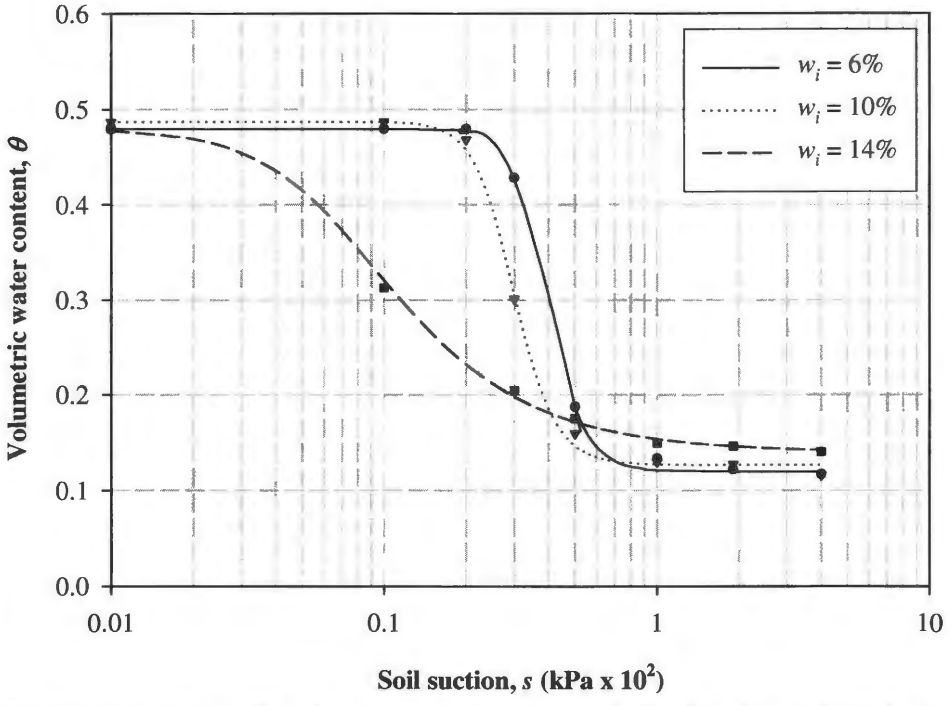

Figure 79 - Variation in soil water characteristic curve behavior due to initial water content at SCS = 100 kPa.

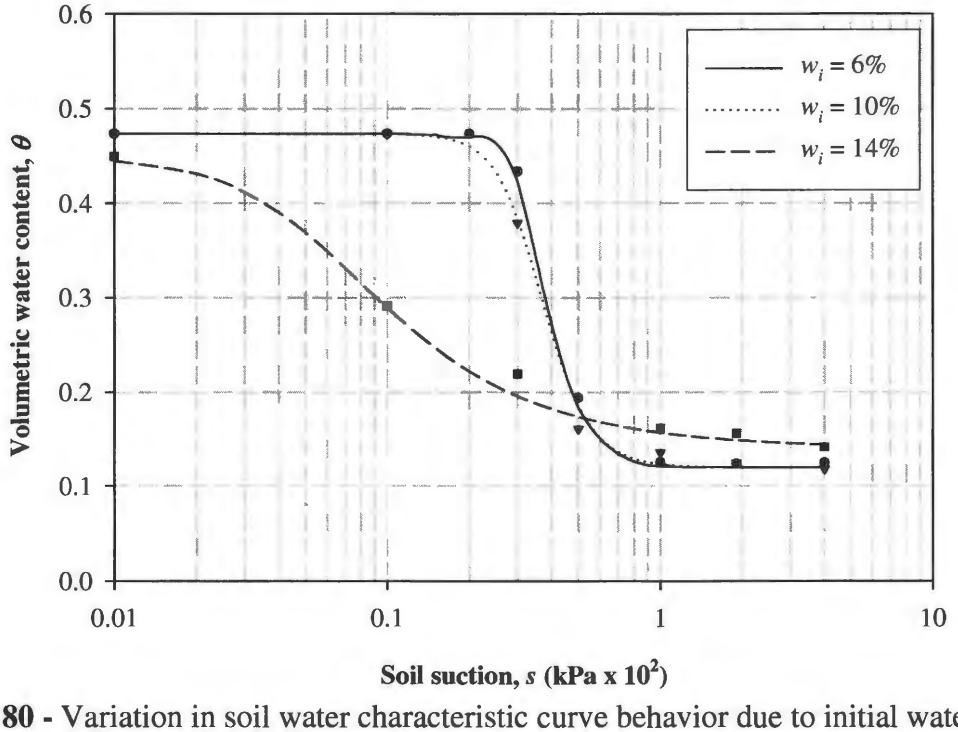

Figure 80 - Variation in soil water characteristic curve behavior due to initial water content at SCS = 200 kPa.

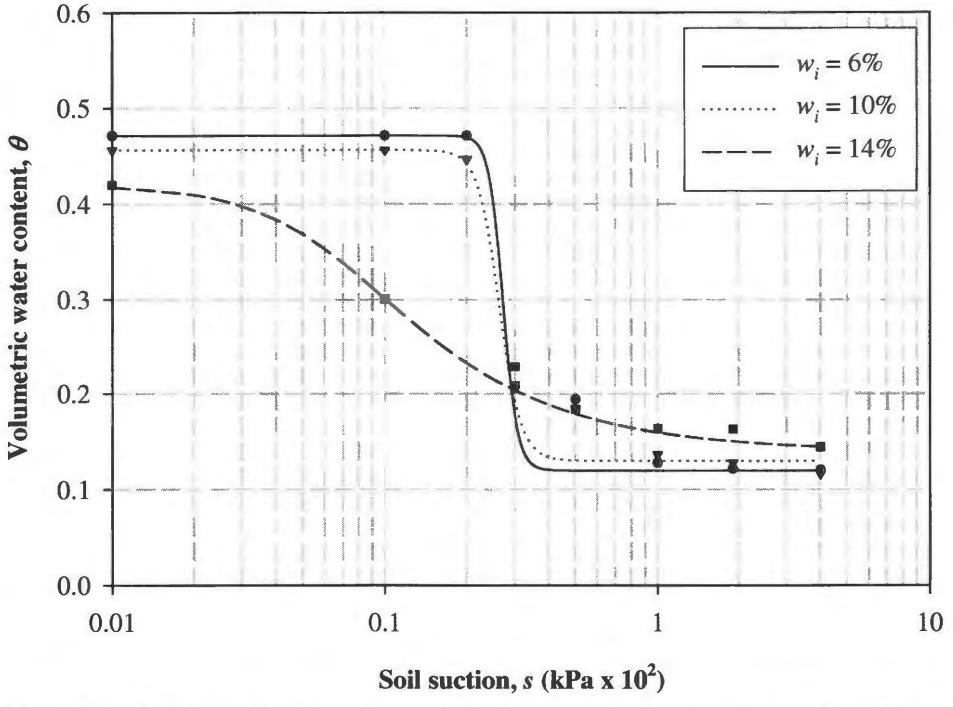

Figure 81 - Variation in soil water characteristic curve behavior due to initial water content at SCS = 300 kPa.

VARIATION OF COLLAPSE POTENTIAL WITH SUCTION

The study is primarily concerned with estimating collapse potential of an unsaturated soil using soil-water characteristic curves. The soil-water characteristic curves were developed on specimens with "initial" conditions similar to those used for the single oedometer collapse tests. Initial water contents were replaced with their respective value of suction using corresponding soil water characteristic curves. Soil samples with the same initial gravimetric water content but compacted using different compaction effort have different volumetric water contents. Therefore, suction can be considered as better fundamental parameter than water content as it is correlated to volumetric water content by means of SWCC. It is difficult to measure volumetric water content directly in the field but

soil suction can be directly measured using devices like psycrometer, tensiometer etc. (Brackley, 1980).

The value of initial water contents, volumetric water contents and corresponding soil suction from respective developed SWCCs are given in Table 17. Volumetric water contents corresponding to 6% initial water contents were found smaller than their residual values in SWCCs. Therefore, no suction data is available that corresponds to 6% water content. Figure 82 shows the variation of collapse potential with varying soil suction. Table 17 and Figure 82 indicate that the values of soil suction increased with increasing static compaction effort from 100 kPa to 300 kPa at constant initial water contents. This can be attributed to the reduction in pore size on increasing compaction efforts. However, on increasing the initial water content from 10% to 14%, the respective suction is reducing which is expected due to increase in positive pore water pressures at the same compaction effort value. From Figure 82, the collapse potential is increasing with increase in initial suction value at constant *SCS* values expect for samples with *SCS* = 300 kPa. The percentage increase in collapse on increasing suction reduced as the static compaction stress value increased.

Table 17 - Initial water contents, volumetric water contents and corresponding suction values.

***SCS* =100 kPa; σ_{fl} = 100 kPa**			***SCS* = 200 kPa; σ_{fl} = 100 kPa**			***SCS* = 300 kPa; σ_{fl} = 100 kPa**		
w_i	θ_i	s_i (kPa)	w_i	θ_i	s_i (kPa)	w_i	θ_i	s_i (kPa)
6.3	0.08	-	6.3	0.08	-	6.1	0.08	-
9.8	0.12	60	9.8	0.13	80	9.6	0.13	100
13.8	0.17	43	14.2	0.18	50	13.8	0.19	60

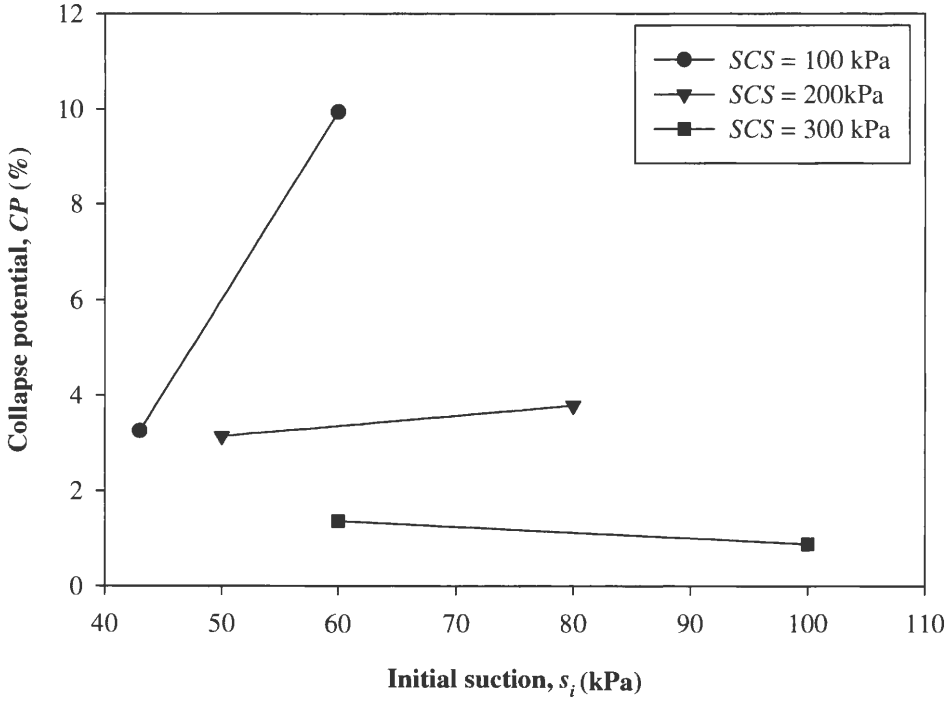

Figure 82 - Summarized collapse potential versus initial soil suction (σ_{fl} = 100 kPa).

CHAPTER 6

CONCLUSIONS AND RECOMMENDATIONS

The main conclusions drawn from the research work described in this thesis, together with recommendations for future work on the behavior of unsaturated collapsible soils is covered in this chapter.

CONCLUSIONS

The research program has provided valuable insight into understanding the behavior of unsaturated collapsible soils and met its objectives. The following subsections summarize the conclusions based on the various aspects of this research:

Volume change behavior

- The collapse potential of a collapsible soil depends on the initial placement conditions i.e., initial water content and initial dry unit weight and on the flooding stress.
- The collapse potential increases as the flooding stress is increased and reaches a maximum value. Thereafter, the collapse potential decreases on increasing flooding stress due to possible yielding of soil prior to inundation. The limiting value of flooding stress at which maximum collapse occurs arrives first for the lowest value of static compaction stress.

- The phenomenon of collapse is sudden as it takes only 1-1.5 hours for the full collapse to occur at any flooding stress and to attain an equilibrium void ratio in an oedometer test.
- The collapse potential decreases linearly with increase in initial water content for specimens statically compacted to a constant dry density.
- The maximum value of collapse potential decreases with increase in compactive effort while the initial water content is kept constant.
- The extent of partial collapse varies with the degree of saturation. As the degree of saturation increases from initial degree of saturation, the extent of partial collapse increases.

Shear strength behavior

- An initial increase in penetration resistance occurs followed by a subsequent decrease as the initial water content increases for specimens prepared at identical placement conditions.
- The penetration resistance increases with the increase in static compaction stress level at constant initial water content. A linear relationship exists between static compaction stress, *SCS* and penetration constant, N_k.
- Undrained cohesion, c_u increases with increasing static compaction stress at constant initial water content.
- The c_u values increases initially with increasing water content and then drops from the peak value.

- An excellent correlation exists between c_u (measured) from Torvane shear test and c_u (predicted) from penetration resistance.

Soil suction study and correlations with collapse potential

- The air-entry value, residual volumetric water content and saturated volumetric water content for a silty soil are smaller than that for clay.
- The slope of the SWCC for loess is almost flat at suction levels between 100 kPa - 400 kPa due to the release of most of the water at low suction levels say 0 - 100 kPa for low plasticity soils.
- The van Genuchten model gives SSR values less than 10^{-3} and therefore, it can be used for the extrapolation of volumetric water contents at high suction values.
- The saturation volumetric water content decreases as the compaction effort increases at constant initial water content. Unsystematic change in the air entry values on increasing compaction effort while, no change occurs in the residual water content value as the static compaction stress is increased.
- The residual water content increases on increasing initial water content. Also, the air entry value decreases as the initial water content increases.
- The collapse potential increases with increase in initial suction value at constant *SCS* values except for *SCS* = 300 kPa for which no effect of increase in initial suction on collapse potential was observed.

RECOMMENDATIONS

The research reported in this thesis has resulted in a better understanding of the unsaturated collapsible soils behavior. However, there is a scope for the future work to

explore further on unanswered questions and to improve the quality of research. These recommendations include:

- Development of oedometer test apparatus which can incorporate the suction measurement together with the volumetric changes.
- Development of oedometer test for partial collapse tests with no loss of moisture.
- Better alternatives for undrained shear strength measurements.
- Comparison of laboratory test results with field test results to check their applicability to the real world problems.
- Better methods to obtain soil water characteristic curves in the laboratory which incorporates the volumetric changes in the samples and can measure suction well below 10 kPa.
- Development of new correlations between the laboratory and field test results along with their limitations.

REFERENCES

Abelev, Y. M. (1948). "The essentials of designing and building on microporous soils," *Stroital Naya Promyshlemast*, No.10.

Al-Amoudi, O. S. B. and Abduljauwad, S. N. (1994). "Suggested modifications to ASTM standard methods when testing arid, saline soils." *Geotechnical Testing Journal*, 17(2), 243-253.

Ananyev, V. P. (1964). *Mineralogical composition and loessial soil properties.* (in Russian)

Anderson, P. J. (1968). "Collapsing soils and their basic parameters in an area in Tucsan, Arizona vicinity," unpublished M.S. thesis, University of Arizona, Tucsan, AZ.

Anderson, W. I. (1998). *Iowa's Geological Past: Three Billion Years of Earth History*, University of Iowa Press, Iowa city, 309-310.

ASTM (2003). *Annual Book of ASTM Standards, Section 4, Construction*. Vol. 04.09, American Society for Testing and Materials, Philadelphia, PA.

Bally, R., and Oltulescu, D. (1980). "Settlement of deep collapsible loessial strata under structures using controlled infiltration," In *Proceedings of the 6th Danube-European Conference*, SMFE, Varna.

Barden, L., McGown, A., and Collins, K. (1973). " The collapse mechanism of partly saturated soil," *Engineering Geology*, 7, 49-60.

Bell, F. G., and Culshaw, M. G. (2001). "Problem soils a British perspective," Problematic soils, *Proceedings of the Symposium*, The Nottingham Trent University, School of Property and Construction, 1-35.

Benites, L. A. (1968). "Geotechnical properties of the soils affected by piping near the Benson area, Cochise County, Arizona," unpublished M.S. thesis, University of Arizona, Tucsan, AZ.

Brackley, I. J. A. (1980). "Prediction of soil heave from suction measurements," *Seventh Regional Conference for Africa on Soil Mechanics and Foundation Engineering,* Accra, 159-166.

Bishop, A. W., Kumapley, N. K., and El-Ruwayih, A. (1975). "The influence of pore water tension on the strength of clay," In *Proceedings of Royal Society*, 278 A, 511-554.

Casagrande, A. (1936). "Determination of the preconsolidation load and its practical significance," In *Proceedings of Ist International Conference on Soil Mechanics and Foundation Engineering*, Cambridge, Mass., 3, 60-64.

Chen, F. H. (1988). *Foundations on Expansive Soils*, Elsevier Science, Amsterdam, The Netherlands.

Clevenger, W. A. (1958). "Experience with loess as foundation material," In *Proceedings, ASCE Journal of Soil Mechanics and Foundations Division*, 85, 151-180.

Coduto, D. P. (2001). *Foundation Design: Principles and Practices*, Prentice Hall.

Croney, D. (1952). "The movement and distribution of water in soils," *Geotechnique*, 3(1), 1-16.

Das, B. M. (1995). *Principles of Foundation Engineering,* PWS Publishing Company, Boston, MA.

Das, B. M. (2002). *Principles of Geotechnical Engineering*, Brooks /Cole, Pacific Groove, CA.

Denisov, N. Y. (1951). *The Engineering Properties of Loess and Loess Loams*, Gosstroiizdat, Moscow, USSR.

Derbyshire, E., and Mellors, T. W. (1988). "Geological and geotechnical characteristics of some loess and loessic soils from China and Britain: a comparison," *Engineering Geology*, 25, 135-175.

Derbyshire, E., Meng, X., Wang, J. T., Zhou, Z., and Li, B. (1995). "Collapsible loess on the loess plateau of China," In *Proceedings of the NATO Advanced Research Workshop on Genesis and Properties of Collapsible Soils*, Loughborough, U.K., 267-293.

El-Ehwany, M., and Houston, S. (1990). "Settlement and moisture movement in collapsible soils," *Journal of Geotechnical Engineering*, ASCE, 116(10), 1521-1535.

Evstatiev, D. (1995). "Design and treatment of loess bases in Bulgaria," In *Proceedings of the NATO Advanced Research Workshop on Genesis and Properties of Collapsible Soils*, Loughborough, U.K., 375-382.

Feda, J. (1964). "Colloidal activity, shrinking and swelling of some clays," In *Proceedings of the Soil Mechanics Seminar*, Loda, 531-546.

Feda, J. (1966). "Structural stability of subsident loess from Praha-Dejvice," *Engineering Geology*, 1, 201-219.

Feda, J. (1995). "Mechanisms of collapse of a soil structure," In *Proceedings of the NATO Advanced Research Workshop on Genesis and Properties of Collapsible Soils*, Loughborough, U.K., 149-172.

Fredlund, D. G., and Rahardjo, H. (1993). "An overview of unsaturated soil behavior," In *Proceedings, ASCE Specialty Series on Unsaturated Soil Properties*, Dallas, TX, October 24-28, 1-33.

Fredlund, D.G., and Xing, A. (1994). "Equations for the soil-water characteristic curve," *Canadian Geotechnical Journal*, 31(3), 521-532.

Gallipoli, D., Gens, A., Sharma, R., and Vaunat, J. (2003). "An elasto-plastic model for unsaturated soil incorporating the effects of suction and degree of saturation on mechanical behavior," *Geotechnique*, 53(1), 123-135.

Gibbs, H. J. (1961). "Properties which divide loose and dense uncemented soils," *Earth Laboratory Report EM-608*, U.S. Department of the Interior, U.S. Bureau of Reclamation.

Grim, R. E. (1962). *Applied Clay Mineralogy*, McGraw-Hill, New York.

Habibahghi, G., and Mokhberi, M. (1998). A hyperbolic model for volume change behavior of collapsible soils," *Canadian Geotechnical Journal*, 35, 264-272.

Handy, R. L. (1973). "Collapsible loess in Iowa,"*Soil Science Society of America Proceedings*, 37, 281-284.

Handy, R. L. (1995). *The Day The House Fell*, ASCE Press, Reston, Virginia, USA.

Haq, I. and Kibria, S. (1994). "Engineering characteristics of arid soils," In *Proceedings of the First International Symposium on Engineering Characteristics of Arid Soils*, London, U.K., A. A. Balkema, Brookfield, VT, p.91.

Hepworth, R. C., and Langfelder, J. (1988). "Settlement and repairs to cement plant in central Utah," *International Conference on Case Histories in Geotechnical Engineering*, University of Missouri-Rolla, MO, 1349-1354.

Holtz, R. D., and Kovacs, W. D. (1981). *Introduction to Geotechnical Engineering*, Hardcover Prentice Hall, 289-293.

Houlsby, G. T., and Sharma, R. S. (1999). "A conceptual model for the yielding and consolidation of clays," *Geotechnique*, 49(4), 491-501.

Houston, S. L., and Houston, W. N. (1997). "Collapsible soil engineering," *Unsaturated Soil Engineering Practice, Geotechnical Special Publication*, 68, 199-232.

Houston S. L., Houston, W. N., and Lawrence, C. A. (2002). "Collapsible soil engineering in highway infrastructure development," *Journal of Transportation Engineering*, 128(3), 295-300.

Houston, S. L., Houston, W. N., and Zapata, C. E. (2001). "Geotechnical engineering practice for collapsible soils," *Geotechnical and Geological Engineering*, 19(34), 333-355.

Houston, S. L., Houston, W. N., and Mahmoud, H. H. (1995 a). "Interpretation and comparison of collapse measurement techniques," In *Proceedings of the NATO Advanced Research Workshop on Genesis and Properties of Collapsible Soils*, Loughborough, U.K., 217-224.

Houston, S. L., Mahmoud, H. H., and Houston, W. N. (1995 b). "Down-hole collapse test system," *Journal of Geotechnical Engineering*, 121(4), 341-349.

Jefferson, I., Tyle, C., and Northmore, K. J. (2001). "Behavior of silt: the engineering characteristics of loess in the UK," Problematic soils, In *Proceedings of the Symposium*, The Nottingham Trent University, School of Property and Construction, 37-52.

Jennings, J. E., and Burland, J. B. (1962). "Limitation to the use of effective stress in partly saturated soils," *Geotechnique*, 12(2), 125-144.

Jennings, J. E., and Knight, K. (1957). "The additional settlement of foundations due to collapse of sandy soils on wetting," In *Proceeding of the 4th International Conference on Soil Mechanics and Foundation Engineering*, 1, 316-319.

Jennings, J. E., and Knight, K. (1975). "A guide to construction on or with materials exhibiting additional settlement due to "collapse" of grain structure," In *Proceedings of the 6th Asian Conference of Soil Mechanics and Foundation Engineering*, Durban, 99-105.

Jones, D. E., and Holtz, W. G. (1973). "Expansive soils – the hidden disaster," *Civil Engineering*, ASCE, 43(8), 49-51.

Kay, G. F., and Apfel, E. T. (1944). *The Pleistocene Geology of Iowa,* Part I, p.37.

Kezdi, A. (1974), *Handbook of Soil Mechanics, Soil Physics,* Vol. 1, Elsevier, Amsterdam, Netherlands.

Knight, K. (1963). "The origin and occurrence of collapsing soils," In *Proceeding of the 3rd Regional Conference for Africa on Soil Mechanics and Foundation Engineering*, 1, 127-130.

Larionov, A. K. (1971). *Research methods of soil structures.*

Lawton, E. C., Fragaszy, R. J., and Hardcastle, J. H. (1989). "Collapse of compacted clayey sand," *Journal of Geotechnical Engineering*, 115(9), 1252-1267.

Livingstone, I., and Warren, A. (1996). *Aeolian Geomorphology: An Introduction*, Longman Singapore Publishers Ltd.

Lutenegger, A. J., and Saber, R. T. (1988). "Determination of collapse potential of soils," *Geotechnical Testing Journal*, 111(3), 173-178.

Leong, E. C., and Rahardjo, H. (1997) ''A review on soil-water characteristic curve equations,'' *Journal of Geotechnical and Environmental Engineering,* 123(12), 1106–1117.

Marinho, F. A., and Chandler, R. J. (1993). ''Aspects of the behavior of clays on drying,'' *Unsaturated soils—Geotechnical special publication No. 39*, S. Houston and W. Wray, eds., ASCE, New York.

Marshall, T.J. (1958). "A relation between permeability and size distribution of pores," *Journal of Soil Science*, 9, 1-8.

Miao, T., Liu, Z., and Niu, Y. (2002). "Unified catastrophic model for collapsible loess," *Journal of Engineering Mechanics*, 128(5), 595-598.

Miller, C. J., Yessiller, K. Y., and Merayyan, S. (2002). "Impact of soil type and compaction conditions on soil water characteristic," *Journal of Geotechnical and Geoenvironmental Engineering*, 128(9), 733-742.

Mitchell, J. K. (1976). *Fundamentals of Soils Behavior*. John Wiley & Sons, New York, N. Y., 222-252.

Mokhberi, M. (1995). "Factors influencing volume change behavior of compacted soils," unpublished M.S. thesis, Shiraz University, Shiraz, Iran.

Mualem, Y. (1986). "Hydraulic conductivity of unsaturated soils: prediction and formulas," In *Methods of soil analysis*. Part I Physical and mineralogical methods. 2nd Edition. Agronomy. American Society of Agronomy, Inc. and Soil Society of America, Inc., Madison. Wis., U.S.A., 799-823.

Osipov, V. I., and Sokolov, V. N. (1995). "Factors and mechanisms of loess collapsibility," In *Proceedings of the NATO Advanced Research Workshop on Genesis and Properties of Collapsible Soils*, Loughborough, U.K., 49-63.

Pengelly, A., Boehm, D., Rector, E., and Welsh, J. (1997). "Engineering experience with in-situ modification of collapsible and expansive soils," *Unsaturated Soil Engineering, ASCE, Special Geotechnical Publication.*

Pereira, J. H. (1996). "Numerical analysis of the mathematical behavior of small collapsing earth dams during first reservoir filling," PhD thesis, University of Saskatchewan, Saskatoon, Sask., Canada.

Pereira J. H., and Fredlund, D. G. (2000). "Volume change behavior of collapsible compacted gneiss soil," *Journal of Geotechnical and Geoenvironmental Engineering,* 126(10), 907-916.

Phani Kumar, B. R., and Sharma, R. S. (2004). "Effect of fly ash on engineering properties of expansive soils," *Journal of Geotechnical ad Geoenvironmental Engineering*, 130(7), 764-767.

Phien-Wej, N., Pientong, T., and Balasubramanian, A. S. (1992). "Collapse and strength characteristics of loess in Thailand," *Engineering Geology*, 32, 59-72.

Poesen, J. W. A., and Wesemael, B. V. (1995). "Effects of rock fragments on the structural collapse of tilled topsoils during rain," In *Proceedings of the NATO Advanced Research Workshop on Genesis and Properties of Collapsible Soils*, Loughborough, U.K., 333-343.

Popescu, M. E. (1986). "A comparison of the behavior of swelling and collapsing soils," *Engineering Geology*, 23, 145-163.

Priklonski, V.A. (1952). *"Gruntovedenie-Vtoraic Chast.*, Gosgeolzdat, Moscow, USSR.

Proctor, R. R. (1933). "Description of field and laboratory methods," *Engineering News Record,* 3(10), 286-289.

Qian, H., Wang, J., Luo, Y., She, G., and Qi, W. (1985). *Foundations on Collapsible Loess.* Publishing House of Chinese Architecture Industry, 470. (in Chinese)

Rao, A. S., Phanikumar, B. R., and Rekha, V. A. (1991). " Swelling behavior of a remoulded expansive soil," *Journal of Institution of Engineers*, India, 76(5), 1-5.

Reznik, Yakov M. (1992). "Determination of deformation properties of collapsible soils," *Geotechnical Testing Journal*, 15(3), 248-255.

Rogers, C. D. F. (1995). "Types and distribution of collapsible soils," In *Proceedings of the NATO Advanced Research Workshop on Genesis and Properties of Collapsible Soils*, Loughborough, U.K., 1-17.

Rollins, K. M., Jorgensen, S. J., and Ross, T. E. (1998). "Optimum moisture content for dynamic compaction of collapsible soils," *Journal of Geotechnical and Geoenviromental Engineering*, 124(8), 699-708.

Rollins, K. M., and Rogers, G. W. (1994). "Mitigation measures for small structures on collapsible alluvial soils," *Journal of Geotechnical Engineering*," 120(9), 1533-1553.

Saber, R. T. (1987). "Collapse potential and pore-size distribution of friable loess soils," unpublished M.S. thesis, Clarkson University, Potsdam, NY.

Sanglerat, G. (1972). *The Penetrometer & Soil Exploration.* Elsevier, Amsterdam, Netherlands.

Schnaid, F. Kratz de Oloveira, L. A., and Gehling, W. Y. Y. (2004). "Unsaturated constitutive surfaces from pressuremeter tests,"*Journal of Geotechnical and Geoenvironmental Engineering*, 130(2), 174-185.

Seed, H. B., and Idriss, I. M. (1971). "Simplified procedure for evaluating soil liquefaction potential," In *Proceedings of the ASCE, Journal of Soil Mechanics and Foundations Division*, 97(SM9), 1249-1273.

Sergeev, E. M., Larionov, A. N. and Komissarova, N. N. (eds) (1986). *Loess in the USSR. (in Russian)*

Sharma, R.S. (1998). "Mechanical behavior of unsaturated highly expansive clays," PhD thesis, University of Oxford.

Sharma, R. S., and Mohamed , M. H. A. (2003a). "An experimental investigation of LNAPL migration in an unsaturated/saturated sand," *Engineering Geology*, 70, 305-313.

Sharma, R. S., and Mohamed , M. H. A. (2003b). "Patterns and mechanisms of migration of light non-aqueous phase liquid in an unsaturated sand," *Geotechnique*, 53(2), 225-239.

Sivakumar, V. (1993). " A critical state framework for unsaturated soil," PhD thesis, University of Sheffield.

Smith, T. D., Slyh, R., and Deal, C. (1994). "Stability of cracked earth dams on collapsible debris fans," In *Proceedings XIII. ICSMFE*, New Delhi, 3, 979-982.

Sokolovski, V. E., and Semkin, V. V. (1984). "Chemical stabilization of loess soils," *Soil Mechanics and Foundation Engineering*, 4, 8-11.

Tadepalli, R., and Fredlund, D. G. (1991)." Collapse behavior of a compacted soil during inundation," *Canadian Geotechnical Journal*, 28(40), 477-488.

Tadepalli, R., Rahardjo, H., and Fredlund, D. G. (1992). "Measurements of matric suction and volume changes during inundation of collapsible soil," *Geotechnical Testing Journal*, 15(2), 115-122.

University of Saskatchewan (1984). *KCAL User's manual. A computer program for calculating unsaturated permeability*, Department of Civil Engineering, University of Saskatchewan. Saskatoon.

Vanapalli, S. K., Fredlund, D. G., and Pufahi, D. E. (1996). "The relationship between the soil-water characteristic curve and the unsaturated shear strength of a compacted glacial till," *Geotechnical Testing Journal*, 19(3), 259-268.

Vanapalli, S. K., Sillers, W. S., and Fredlund, M. D. (1998). "The meaning and relevance of residual state to unsaturated soils," *51st Canadian Geotechnical Conference, Edmonton, Alberta,* 1-8.

Van Genuchten, M. T. (1980). ''A closed form equation for predicting the hydraulic conductivity of unsaturated soils,'' *Soil Science Society of America Journal*, 44, 892-898.

Van Genuchten, M., Leij, F., and Yates, S. (1991). ''The RETC code quantifying the hydraulic functions of unsaturated soils,'' *Report No. EPA/600/2-91/065*, U.S. EPA, Office of Research and Development, Washington, D.C.

Wheeler, S. J., Sharma, R. S., and Buisson, M. S. R. (2003). "Coupling of hydraulic hysteresis and stress-strain behavior in unsaturated soils," *Geotechnique*, 53(1), 41-54.

Zapata, C. E., Houston, W. N., S. L. Houston, and Walsh, K. D. (2000). "Soil-water characteristic curve variability,"In *Proceeding of GEO-DENVER 2000 - Advances in Unsaturated Geotechnics*, 99, 84-124.

APPENDIX A

Table A1 - Variables used in the Test Series No. 1 of study of volume change characteristics.

SCS (kPa)	σ_{fl} (kPa)	w_i (%)	γ_d (kN/m^3)	S_{ri} (%)	w_{sat} (%)	e_o	e_1
100	6	6.00	12.24	13.79	24.60	1.140	1.133
100	12	6.30	12.36	14.74	26.47	1.120	1.111
100	25	5.70	12.25	13.12	25.19	1.138	1.123
100	55	6.00	12.30	13.92	26.20	1.129	1.097
100	100	6.20	12.28	14.33	27.46	1.134	1.090
100	200	6.50	12.25	14.25	26.39	1.139	0.990
100	400	6.50	12.37	14.54	26.92	1.118	0.917
200	50	6.30	12.88	15.97	26.69	1.036	1.013
200	100	6.30	12.95	17.26	25.23	1.020	0.953
200	200	6.00	12.99	15.46	26.43	1.018	0.874
200	400	5.80	12.89	14.71	26.90	1.033	0.810
200	800	6.30	12.95	16.14	26.96	1.023	0.736
300	50	6.00	13.17	15.89	22.79	0.991	0.939
300	100	6.10	13.30	17.38	25.90	0.969	0.940
300	200	5.70	13.16	15.08	25.28	0.992	0.926
300	400	6.20	13.26	16.65	24.57	0.976	0808

Table A2 - Variables used in the Test Series No. 2 of study of volume change characteristics.

SCS (kPa)	σ_{fl} (kPa)	w_i (%)	γ_d (kN/m^3)	S_{ri} (%)	w_{sat} (%)	e_o	e_1
100	100	6.20	12.28	14.33	27.46	1.134	1.090
100	100	10.00	12.35	23.35	25.38	1.122	1.076
100	100	13.80	12.06	30.85	25.60	1.172	0.957
200	100	6.30	12.95	17.26	25.23	1.020	0.953
200	100	9.80	12.73	24.26	28.02	1.058	1.006
200	100	14.42	12.72	35.64	26.55	1.060	1.010
300	100	6.10	13.30	17.38	25.90	0.969	0.940
300	100	9.80	13.06	25.5	26.85	1.007	0.965
300	100	13.80	13.27	37.12	26.49	0.974	0.929

Table A3 - Variables used in the Test Series No. 3 of study of volume change characteristics.

SCS (kPa)	σ_{fl} (kPa)	w_i (%)	γ_d (kN/m^3)	S_{ri} (%)	S_{rf} (%)	w_f (%)	e_o	e_1
100	100	6.50	12.22	15.77	25.36	9.61	1.145	1.079
100	100	6.50	12.23	15.54	47.28	17.22	1.139	1.094
100	100	6.50	12.23	15.71	63.28	22.43	1.139	1.082
100	100	6.50	12.20	16.03	78.17	27.04	1.147	1.061
100	100	6.20	12.28	14.89	100.00	27.46	1.134	1.090
200	100	5.60	12.87	14.87	25.33	9.01	1.036	0.986
200	100	5.70	12.89	15.00	35.78	12.50	1.032	0.995
200	100	6.00	12.73	16.32	45.99	15.68	1.031	0.962
200	100	5.60	12.87	14.68	52.61	18.65	1.035	0.998
200	100	5.40	12.79	13.92	87.00	29.84	1.049	1.014
200	100	6.30	12.95	17.26	100.00	25.23	1.020	0.953
300	100	5.40	13.07	14.75	25.45	9.11	1.000	0.958
300	100	5.40	12.82	14.60	33.10	11.77	1.008	0.968
300	100	5.70	12.82	15.55	39.59	13.74	1.011	0.959
300	100	5.70	12.87	15.40	48.59	17.37	0.986	0.952
300	100	5.70	12.92	15.13	84.71	29.24	1.028	0.986
300	100	6.30	13.30	17.26	100.00	25.23	0.969	0.940

Table A4 - Variables used in the study of shear strength characteristics by using Proctor penetrometer.

w_i (%)	γ_d (kN/m^3)
6.20	12.28
9.80	12.37
13.80	12.06
6.30	12.95
9.80	12.73
14.40	12.72
6.10	13.30
9.80	13.06
13.80	13.27

Table A5 - Variables used in the study of shear strength characteristics by using Torvane shear tester.

w_i (%)	γ_d (kN/m^3)
6.46	12.25
10.06	12.34
13.81	12.06
5.74	13.02
10.20	12.68
13.69	12.80
6.06	13.30
10.00	13.04
13.41	13.32

APPENDIX B

Table B1 - Experimental and fitted data for SWCC with w_i = 6% and SCS = 100 kPa.

Applied suction, s (kPa)	Experimental θ	Fitted θ using VG model
0.01	0.48	0.48
0.10	0.48	0.48
0.13	0.48	0.48
0.15	0.48	0.48
0.20	0.48	0.48
0.30	0.43	0.43
0.50	0.19	0.19
1.00	0.13	0.12
1.90	0.12	0.12
4.00	0.12	0.12

Table B2 - Experimental and fitted data for SWCC with w_i = 6% and SCS = 200 kPa.

Applied suction, s (kPa)	Experimental θ	Fitted θ using VG model
0.01	0.47	0.47
0.10	0.47	0.47
0.20	0.47	0.47
0.30	0.43	0.42
0.50	0.19	0.18
1.00	0.13	0.12
1.90	0.12	0.12
4.00	0.13	0.12

Table B3 - Experimental and fitted data for SWCC with w_i = 6% and SCS = 300 kPa.

Applied suction, s (kPa)	Experimental θ	Fitted θ using VG model
0.01	0.47	0.47
0.10	0.47	0.47
0.20	0.47	0.47
0.30	0.21	0.18
0.50	0.19	0.12
1.00	0.13	0.12
1.90	0.12	0.12
4.00	0.12	0.12

Table B4 - Experimental and fitted data for SWCC with w_i = 10% and *SCS* = 100 kPa.

Applied suction, s (kPa)	Experimental θ	Fitted θ using VG model
0.01	0.49	0.49
0.10	0.49	0.49
0.20	0.47	0.46
0.30	0.30	0.31
0.50	0.16	0.15
1.00	0.13	0.13
1.90	0.13	0.13
4.00	0.12	0.13

Table B5 - Experimental and fitted data for SWCC with w_i = 10% and *SCS* = 200 kPa.

Applied suction, s (kPa)	Experimental θ	Fitted θ using VG model
0.01	0.47	0.47
0.10	0.47	0.47
0.30	0.38	0.38
0.50	0.16	0.19
1.00	0.14	0.12
1.90	0.12	0.12
4.00	0.12	0.12

Table B6 - Experimental and fitted data for SWCC with w_i = 10% and *SCS* = 300 kPa.

Applied suction, s (kPa)	Experimental θ	Fitted θ using VG model
0.01	0.46	0.46
0.10	0.46	0.46
0.20	0.45	0.44
0.30	0.21	0.19
0.50	0.18	0.13
1.00	0.14	0.13
1.90	0.13	0.13
4.00	0.12	0.13

Table B7 - Experimental and fitted data for SWCC with w_i = 140% and *SCS* = 100 kPa.

Applied suction, s (kPa)	Experimental θ	Fitted θ using VG model
0.01	0.48	0.48
0.10	0.31	0.32
0.30	0.20	0.20
0.50	0.18	0.17
1.00	0.15	0.15
1.90	0.15	0.15
4.00	0.14	0.14

Table B8 - Experimental and fitted data for SWCC with w_i = 14% and SCS = 200 kPa.

Applied suction, s (kPa)	Experimental θ	Fitted θ using VG model
0.01	0.45	0.44
0.10	0.29	0.29
0.30	0.22	0.19
1.00	0.16	0.16
1.90	0.16	0.15
4.00	0.14	0.14

Table B9 - Experimental and fitted data for SWCC with w_i = 14% and SCS = 3200 kPa.

Applied suction, s (kPa)	Experimental θ	Fitted θ using VG model
0.01	0.42	0.42
0.10	0.30	0.30
0.30	0.23	0.20
0.50	0.18	0.18
1.00	0.16	0.16
1.90	0.16	0.15
4.00	0.14	0.14